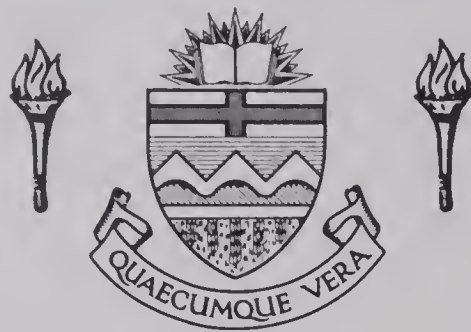


# **For Reference**

---

**NOT TO BE TAKEN FROM THIS ROOM**

Ex LIBRIS  
UNIVERSITATIS  
ALBERTAE NSIS











THE UNIVERSITY OF ALBERTA

RELEASE FORM

NAME OF AUTHOR\ ...Suzanne Mickey Costaschuk.....  
TITLE OF THESIS ...Uraniferous Pegmatites in the Grease River  
Area, Northern Saskatchewan.....  
.....  
DEGREE FOR WHICH THESIS WAS PRESENTED ...M.Sc.....  
YEAR THIS DEGREE GRANTED ...Fall, 1979.....

Permission is hereby granted to THE UNIVERSITY OF  
ALBERTA LIBRARY to reproduce single copies of this  
thesis and to lend or sell such copies for private,  
scholarly or scientific research purposes only.

The author reserves other publication rights, and  
neither the thesis nor extensive extracts from it may  
be printed or otherwise reproduced without the author's  
written permission.

(Sig  
PER

DATED ...October..... 19 79



THE UNIVERSITY OF ALBERTA

URANIFEROUS PEGMATITES IN THE GREASE RIVER AREA, NORTHERN  
SASKATCHEWAN

by



SUZANNE MICKEY COSTASCHUK

A THESIS

SUBMITTED TO THE FACULTY OF GRADUATE STUDIES AND RESEARCH  
IN PARTIAL FULFILMENT OF THE REQUIREMENTS FOR THE DEGREE  
OF MASTER OF SCIENCE

DEPARTMENT OF GEOLOGY

EDMONTON, ALBERTA

FALL, 1979



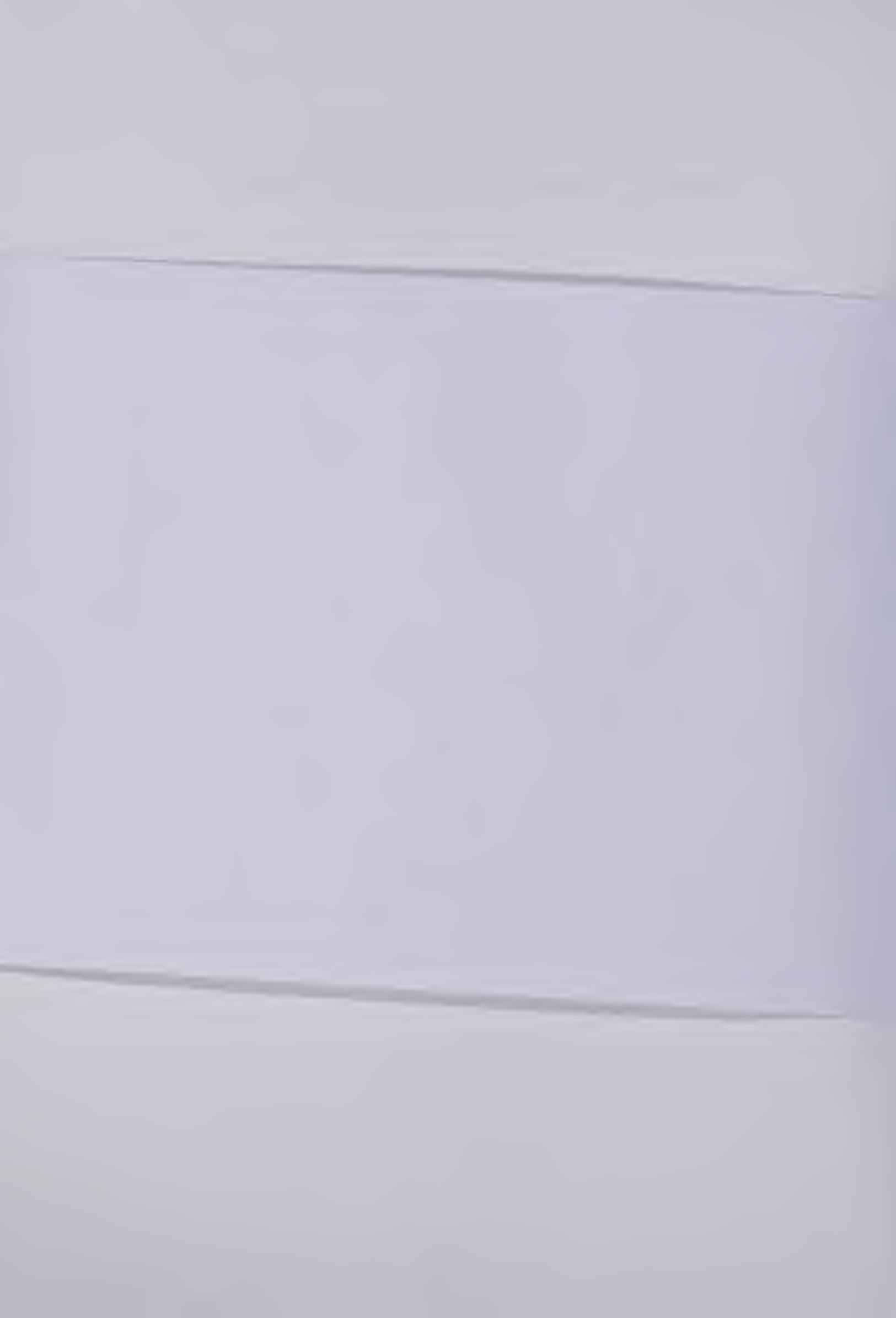


Digitized by the Internet Archive  
in 2019 with funding from  
University of Alberta Libraries

<https://archive.org/details/Costaschuk1979>

THE UNIVERSITY OF ALBERTA  
FACULTY OF GRADUATE STUDIES AND RESEARCH

The undersigned certify that they have read, and recommend to the Faculty of Graduate Studies and Research, for acceptance, a thesis entitled URANIFEROUS PEGMATITES IN THE GREASE RIVER AREA, NORTHERN SASKATCHEWAN submitted by SUZANNE MICKY COSTASCHUK in partial fulfilment of the requirements for the degree of MASTER OF SCIENCE.





To my parents,

for all they have taught me.



## Abstract

This study involves a portion of the Western Craton subdivision of the Churchill structural province of northern Saskatchewan. It is a detailed study of radioactive pegmatites bordering the Grease River in the Fond-du-Lac map area. Results from field, microscopic, oxygen stable isotope, U-Th-Pb mineral age dating, heavy mineral and electron microprobe mineral studies are used to summarize the geology and uranium mineralization of the Grease River property.

The Precambrian basement is comprised of Tazin Group biotite gneisses and pink felsic gneisses. The thinly banded plagioclase-quartz -biotite gneisses developed under middle amphibolite facies metamorphism. The coarser-grained, leucocratic, K-feldspar-plagioclase-quartz-biotite gneisses are evidence of upper amphibolite facies conditions.

The pelitic and felsic gneisses formed contemporaneously during a regional metamorphic event involving high temperatures and pressures. Petrological evidence suggests the biotite gneisses formed from low Al, Ca and high Fe, Mg, Ti argillaceous sediments, while the granitic rocks were derived by partial melting of a source similar in composition to the more mafic units.

White, massive pegmatites intrude and migmatize the Tazin Group assemblages. They mainly vary in composition from trondhjemite to two-feldspar and alaskite granites depending





on the extent of K-metasomatism. The initial plagioclase-quartz-biotite trondhjemitic melt likely formed at temperatures greater than 685°C. At the time of intrusion, high temperatures existed which thermally metamorphosed and melted the gneisses. A later intrusive phase involving quartz-muscovite veining, transformed some white pegmatites into quartz-rich granitoids and quartzolites. The silicification took place during hypothermal conditions (300 to 500°C) which, consequently caused extensive alteration of the affected rocks.

Zircon separates from biotite and granitic gneisses yield mid-Aphebian U-Pb dates of 2250 Ma. These results are interpreted as Kenoran (2500 Ma) survival ages, up-dated by the younger Hudsonian orogeny which essentially re-set their U-Pb radiometric clocks. The white pegmatites have originated from more intensely remobilized portions of the Archean crust. The main trondhjemitic to granite pegmatite is dated at 1970 Ma, while the late-stage quartz enrichment yields 1845 Ma ages.

Considerable tectonic activity occurred during the Hudsonian reactivation. Shearing, plastic deformation and major faulting of the biotite and granitic gneisses are observed in the affected portions of the Grease River linear belt. Also, structural control of the emplacement of the syntectonic pegmatites is inferred since they form in an elongated, discontinuous zone paralleling the NE regional strike.





Uranium mineralization is localized in the white pegmatites. Two periods of uranium enrichment are inferred from radiometric, geochronological, petrological and probe studies. In the first, cubic, Th-rich uraninite crystallized with the plagioclase-quartz-biotite assemblage. Common accessories are zircon, molybdenite, apatite, sphene, thorite and iron opaques. A second mineralization period occurred during the hydrothermal silicification of the initial pegmatites. Uranium enriched zircons, thorium-bearing minerals and yellow uranyl mineralization are believed to have formed during this time.



## Acknowledgements

The author wishes to express her gratitude to Dr. R.E. Folinsbee for his undiminished guidance and interest in all the aspects of thesis work, and for his financial support both, in the field and with the departmental teaching assistantship.

The author also wishes to acknowledge the following persons:

Dr. H. Baadsgaard for his tremendous generosity of time, help and enthusiasm spent in accomplishing the heavy mineral and age dating analyses.

Dr. D.G.W. Smith for his suggestions regarding the electron microprobe study, his views on the interpretation of the geochemical results, and his help in financing the commercially made electron microprobe thin-sections.

Dr. K. Hattori for conducting the oxygen stable isotope analysis and providing the author with insight into the interpretation of the results.

Drs. J. Krupicka, R.D. Morton, R. St. J. Lambert, F. Longstaffe, R.A. Burwash and K. Muehlenbachs for their helpful comments on the petrological, structural and oxygen isotope results.

Mrs. Alice Leech for accompanying the author to the Grease River area and for offering her hospitality during the last three years.



Permission to use and publish Urangesellschaft's geological map, radiometric map and U3O8 assay results is also acknowledged.

Many thanks are also extended to: S. Launspach, D. Tomlinson and C. Gold for their greatly appreciated help in obtaining mineral compositional analysis; F. Dimitrov who helped photograph the hand specimens; A. Stelmach who helped stain the rocks.

Special thanks are due to the University of Alberta, Geology Department for financing the typing of the thesis and especially to Mrs. Ella Ritz from Computing Services for her friendly and continued help in preparing a final draft.





## Table of Contents

Chapter	Page
I. Introduction.....	1
A. General Statement.....	1
B. The Thesis Area.....	3
Location.....	3
Previous Work.....	3
Work Done by the Author.....	7
II. Regional and Local Geological Setting.....	8
A. Geological and Mining Developments in Northwestern Saskatchewan.....	8
B. Regional Geology.....	12
C. Local Geology.....	18
III. Petrography and Mesosstructural Analysis of the Grease River Property.....	21
A. Textural Classification of the Rocks.....	22
B. Compositional Classification of Rocks at the Main Showing.....	25
C. Description of the Mineralized Rocks.....	31
D. Mesosstructural Analysis.....	32
E. Discussion of Chapter III.....	35
IV. Petrology, Petrogenesis and Oxygen Isotopes of the Grease River Property.....	37
A. Petrological Examination.....	37
Biotite Gneiss.....	38
Two-Feldspar Granites.....	39
Alaskite.....	42



Quartz-Rich Granitoid and Quartzolite.....	43
Trondhjemite.....	44
Summary of Petrological Results.....	46
B. Petrogenesis.....	49
C. Oxygen Stable Isotope Analysis.....	56
Analytical Procedures.....	56
Geological Applications of Oxygen Stable Isotope Analyses.....	57
Results.....	58
Interpretations of the Results.....	61
V. Geochronology.....	63
A. U-Th-Pb Dating Method.....	63
Introduction.....	63
Theory of Radioisotope Dating.....	64
B. Analytical Procedures.....	66
C. U-Th-Pb Isotope Results and Mineral Dates.....	67
D. Interpretation of Results.....	72
VI. Mineral Geochemistry of the Mineralized Zone.....	78
A. Analytical Approach.....	78
B. Minerals Analyzed by the Electron Microprobe...80	
Biotite Analyses.....	80
Zircon Analyses.....	95
Uraninite Analyses.....	105
C. Summary of Chapter VI.....	114
VII. Uranium Mineralization in the Grease River Area..	115
A. Radiometric Survey, Ore Grades and Economic Potential of the Grease River Property.....	115
B. Discussion of the Geology and Economic Evaluation of the Grease River Property.....	120



C. Comparison with Similar Pegmatitic Uranium Occurrences.....	124
VIII. Summary and Conclusion.....	130
PHOTOGRAPHIC PLATES.....	135
REFERENCES.....	151
Appendix A.....	160
Sample Descriptions.....	160
Appendix B.....	163
Heavy Minerals.....	163
Appendix C.....	164
Geochronology Analytical Procedures.....	164
Heavy Mineral Analysis.....	164
Isolation of Mineral Separates.....	164
Notes on Zircon and Uraninite Separates.....	165
Chemical Procedure.....	166
Isotope Analysis.....	167
Appendix D.....	168
Electron Microprobe Methodology.....	168
Energy Dispersive Analysis.....	168
Instrumentation and Operating Conditions.....	168
Standardization of Operating Conditions.....	169
Standards used to obtain Chemical Results.....	169
Data Accumulation.....	170
Data Processing.....	170
Semi-Qualitative Analysis.....	172
Wavelength Dispersive Analysis.....	172
Instrumentation and Operating Conditions.....	172
Data Accumulation.....	173
Data Processing.....	173





## List of Tables

Table	Description	Page
1.	Modal composition of granitic rocks from the Grease River area.....	26
2.	Modal composition of quartz-rich rocks from the Grease River area.....	27
3.	Modal composition of trondhjemitic rocks from the Grease River area.....	27
4.	Characteristic features of essential minerals, secondary minerals and predominant textures observed in rocks from the thesis area.....	47
5.	$\delta O^{18}$ values in % for minerals from Grease River area pegmatites and from granitoids of igneous and metamorphic origin.....	59
6.	U-Th-Pb isotopic results for zircons and uraninites.....	68
7.	U-Pb, Pb-Pb, Th-Pb dates, Grease River area, N. Saskatchewan.....	68
8.	K-Ar, Rb-Sr, U-Pb mineral and whole rock ages (Ma) from the Western Craton of Saskatchewan, Alberta and the Northwest Territories.....	73
9.	Chemical analyses in weight percentages of biotites from the Grease River area, N. Saskatchewan.....	81
10.	Structural formulae of biotites from the Grease River area, N. Saskatchewan.....	83
11.	Chemical analyses in weight percentages of zircons from the Grease River area, N. Saskatchewan.....	97
12.	Chemical analyses in weight percentages of uraninites from the Grease River area, N.	



	Saskatchewan.....	107
13.	Subtotals, ratios and chemical ages calculated for uraninites from the Grease River area, N. Saskatchewan.....	109
14.	Average grade (% U308) and spectrometric results for trenches in white pegmatites and migmatites at the Grease River property.....	119
15	Time stratigraphic sequence of events, Grease River Area, northern Saskatchewan.....	131
16.	Heavy minerals found in gneisses, migmatites and pegmatites from the Grease River area, N. Saskatchewan.....	163
17.	Standards used for the elements detected in biotites and zircons analyzed using EMP-EDA methods.....	171
18.	Basic data regarding the elements (El) analyzed and the standards used to obtain EMP-WDA compositional analyses of uraninite.....	174



## List of Figures

Figure	Description	Page
1.	Location and claim map of the Grease River property.....	4
2.	Major lithostructural subdivisions of the Saskatchewan shield.....	13
3.	Metamorphic map of the Saskatchewan shield.....	14
4.	Simplified geological map of the Fond-du-Lac area.	16
5.	Geological map of the thesis area.....	19
6.	Quartz-plagioclase-K-feldspar diagram showing the distribution of rock types in the thesis area.....	28
7.	Equal-area projection of poles to foliation planes in gneisses and migmatites at the main showing.....	34
8a.	Diagram of metamorphic grade.....	50
8b.	Diagram of metamorphic facies.....	50
9.	$\delta O^{18}$ mineral results for pegmatites from the Grease River area.....	60
10.	Concordia curve for zircons and uraninites from the Grease River area.....	70
11.	U-Th-Pb evolution diagram for uraninites from the Grease River area.....	71
12.	Distribution of the oxides found in biotites from the Grease River area.....	86





13a.	Plot of SiO <sub>2</sub> vs. H <sub>2</sub> O in unaltered and partially chloritized biotites.....	87
13b.	Plot of K <sub>2</sub> O vs. H <sub>2</sub> O in unaltered and partially chloritized biotites.....	87
14.	SiO <sub>2</sub> vs. Al <sub>2</sub> O <sub>3</sub> for biotites.....	88
15.	MgO vs. FeO for biotites.....	90
16.	(FeO+MnO) - TiO <sub>2</sub> - MgO plot for biotites from the Grease River area.....	93
17.	Triangular diagram for contents of MgO, FeO, Al <sub>2</sub> O <sub>3</sub> for biotites in the Grease River area.....	94
18.	ZrO <sub>2</sub> vs. SiO <sub>2</sub> in migmatitic and pegmatitic zircons.....	98
19.	Plot of the chemical variations in zircons from the Grease River area.....	101
20.	Distribution of major and minor oxides found in the uraninites from the Grease River area.....	110
21.	Chemical trends of uraninites in pegmatites from the Grease River and Charlebois Lake areas.....	112
22.	Histogram of the spectrometric and U308 results, Grease River area.....	117



## List of Photographic Plates

Plate	Description	Page
1.	Photographs of the Grease River area.....	136
2.	Photographs illustrating field relationships...	137
3.	Photographs illustrating field relationships...	138
4.	Photographs of the migmatized biotite gneiss...	139
5.	Photographs of the white pegmatites.....	140
6.	Photographs and radioluxographs of radioactive samples.....	141
7.	Photographs and radioluxographs of radioactive samples.....	142
8.	Radioluxographs of electron microprobe mounts and petrographic thin sections.....	143
9.	Reflected light photomicrographs of zircon and allanite.....	144
10.	Elemental photographs of zircon D9-6.....	145
11.	Reflected light photomicrographic mosaic of trondhjemitic pegmatite sample 14.....	146
12.	Reflected light photomicrographs of uraninite..	147
13.	Backscatter electron and elemental photographs of uraninite 32-A.....	148
14.	Backscatter electron and elemental photographs of uraninites 32-B and 32-C.....	149



15.	Elemental photographs of extensively altered uraninites.....	150
-----	---	-----





## Index of Maps

Map	Title
1.	Grease River: Main Showing Geological Map.....
2.	Grease River: Main Showing Radiometric Survey and Trench Sampling Results.....
3.	Grease River: Main Showing Structural Geology.....

(all maps in pocket)



## **I. Introduction**

### **A. General Statement**

Low-grade uranium pegmatites are found in Precambrian Shield areas throughout the world. They commonly occur in regionally metamorphosed terrains that have been extensively granitized. The pegmatites are usually of silicic or alkalic composition and host a variety of radioactive minerals of which uraninite is the most common. These uranium pegmatitic occurrences generally have low ore grades and low tonnages. Typical assay grades rarely run above .05 percent U<sub>3</sub>O<sub>8</sub> and yields are usually under 20,000 ton U<sub>3</sub>O<sub>8</sub>. Furthermore, uranium is frequently disseminated throughout small, discontinuous pegmatitic lenses and pods which make them even higher-risk mining targets.

Despite the dim foregoing appraisal of pegmatitic uranium deposits, these occurrences have recently attracted much interest from the mining community. The soaring world demand for uranium has initiated intensive uranium exploration programs aimed at locating even low-grade deposits. This concern is likely to continue because of the increased use of uranium as a nuclear fuel by the industrialized and developing nations. Although to-date, only a few of these usually sub-economic deposits have been exploited, namely at Bancroft, Canada and Rossing, South-West Africa, they continue to be assessed as potential uranium producers for the future.



This thesis was initiated in order to provide an in depth evaluation of a potential deposit in Canada; the pegmatitic uranium occurrence situated along the Grease River fault zone in the Lake Athabasca - Stony Rapids area of northern Saskatchewan. Specific objectives are:

1. to describe the geology of the study area,
2. to determine the age of the uraniferous pegmatites and,
3. to obtain mineral geochemical data in hopes of determining the factors governing the emplacement of the pegmatites and genesis of the uranium mineralization.

Chapter II describes the regional and local geological settings. A synthesis of field work and subsequent hand sample examination used to classify the rocks is presented in Chapter III. In Chapter IV, emphasis has been placed on detailed petrologic thin-section examinations and stable oxygen isotope results. The theory, methodology and results of U-Th-Pb isotope dilution methods used to date the rocks are contained in Chapter V. Chapter VI describes electron microprobe mineral compositional analyses. Chapter VII describes the uranium mineralization and ore grades of the Grease River area pegmatites and several other similar occurrences. Finally, Chapter VIII is a summary and conclusion of the significant results of this study.





## B. The Thesis Area

### Location

The study area is located on the Grease River in the north-central Saskatchewan shield region, approximately 150 km east of Uranium City, Saskatchewan. (59° 30'N, 106° 22'W). The area of concern lies within three adjacent claim blocks (CBS 2745, CBS 5398 and CBS 3424), each covering an area of approximately 4.1 km<sup>2</sup> (Figure 1). These properties are presently accessible only by air from Stony Rapids, 40 km to the southeast and from Uranium City.

The physiography of the Grease River area is typical of glaciated regions of the Canadian Shield. It is comprised of elongated hills and valleys of bedrock with moderate relief (up to 300 m elevations), mantled by a broken cover of glacial sediments. Numerous lakes and rivers drain southwest, following a strong regional trend, and eventually empty into Lake Athabasca. The Grease River originates from Fontaine Lake, 25 km north of the property, and empties into Fond-du-Lac Channel east of Lake Athabasca 40 km to the south. A major waterfall, known as Lefty's Falls, is located on the river only .8 km from the main showing.

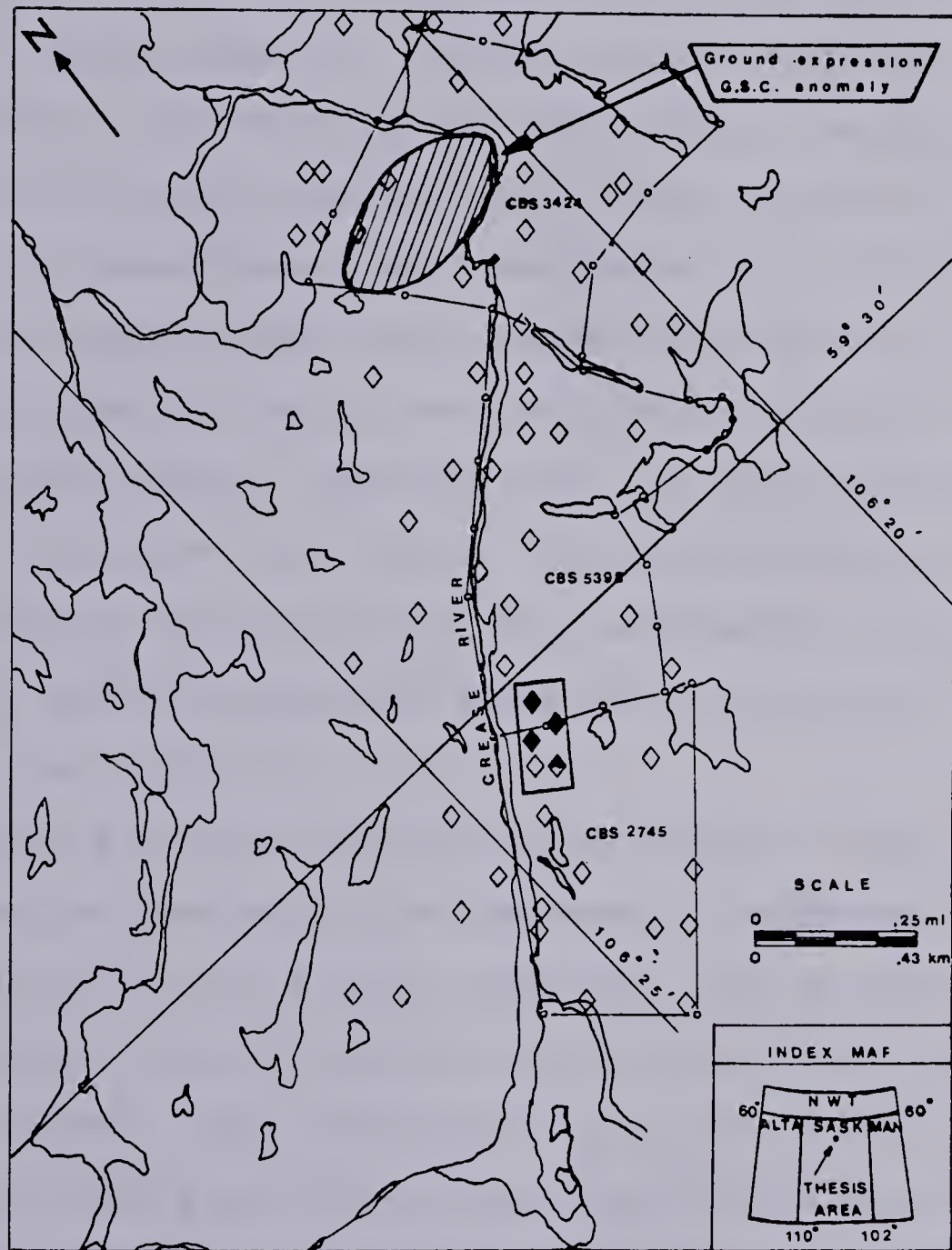
### Previous Work

Since the discovery in 1950 of the radioactive pegmatites in the study area, the property has changed ownership three times. Al Hemingson, first to work on the uranium showings, staked and restaked CBS 2745 from 1954 until 1974. His work included trenching and blasting of the





FIG. 1: LOCATION AND CLAIM MAP OF THE GREASE RIVER PROPERTY



LEGEND:

Radiometric  
anomaly

1st order  
2nd order  
3rd order



Claim post



Claim boundary





radioactive sites in 1964-65. The pits and trenches, averaging .7 m deep extended over a distance of 6.4 km on a ridge paralleling the Grease River. Several chip samples were assayed for their U308 content.

Results of a Geological Survey of Canada (G.S.C.) funded airborne gamma ray spectrometry survey of northern Saskatchewan (Richardson et al. 1974) showed the existence of a radioactive anomaly on the Grease River property. The radiometric measurements were obtained using a Skyvan four-window spectrometer with twelve 22.86 cm by 10.16 cm NaI(Tl) detectors flown at an elevation of 150 meters and a speed of 190 km/hour. The high U and low Th responses obtained on flight line 15 over the Grease River property were anomalous for the region. This radiometric anomaly (see Figure 1) provided incentive for further exploration in the Grease River district.

During 1974, Fosago Exploration Limited staked CBS 3425 and later CBS 5398 which lie northeast of Hemingson's property. Beginning in 1974, assessment work of the Grease River property was conducted by several geologists on Fosago's behalf. The Folinsbee and Leech field party worked primarily at the main showing where the most radioactive pegmatites had been discovered (Folinsbee et al. 1974). Two main baselines, 040 AND 085, and perpendicular secondary lines were laid out in order to give grid-coordinates to Hemingson's trenches and to run a radiometric survey. Six chip samples were assayed for U and Th. Fosago's continued



interest in the property resulted in two geologic and radiometric reconnaissance reports: Sassano (1974); Donaghy (1975). Other work was done by D. Robertson but no report is available.

The three claim blocks comprising the Grease River property were optioned by Urangesellschaft Canada Limited in 1976. Urangesellschaft's exploration program included an airborne gamma ray spectrometer and magnetometer survey (Beesley, 1977). The geophysical survey was flown with a fixed-wing Beaver system at an altitude averaging 53 meters above ground and a speed of 137 km/hour. A total of 9 flight lines, each 8 km long and at 130 degrees across the regional strike, were flown at .4 km intervals. The geophysical crew detected one second and three first order radioactive anomalies plus numerous others of third order.

Later in 1976, Urangesellschaft's field party carried out a reconnaissance geological survey of the property in order to explain the various anomalies recorded by the airborne survey. It was found that the stronger radioactive signals coincided with the main mineralized zone previously outlined by Hemingson and Fosago (Beesley, 1977). However, many of the third order anomalies detected over areas adjacent to the main showing could not be located or explained by the ground follow-up crew. Detailed geologic and radiometric surveys were conducted over the main showing where the principal uraniferous pegmatites are exposed.





### Work Done by the Author

During the first week in August, 1976, the author went with A. Leech, D. Robertson, and a summer assistant to the thesis location. Fosago's map outlining the basic geology and radiometric results of the main showing were used in the field. A. Leech who had previously surveyed the Grease River property helped to carry out the following tasks:

1. structural analyses consisting primarily of taking orientations of the metasediments and their contacts with the intruding white pegmatites.
2. geologic mapping.
3. collecting grab samples and bulk samples.
4. ground radiometric work.

Subsequent to the field work, the structural data was plotted on a map and stereogram in order to assess the tectonic disturbance associated with the intruding white pegmatites.

Petrologic thin-sections were prepared from the 36 samples collected from the Grease River property. On the basis of petrological examinations, the samples suitable for heavy mineral analyses, U-Pb geochronology, and probe study were selected.

Upon receiving in 1978, Urangesellschaft's report on the thesis location, the radiometric survey results and U308 ore grades were closely examined and correlated with the author's geologic findings.





## II. Regional and Local Geological Setting

In this chapter the geological background information relevant to the Grease River study is given. Section A is a review of the geological and mining developments that have taken place in northwestern Saskatchewan. Section B is the summary of the geology of the Western Craton north of Lake Athabasca and of the Fond-du-Lac region in which the thesis area occurs. The local geological setting is presented in the last section, C.

### A. Geological and Mining Developments in Northwestern Saskatchewan

Geological surveys of northwestern Saskatchewan were initiated by the end of the 19th century. The land primarily north of Lake Athabasca but west of the Grease River area was explored by many geologists, whose findings have been outlined by Beck (1966, 1969) and Tremblay (1972). In particular, Alcock (1936) described the extensive Tazin Group of metamorphosed sedimentary rocks which were later recognized in both northeastern Alberta and the Northwest Territories as well as the thesis area which lies to the east.

Regional mapping of the Saskatchewan Shield continued through to the late 1960's. This resulted in a number of G.S.C. publications outlining the geology of the Lake Athabasca region (see Beck, 1966). For the regions closer to



the study area, reports describing the rock types, structure and economic potential in the Fond-du-Lac and Stony Rapids area were completed in 1963 by the Saskatchewan Department of Mines and Resources, and subsequently compiled into a G.S.C. Fond-du-Lac paper and map sheet (see Baer, 1968).

During this time geophysical surveys of northern Saskatchewan were carried out in order to help interpret the geology. The gravity (Can. Dept. Mines Tech. Serv., 1962) and aeromagnetic (Sask. Dept. Miner. Resour. et al. 1964) results suggested that the Saskatchewan crystalline basement was composed of several distinct tectonic units. Since these units were traceable to the Cordilleran fold belt in southwestern Alberta, they were perceived as deep crustal entities.

The ensuing geological studies of Saskatchewan's Precambrian basement rocks were of a broader scope, encompassing structural, petrological, geochemical and geochronological investigations. A number of important papers, particularly those of Burwash (1978, 1979), Burwash et al. (1962, 1969, 1970), Koster et al. (1970) and Lewry et al. (1978) described the four tectonic or lithostructural units presently recognized in Saskatchewan. Several of these publications also dealt with the main events leading to the final stabilization of this part of the Churchill structural province. It is now certain that much of the Archean craton in Saskatchewan was reactivated during the Hudsonian orogeny which lasted from 1900 to 1700 Ma (Burwash et al. 1969). The



reactivation, consisting of extensive polymetamorphism, granitization and K-metasomatism, affected much of the shield region of Saskatchewan.

Mining activities in northern Saskatchewan flourished after the initial discovery of U, Au, Fe, Cu and Ni mineralization in the Lake Athabasca region (Beck, 1966; Tremblay, 1972). As early as 1914, ore minerals were associated with the Tazin Group of supracrustal and granitoid rocks located in the Beaverlodge mining district on the north shore of Lake Athabasca (Figure 1). Although Au-quartz veins were mined for several years, the tremendous economic worth of the rich epigenetic and syngenetic uranium occurrences was soon realized. As a result, numerous uranium staking and prospecting ventures were initiated.

Exploitation of these radioactive deposits began in 1942 because of an immediate requirement for nuclear fuels. The ores were mined under the sole jurisdiction of Eldorado Mining and Refining, a Crown Corporation. In 1948 the end of the wartime ban on uranium prospecting caused a second intensive uranium exploration boom in northern Saskatchewan (Northern Miner, July 1978). This continued until the late 1950's when the world demand for uranium had dwindled.

The uranium prospecting interests in northern Saskatchewan were renewed in the 1960's by German, French and American geologists (Northern Miner, July, 1978). Since





then the increasing world demand and price for U, coupled with the energy crisis in the 1970's set going a third wave of uranium prospecting in Saskatchewan. The mounting economic interest resulted in a grand-scale, joint Federal-Saskatchewan Government, Uranium Reconnaissance Program involving high-sensitivity airborne gamma-ray spectrometry (Darnley et al. 1975; Richardson et al. 1975). The surveys were flown over Precambrian shield areas with good exposures of bedrock and uniform topography.

The prime objectives in obtaining such high-quality reconnaissance data were to (1) evaluate the regional U-potential and (2) provide incentive for follow-up U-exploration programs by making available the background radiometric and geochemical information which would be otherwise both costly and time-consuming to accumulate.

The airborne gamma-ray spectrometer results proved the existence of a uranium enriched province in northern Saskatchewan. Many radioactive anomalies were discovered in the younger Proterozoic belts in the western and central shield area (Richardson et al. 1975).

Meanwhile, the theoretical possibility of sandstone-unconformity type uranium deposits occurring at the crystalline basement-Athabasca Formation contact in northern Saskatchewan was soon realized. The discoveries of rich pitchblende ores at Rabbit Lake, Cluff Lake, Key Lake and Midwest Lake signified the geographical extent of epigenetic U-mineralization at the Proterozoic unconformity.





It was soon apparent that the uranium in these high-grade ores was remobilized from the underlying Precambrian basement rocks.

## B. Regional Geology

The four lithostructural units of the Saskatchewan shield area are shown in Figure 2. The significant features of these northeast trending domains are described in a paper by Lewry et al. (1978). The following is a summary of the sections dealing with only the two most westerly units since these contain most of the radioactive anomalies discovered in Saskatchewan.

The first is the Western Craton which is comprised of an Archean basement complex of granitoids, migmatites and high-grade metamorphic rocks. Reactivation of the craton during the Hudsonian orogeny (1900 to 1700 Ma; Burwash et al. 1969) resulted in a series of younger mobile belts which surround the older stable blocks (Beck, 1969). Here the Kenoran ages (2500 Ma.) have been up-dated to give a range of ages from 2360 to 1750 Ma. depending on the degree of reactivation. Figure 3 shows that the Hudsonian metamorphic overprinting occurred under conditions of lower amphibolite and greenschist, facies.

East of the Western Craton, the Cree Lake Zone represents a second subdivision where the Archean craton has been reactivated. Here extensive anatexis of the older metamorphic rocks has produced a zone of plutonic granitoid



FIG. 2: MAJOR LITHOSTRUCTURAL SUBDIVISIONS OF THE SASKATCHEWAN SHIELD. (from Lewry et al. 1978)

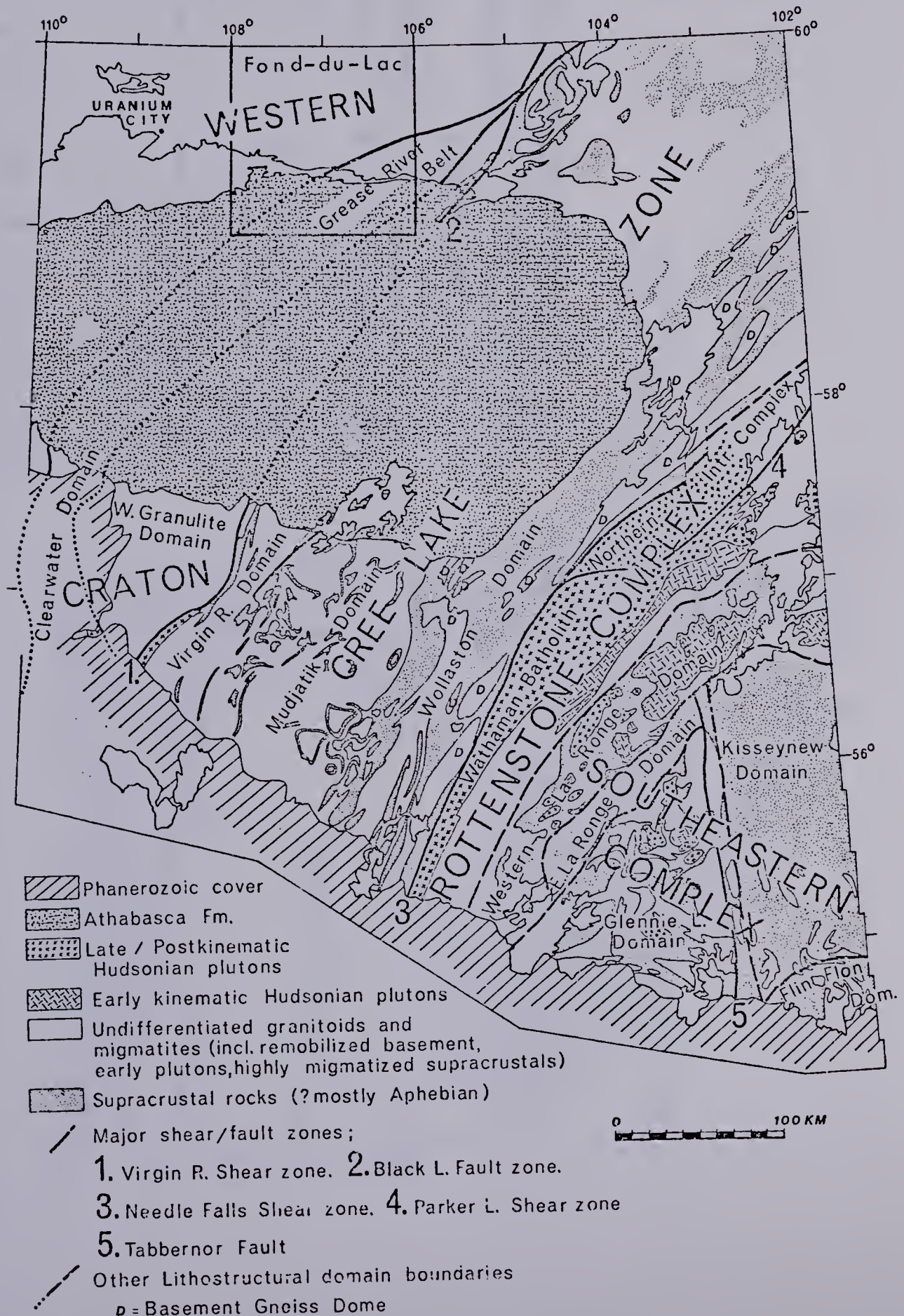
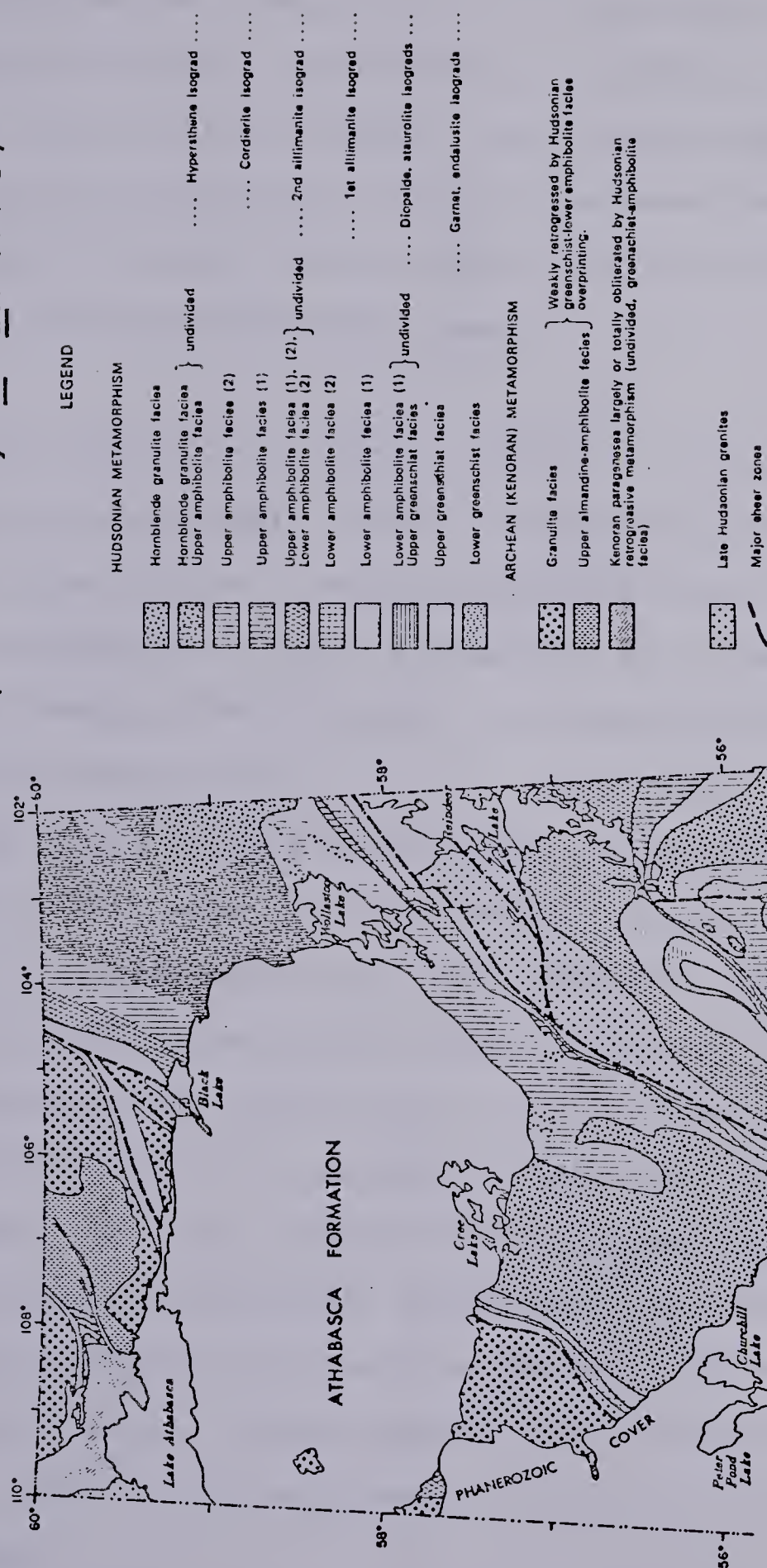






FIG. 3 : METAMORPHIC MAP OF THE SASKATCHEWAN SHIELD  
(from Lewry et al. 1978)





rocks of Hudsonian age with variable macrostructures depending on the pressure (P) and temperature (T) conditions prevailing at the time of melting. Gneissic domes developed in the cooler margins (Virgin River Domain and Wollaston Domain) while migmatitic nappes of basement mobilizate intruded the higher level crystalline rocks in the hotter central portion (Mudjatic Domain).

The Fond-du-Lac district occurs in the northeastern portion of the Western Craton. A simplified geological map of the area (Figure 4) has been adapted from Baer (1968). The Precambrian basement is comprised of Archean Tazin Group metasediments and Proterozoic granodiorite, granite and mylonite assemblages.

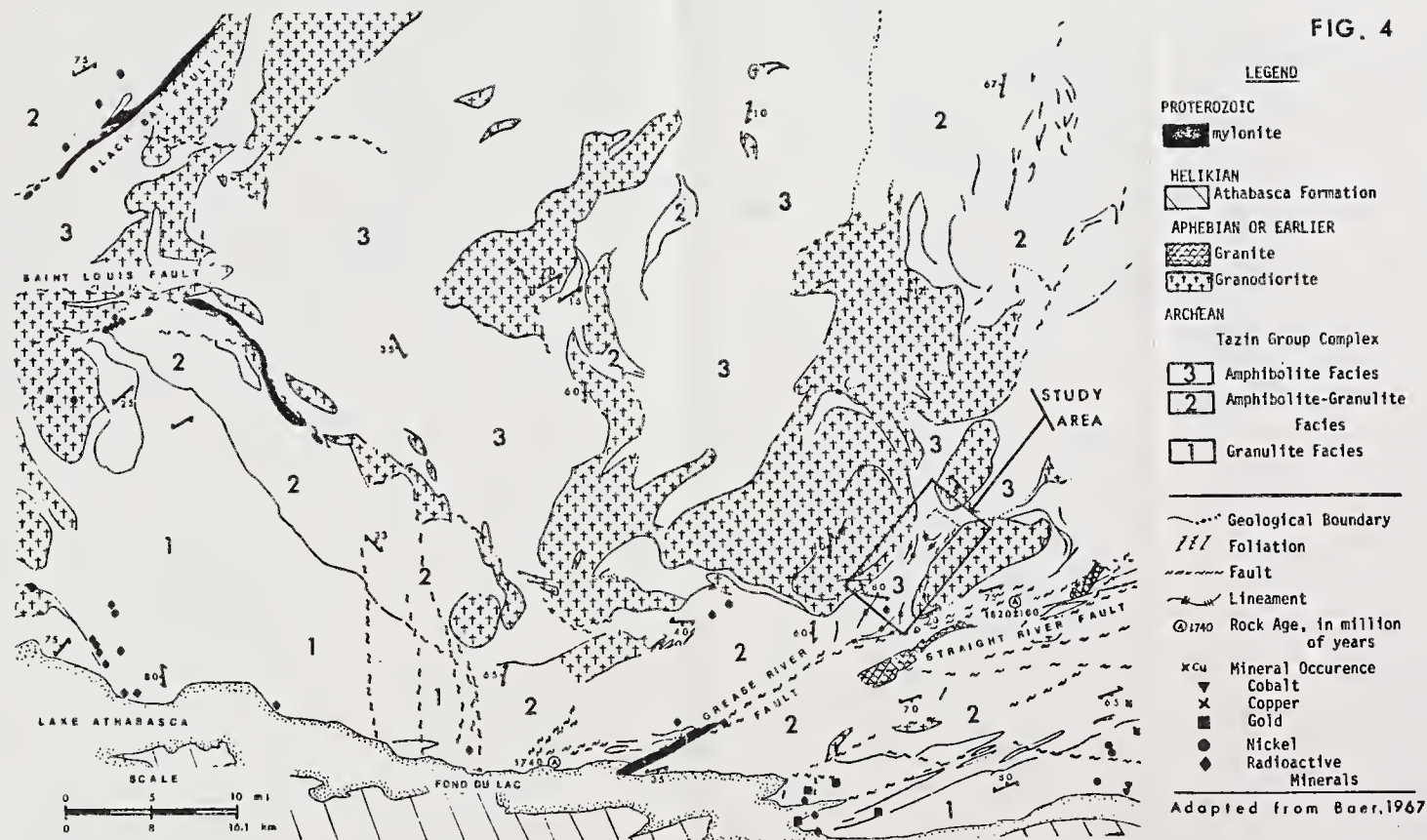
The Tazin Group paragneisses are classified according to Baer (1968) into three metamorphic facies: granulite (unit 1), amphibolite with relic granulite features (unit 2), and amphibolite facies (unit 3). As seen in Figure 4, the pyroxene and garnet bearing granulite gneisses and amphibolites (unit 1) are found immediately north of Lake Athabasca. The lower grade biotite gneisses and amphibole-pyroxene-biotite gneiss (unit 2) exist in a somewhat elongated form between the amphibolite facies and granulite facies. The hornblende and biotite gneisses (unit 3) are found in the northcentral portion of the Fond-du-Lac map sheet.

The granodioritic rocks (unit 4) are predominately





FIG. 4





associated with the amphibolite facies biotite gneisses. They are generally gneissic domes but massive granodioritic rocks have been observed immediately north of the thesis area in the Fontaine Lake area (Figure 4). The contacts between the paragneisses and the granodiorites generally fold around the felsic bodies and are either gradational (Baer, 1968) or extensively migmatized (Colborne et al. 1962; Sassano, 1974). The granodiorites yield Rb-Sr ages of 2360 Ma (Beck's 1966 dates revised by Baadsgaard, per. comm., 1979) which are suggestive that these rocks were not entirely recrystallized during the Hudsonian reworking.

Granitic rocks (unit 5) intrude the granodiorites and Tazin Group gneisses. They are white, coarse-grained, massive rocks containing muscovite and minor biotite. Pegmatitic dykes are frequently associated with the granites and are occasionally tourmaline bearing. Although many of these granitic and pegmatitic rocks have been mapped in the Fond-du-Lac area, only one is of size large enough to appear in Figure 4 (south of the Straight River fault zone). These granites are the youngest crystalline rocks in this part of the Western Craton, giving ages of  $1820 \pm 100$  Ma. (Lowdon, 1961).

Mylonite occurs along the Black Bay, Saint Louis and Straight River fault zones. These major faults are thought to have originated during the late phases of deformation accompanying the emplacement of the granodiorites (Baer, 1968).



### C. Local Geology

The geology of the Grease River area is shown in Figure 5 (adapted from Colborne et al. 1962 and Sassano, 1974). The Tazin Group metasediments are comprised of amphibolite facies biotite and biotite-hornblende bearing paragneisses and paraschists that are sometimes referred to as the Straight River Complex (Sassano, 1974). In this part of the Grease River mobile belt (Beck, 1964), granodioritic domes and lenses intrude the mafic assemblages. Their contact zones are frequently migmatized, feldspathized and are host to uranium mineralization (Sassano, 1974).

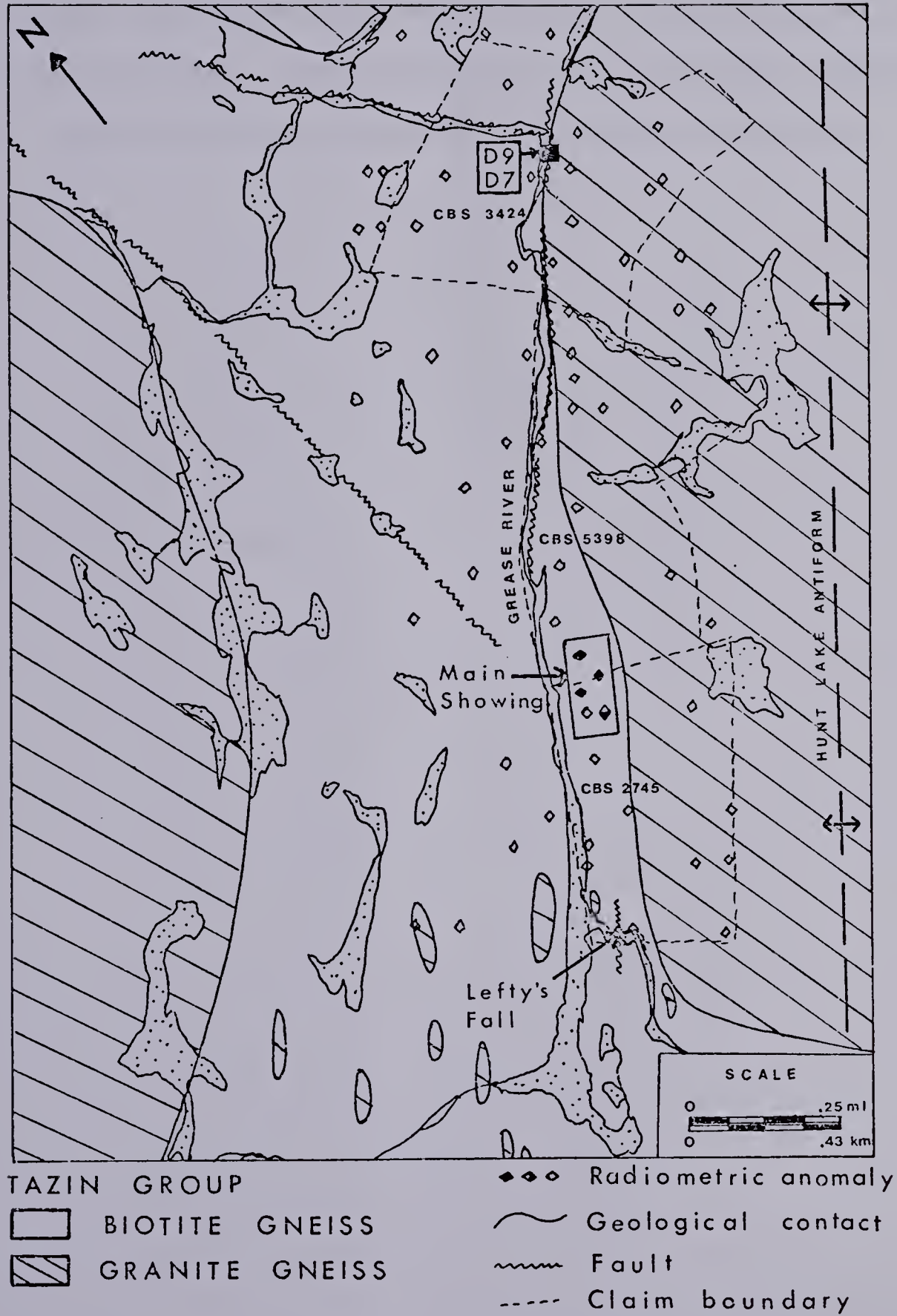
The metasediments in the Grease River linear belt have been formed into tight isoclinal folds that strike to the northeast with nearly vertical dips. Folding of the gneisses is thought to have developed during the emplacement of the granodioritic domes. Southeast of the Grease River, the gneisses occur on the north flank of the Hunt Lake antiform (Figure 5) and thus dip to the northwest. The major faults occurring in the gneisses parallel the edges of the large granodiorite bodies.

Geophysical data for the area includes aeromagnetic maps for the Wiley Lake and Fontaine Lake areas as well as the larger Fond-du-Lac region (Sask. Dept. Miner. Resour. et al. 1962a, 1962b, 1964). In summary, the character of the magnetic response is only slightly disturbed in passing from the leucocratic, granodiorite domes into the biotite





FIG. 5 : GEOLOGICAL MAP OF THE THESIS AREA







gneisses. This is interpreted to mean that the metasediments in the belt are shallow, and are probably underlain by the more felsic rock units surrounding them. The geology of the area supports these interpretations since numerous granitoid lenses outcrop throughout the belt of biotite gneisses (Figure 5).



### III. Petrography and Mesosstructural Analysis of the Grease River Property

The textural and compositional classifications of the rocks occurring in the thesis area are given in sections A and B, respectively. A description of the mineralized rocks is found in section C. Field mesosstructural analysis of the main showing is included in section D. A discussion of the results presented in this chapter is found in section E.

The locations of the outcrops and trenches sampled by the author are indicated in the geological map of the main showing (Map 1). Most of the thirty-four samples collected are examples of the radioactive white pegmatites. Two samples, D9 and D7, obtained by D. Robertson during the 1976 field season, are radioactive pegmatites from the southeast shore of the Grease River in CBS 3424 (Figure 5). They are examples of white pegmatitic rocks believed to be the source of the GSC Skyvan-airborne radioactive anomaly (see Figure 1).

Hand specimen descriptions of the most representative samples collected are listed in Appendix A. The inequigranular nature of the highly migmatized biotite gneisses and some of the pegmatites sometimes makes their textural classification difficult. However, samples with both igneous fabrics and average grain sizes greater than 5 mm are called pegmatites. Granofels is a textural name applied to those samples retaining traces of metamorphic character.



The grain size category used in this thesis is as follows:

fine	<1 mm
medium	1-5 mm
coarse	5-30 mm
very coarse	>30 mm

## A. Textural Classification of the Rocks

Peripheral to the migmatized zone at the main showing, the metasediments are thinly to coarsely banded biotite gneisses. The thinly layered gneisses are often higher in biotite content, fine grained and nearly schistose in places. The more coarsely banded gneisses appear to be lighter in colour and less mafic (Plate 3B). Due to extensive weathering (or alteration) the gneisses flanking the main showing are a rusty colour.

From field observation and hand specimen examination, the gneisses show only one metamorphic orientation which is defined by the parallel arrangement of biotite grains and the gneissic layering composed of dark mafic and light felsic bands. The compositional layers are uniform in width, rarely greater than 3 cm thick, and in places, continuous for the length of the outcrop (Plates 2D, 3D). The gneisses have a nearly uniform grain size, lack conformable pegmatitic layers and are devoid of porphyroblasts. Exceptions are exemplified by samples 2 and 4 which contain garnet porphyroblasts ranging up to 4 mm in diameter. The garnets are inferred to be of post-kinematic origin (Spry,





1969; Vernon, 1976) or formed during the intrusion of the white pegmatites. Folding, faulting and cross-cutting by pegmatitic stringers as seen in Plates 2D and 3A, are uncommon features of the unmigmatized biotite gneisses.

The migmatized biotite gneisses are texturally inhomogeneous. Coarse to very coarse grained, conformable felsic layers are mixed with finely laminated biotite-rich gneisses (Plates 4B, 4C, 4F). The fine-grained, thinly banded gneissic to schistose portions are dark grey to black. Their contacts with the pegmatitic feldspar-quartz-(biotite) bands are either sharp (Plate 4F) or gradational (Plate 4B, 4C), depending on the degree of biotite recrystallization. Fine-grained, leucocratic bands prominent in the unmigmatized biotite gneisses (Plates 2D, 3A, 3B) are not normally found in these rocks.

The development of lenticular and porphyroblastic textures in the pegmatitic layers often disturbs the original metamorphic fabric (Plates 4C, 4E, 4F). Boudinage and non-uniform thickening of compositional bands are frequently accompanied by warping and folding of the layers. Plates 2B, 2C, 2D, 3C, 3D illustrate the usual textures observed in the migmatized gneisses.

Simple, unzoned, white pegmatite lenses and pods showing only igneous-plutonic textures intrude the migmatized gneisses. Two textural varieties of the white pegmatite occur at the main showing: (1) a granular, equidimensional, predominantly coarse-grained structureless



type (Plate 5B, 5D) and (2) a porphyritic feldspar-rich type confined mostly to the central portion of the intrusives (Plate 5A, 5C, 5E). Graphic granite is common in the extremely coarse grained variety.

The white pegmatites outcrop discontinuously in a zone 500 meters long and 60 meters (Map 1). They are intimately associated with the migmatized gneisses and often intrude (Plate 2C), surround or completely engulf (Plates 2B, 3C, 3D) portions of the gneisses. The contacts are frequently irregular due to the corrosion of the gneissic blocks (Plates 2B, 2C, 3C, 3D). Assimilation of the intruding magma and metasedimentary materials is evidenced in Plate 2B, where darker patches remaining in the white pegmatite are continuous with mafic bands in the migmatized gneiss. Sharper contacts are seen in zones where only small pods and stringers of pegmatite intrude.

Gneissic, pink to white pegmatite are exposed at a lower structural level at the main showing (see Map 1). They are medium to coarse grained rocks with granitic and occasionally porphyritic textures. The range in colour from pink to white is caused by an abundance of feldspars that have been iron stained.

The largest granite body outcrops in several places on the west side of the main showing (Plates 1C, 2A). It is estimated to be continuous for 120 meters with its longest dimension in an eastwest direction. Its contact with the migmatized biotites gneiss is often sharp and oblique to the



regional NE strike of the paragneiss.

Although faintly gneissic, these rocks are essentially igneous-plutonic in appearance and lack xenoliths of migmatized gneiss. Thus, according to Mehnert's (1967) macrostructural classification of migmatites, these gneissic granites may be anatexites since no original metamorphic textures and structures are discernible.

## B. Compositional Classification of Rocks at the Main Showing

Most of the rock samples collected in the thesis area have been stained for potash feldspar identification, and subsequently used to determine their modal compositions. Results of the modal analyses calculated for the stained rocks reveals that three compositional varieties are found: granitic (Table 1), quartz-rich (Table 2) and plagioclase-rich (Table 3). All of the highly migmatized gneissic and pegmatitic samples are of granitoid composition (Figure 6) according to the classification used by the IUGS Subcommission on the Systematics of Igneous Rocks (1973).

The completely unmigmatized biotite gneisses (portion seen in Plate 4B) are characterized by plagioclase-quartz-biotite. Little K-feldspathization has occurred and biotites remain fine grained in a sharp parallel arrangement. However, where the metasediments have been granitized and migmatized, the K-feldspar content increases sharply resulting in the two-feldspar granitic rocks (Table 1). Increasing potash feldspar content and





Table 1: Modal composition of granitic rocks from the Grease River area.

No.	description	qtz.	K-feld	plag.	bio.	acc.
2	qtz-bio gneiss	45	10		45	
2	K-feld-qtz graphic peg.	27	55	15	3	
3	porphyritic granite	20	35	35	4	
4	porphyroblastic garnet biotite gneiss	20	25	25	25	45
5	porphyritic granite	25	40	15	7	
5	K-feld-qtz peg.	30	50	17	3	
7	feld-qtz granite	30	25	44	1	
8a	zoned white pegmatite	20	38	40	2	
9	plag-bio-K-feld-qtz migmatite	20	15	25	40	
10	feld-qtz-bio granite	25	20	40	15	
13	K-feld-qtz-plag migmatite	25	70	3	2	
17	feld-qtz-bio pink migmatite	30	30	30	10	
18	plag-K-feld qtz-bio pink peg.	30	30	34	5	41
20	feld-qtz porphyrite peg.	36	45	15	4	
22	feld-qtz-bio gneiss	25	27	38	10	
25	K-feld-qtz alkali granite peg.	35	62	1	2	
26	K-feld-qtz alkali granite peg.	25	62	3	10	
28	feld-qtz-bio granite	25	35	35	5	
29	K-feld-qtz-bio alkali granite mig.	30	53	4	13	
30	feld-qtz-bio granite mig.	35	30	30	5	
32	feld-qtz granitic granofels	35	34	30	1	





Table 2: Modal composition of quartz-rich rocks from the Grease River area.

No.	description	qtz.	K-feld	plag.	bio.	acc.
6	qtz-plag granitoid granofels	70	3	26	1	<1
12	qtz - plag. quartzolite peg.	80	1	7	10	<1
15	qtz-plag-granitoid mig.	77	2	18	3	
21	qtz-K-feld-bio granitoid granofels	65	25	3	7	
24	qtz-feld-bio granitoid peg.	55	25	10	10	

Table 3: Modal composition of trondhjemitic rocks from the Grease River area.

No.	description	qtz.	K-feld	plag.	bio.	acc.
1	plag-qtz-bio pegmatite	10	<1	70	3	
3	plag-qtz-bio migmatite	40	1	54	5	
6	plag-qtz-bio granofel	45	3	50	2	<1
8	plag-qtz-bio gneiss	25		25	40	
10	plag-qtz pegmatite	33	7	55	5	
14	plag-qtz-bio granofel	44	1	45	10	
17a	plag-qtz-bio gneiss	18	5	70	7	
27	plag-qtz-bio migmatite	30		50	20	
31	plag-qtz granofel	28	1	70	1	







average grain size are evidenced even in rocks where metamorphic textures still predominate (Plate 4A). In areas where the felsic mineral constituents have migrated out of the gneissic bands (Plates 4C, 4F) nearly coarse grained recrystallized biotite plates and books remain in sub-parallel orientation. Aplitic to micro-granitic plagioclase + quartz + K-feldspar lenses often separate the biotite-rich bands from the pegmatitic plagioclase + quartz + K-feldspar zones (Plates 4C, 4E, 4F).

The white pegmatites are mainly grouped into three rock types, defined here in order of increasing K-feldspar content: tonalite, granite and alkali-feldspar granite. The compositional varieties are intimately mixed in most outcrops, in gradations determined primarily by textural differences. Because of their low mafic contents (generally less than 10 percent biotite) and holocrystalline-granular plutonic textures, the alkali-feldspar granite pegmatites and the plagioclase rich 'tonalite' type pegmatites shall be referred to as alaskites and trondhjemites, respectively.

The trondhjemite pegmatites are often mixed with the two-feldspar granites. A common textural feature which accompanies the K-feldspathization of the plagioclase-rich pegmatites, is the corrosion of the plagioclase grains. In the trondhjemites, the predominately subhedral white plagioclases form sharp boundaries with the surrounding light grey quartz while in the granites, smaller and less well defined anhedral plagioclases occur within or adjacent





to K-feldspar blasts (Plate 5B).

The alaskite pegmatite samples 2, 25 and 26 (see Table 1 and Figure 6) are comprised almost entirely of porphyritic K-feldspar with quartz in graphic granite intergrowth (Plate 4B, 5A). The potash-feldspar enriched zones occasionally border the trondhjemitic zones (Plate 4B) but are more commonly developed in the two-feldspar granite portions of the pegmatites. Not all of the alkali-feldspar rocks are pegmatitic. Some of the finer-grained aplitic and granitic textural types have a majority of K-rich rather than Na-rich feldspars. Two examples are sample 13, a very faintly gneissic leucocratic rock and sample 29, a biotite-rich granofels.

The quartz-rich granitoids and quartzolite samples (see Table 2 and Figure 6) contain from 55 to 80 percent quartz and less than 10 percent biotite. The quartz is colourless to very dark grey, frequently clear and free of inclusions and often the last phase to crystallize. In these extensively silicified rocks, the quartz corrodes all of the essential feldspar and biotite silicate minerals. Whether plagioclase or potash feldspar predominate, the textural features are the same: rounded feldspars are surrounded by quartz. The feldspars may be white but are usually reddish due to iron staining (samples 6, 15, 24). Both plutonic and gneissic textures have been observed in the moderately silicified granitoids (Plates 5C, 5D, 6C, 7B).



### C. Description of the Mineralized Rocks

The more radioactive samples (6, 12, 14, 15, 16, 21, 24, 27, 29, 30, 32, 34, D9) studied by the author are the white pegmatites and migmatites. The radioactivity is concentrated in the quartz-rich (Plates 5C, 5D, 6C, 7B) and the trondhjemite (Plates 5E, 6B, 7D) compositional varieties. Occasionally, the two-feldspar granite pegmatites contain scattered mineralization. However, the alaskite or alkali-feldspar granite pegmatites are rarely radioactive.

The radioactivity is produced by (1) primary U and Th opaques, (2) yellow secondary U<sup>6</sup> mineralization and (3) large, dark coloured zircons readily observed in hand specimens 6 and 12. The secondary mineralization frequently coats rock samples already containing an abundance of the primary ore minerals, but is also sometimes found on pegmatite samples barren of the highly radioactive opaques (samples 1, 3, 6).

Uraninite is the principal ore mineral in the pegmatites found in the Grease River area. Its presence was confirmed through powder x-ray diffractometry, chemical tests and radioluxography (Dooley, 1977). In the pegmatites and granofels, isolated uraninite grains may be scattered throughout the sample, or, are more commonly associated with large blocks of biotite (Plates 5C, 5E, 7B, 7D) or biotite-rich bands (Plates 6B, 6C, 6D, 7A, 7C). In the migmatites, occasional uraninite grains will occur in the coarser-grained quartz-feldspar portions of the rock. In the



case of samples 24 and D9, it is possible that isolated uraninite grains form along lineaments or fine fractures (in Plate 7B, the arrows point in the direction of the suggested lineament).

The biotite gneisses and the finer-grained K-feldspathized and folded biotite gneisses (Plate 4A, 4G) are essentially unmineralized. With even prolonged exposure times of up to 36 hours to the radioluxography film, these samples show no presence of radioactive grains. This observation is confirmed by field examination and radiometric survey results obtained on the unmigmatized gneisses. In the field, the biotite gneisses are never seen with secondary yellow uranyl mineralization nor do they host any of the radiometric anomalies discovered in the thesis area.

#### D. Mesosstructural Analysis

The most prominent structural trend in the thesis area is produced by the biotite gneisses which strike NE and dip steeply NW. The structural data accumulated by the author on the in-situ biotite gneiss and the gneissic xenolith blocks incorporated in the white pegmatites appears in Map 2.

Where the metasediments are extensively migmatized and intruded by the white pegmatites, the strikes and dips deviate from the regional trend. Plate 2C exemplifies areas where the structural disturbance is minimal, while Plate 3D illustrates regions where room-size blocks are rotated by





the white pegmatite.

The poles to the foliation planes in the gneisses exposed at the main showing have been plotted and contoured on an equal-area stereogram (Figure 7). Two patterns are apparent from the distribution of poles, namely, a polar concentration and a polar spread. The polar concentration in the SE quadrant likely reflects the regional tight isoclinal folds of the unmigmatized biotite gneisses. The greatest accumulation of poles corresponds to an approximate regional strike of  $40^{\circ}$  and a dip of  $80^{\circ}\text{NW}$ . The spread is likely due to warping and displacement of the biotite gneisses under the force of pegmatite emplacement (Whitten, 1966).

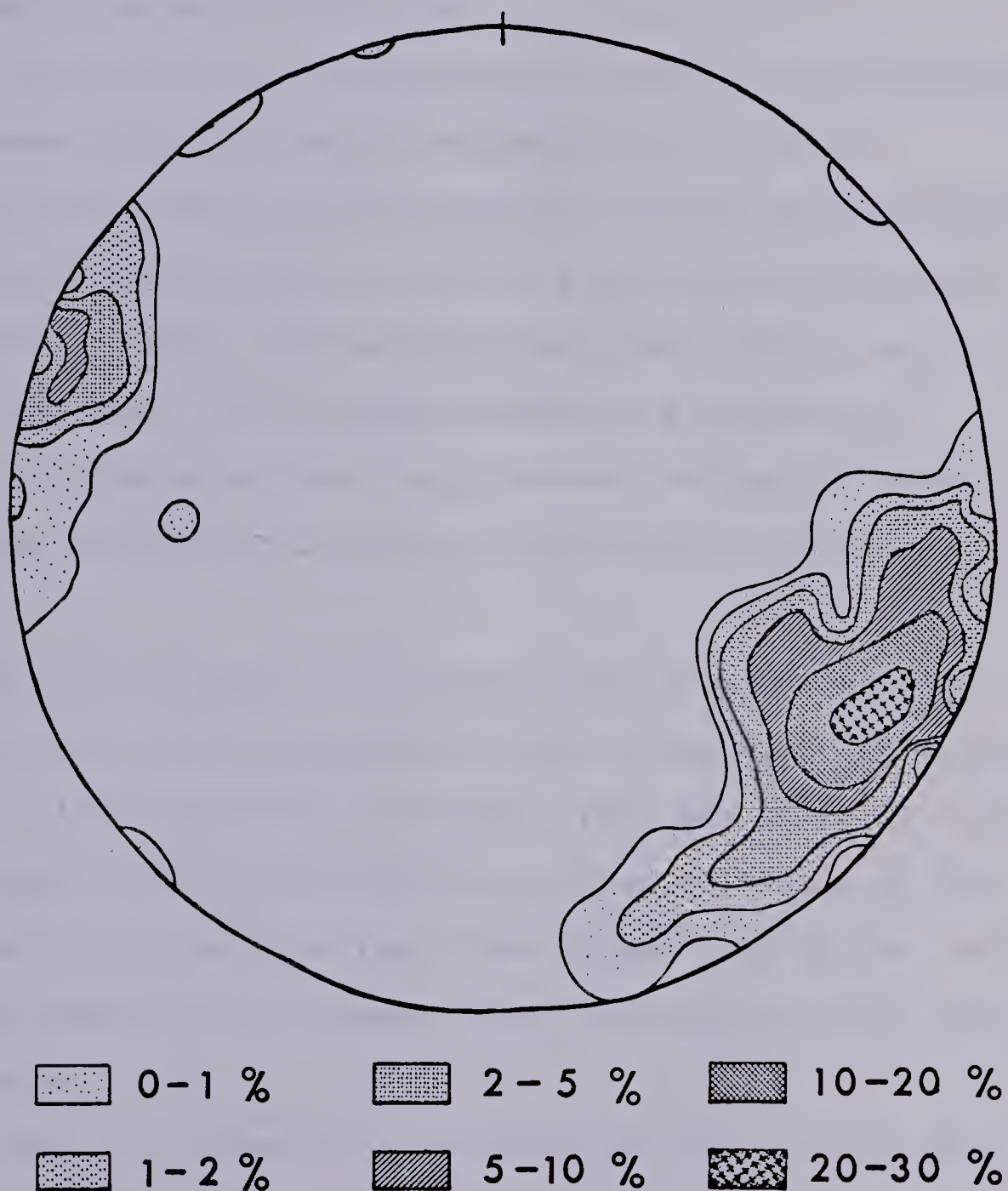
Small scale folds, ptygmatic folds, and drag folding and faulting of the type seen in Plates 2D and 3A are usually associated with stringer pegmatites and therefore, are believed to have formed at the time the biotite gneiss was migmatized and intruded by the white migmatite. Major faulting is also thought to exist at the main showing.

Although these faults have not been mapped systematically, they are likely the cause of a prominent escarpment which frequently borders the southeast side of the main showing. Also, Sassano (1974) and Beesley (1977) refer to extensive faulting primarily in areas where the white pegmatites have been developed to their maximum thickness (ie. near 900 N on the 040 baseline). In one instance, a normal fault with a displacement of approximately 100 meters is thought to exist at the main





FIG. 7 : EQUAL-AREA PROJECTION OF POLES TO FOLIATION PLANES IN BIOTITE GNEISS, MAIN SHOWING, GREASE RIVER AREA





showing (Beesley, 1977). Faulting at the main showing is also likely since major faults occurring on strike appear to the northeast along the Grease River and to the southwest at Lefty's Fall (Figure 5).

### E. Discussion of Chapter III

The biotite-plagioclase-quartz gneisses in the thesis area have been regionally metamorphosed to middle amphibolite facies. The segregation of mineral components seems to have been restricted to a few millimeters since these Tazin Group biotite gneisses remain thinly banded and well foliated. The minerals present are typical of regionally metamorphosed argillaceous sediments (namely, pelites) containing relatively high Mg-Fe content (Bayly, 1968).

The pink pegmatites existed prior to the regional metamorphic event since their faint gneissosity parallels that of the surrounding gneisses. They are probably coeval with grey to pink granodioritic lenses (situated in the metasediments north of the Grease River) and larger gneissic blocks bordering the Grease River metamorphic belt (see Figure 5).

The white pegmatites of trondhjemite, granite and alaskite composition are evidence of one major igneous event and differ only according to the extent to which they have been affected by late-phase K-metasomatism. The potassium-rich metasomatizing solutions have transformed



nearly all the plagioclase-quartz-biotite trondhjemite rocks into the two-feldspar and alkali feldspar granites. It is suggested that the metasomatizing solutions permeated some portions of the felsic rocks more thoroughly than others, thereby producing the three compositional varieties.

According to Augustithis (1973), these results could be due to (1) the impenetrability of the potassium-rich solutions due to consolidation of the initial plagioclase-quartz-biotite magma or (2) an insufficient quantity of potassium to K-feldspathize all the rocks.

High temperatures and pressures at the time of emplacement caused the biotite gneisses to melt (anatexis) or be thermally metamorphosed. Temperatures in the order of 600°C to 750°C were needed to melt the felsic constituents (metatexis) and eventually the biotite fraction (diatexis) (Mehnert, 1968, 1973; Winkler, 1974). With temperatures falling below those required for melting, the biotite gneisses were thermally metamorphosed to the upper amphibolite facies with the development of almandine garnets. The garnet porphyroblasts are found in the biotite-rich gneisses (samples 2, 4, 9) and are clearly of post-kinematic origin since they do not disturb the regional metamorphic foliation (Whitten, 1966).





#### **IV. Petrology, Petrogenesis and Oxygen Isotopes of the Grease River Property**

In part A, results of the petrological microscope study on the gneisses and pegmatites occurring in the Grease River area are presented. In part B, mineral and textural relationships as established from field, petrological and heavy mineral examinations will be discussed in regards to the petrogenesis of the thesis area. Oxygen stable isotope mineral analysis, results and interpretations obtained on five rock samples from the Grease River property are included in part C.

##### **A. Petrological Examination**

Optical, radioluxcgraphy and K-feldspar staining techniques have been used to identify minerals in the petrographic thin sections. The results include descriptions of the essential, varietal, accessory and secondary minerals common to each rock type. The accessory heavy minerals are listed in Appendix B. Since thin-section modal analyses have not been determined due to the coarseness and inhomogeneity exhibited in most samples, the reader is referred to the hand-sample modal compositions presented in Chapter III.

Identification of the plagioclase feldspars has often been problematic. In the coarse grained samples, here the low frequency of plagioclases, coupled with the occurrence of either untwinned or severely altered varieties, has made positive identification difficult.



## Biotite Gneiss

Plagioclase feldspars form up to 50 percent of the mineral constituents in the ungranitized fine-grained gneisses. They are common as untwinned, subhedral, equidimensional grains rarely exceeding 2 mm in length. Only albite twins are developed, giving a compositional range from albite to oligoclase. In places, the plagioclases are slightly altered.

Anhedral, nearly equidimensional quartz grains are closely associated with plagioclases. Although, frequently strained and occasionally recrystallized, the quartz boundaries are usually sharp.

Euhedral biotite books, plates and flakes averaging 1.5 mm long are rarely undulosed and are distinctly free of corrosion and alteration, especially rarely to chlorite. They are strongly pleochroic, with the colours ranging from brownish yellow to reddish brown.

Muscovite, where present, is always associated with biotite and forms as elongated euhedral grains likely pseudomorphic after the biotite. The muscovite grains are weakly pleochroic from colourless to pale yellow.

The accessory minerals found in biotite gneiss are given in Appendix B. Zircon, apatite and iron opaques are the most common, with epidote and garnet found locally, and uraninite occurring rarely.

The zircons are small, subhedral, slightly elongated colourless grains with high relief. They are usually free of



inclusions and zoning but believed to contain small amounts of radioactive elements since they have produced dark haloes in the biotites in which they are found. Low first order grey interference colours are suggestive of a metamict state.

Apatite is characterized by moderately high relief, bright white colour, and first order grey interference colour. The slightly elongated, bipyramid unzoned grains are often slightly rounded with partially corroded edges and are found in the plagioclase-quartz bands.

Isolated cubic iron opaques up to .05 mm in diameter and relatively free from alteration, are usually found with unaltered biotites. However, with the initial grantization and folding of the biotite gneisses, irregular shaped blebs and disseminations of altered iron opaques are very closely mixed with corroded biotites.

### Two-Feldspar Granites

Here plagioclases are virtually always equigranular, anhedral grains averaging 4 mm in diameter. When not completely altered, albite twins are visible in most grains, the composition of the plagioclases lie in the albite to oligoclase range. Occasional Carlsbad twins and rarer Perthite twins occur in the albite twinned grains. The alteration to clay minerals, sericite, muscovite and epidote is usually extensive. Twin plane and patch type replacement antiperthite is sometimes accompanied by albitization of the plagioclase rims.





Poikilolitic, subhedral to anhedral microcline blasts often enclose relict biotite, plagioclase, quartz, zircon and uraninite grains. Less frequently, small microcline grains are found restricted to the interstitial boundaries. The grid-twinned K-feldspar is low in relief, white in transmitted light and commonly fresh in appearance, although locally secondary muscovite will develop (sample 16). When vein, flame and patch microscopic perthites are present, they invade the grid-twinned portions while string and stringlet cryptocrystalline perthites are commonly linked to the untwinned portions of the microcline blasts.

Myrmekite, consisting of parallel and radiating quartz and plagioclase intergrowths is abundant in the pegmatites and coarser grained migmatized gneisses. It is bounded by fresh microcline and extensively altered plagioclase grains. The growths are often rounded, slightly elongated and protruding into the plagioclase.

Equidimensional or slightly elongated quartz grains are found between the larger feldspar grains. The quartz is usually strained and frequently recrystallized with sutured boundaries, resulting in the development of seriated or amoeboid textures.

Corroded and altered biotite stringers and flakes have strong pleochroic colours from either yellow to reddish brown to black or pale yellow to greenish black. Common alteration minerals are muscovite, epidote, chlorite bleached biotite, iron opaques and probably sphene.





Undulosed and kinked biotites are not uncommon. Frequently visible within biotite grains, small darkened areas are caused by radioactive decay of minute grains and uraninite inclusions.

Muscovite patches and rarely euhedral grains develop from the feldspars and biotite. Although muscovite is slightly pleochroic from colourless to pale yellow, it is often confused with epidote since optical examination is impossible on the smaller grains.

The extent of epidotization is always significantly less than muscovitization of biotite. Euhedral epidote grains with moderate relief are usually colourless or pale yellow. Twinned stubby crystals with parallel extinction show second order blue interference colours.

The accessory minerals are more abundant and varied in the granitic rocks than in the biotite gneisses (Appendix B). Zircon, apatite, sphene, uraninite and Fe-opaques are common while allanite and garnet are found locally.

Large (up to 2 mm long), zoned, rounded zircons often containing zircon cores or opaque inclusions are found in most samples (Plate 10F). These grey and light brown coloured zircons with high relief are metamict and filled with microfractures.

Apatite grains are small, white, euhedral slightly rounded dipyrramids often contained as inclusions in quartz grains.

Cubic grains of uraninites and their reaction rims are



found either enclosed in plagioclase, quartz and microcline or bordering biotite grains. Red and yellow coloured stains lining cracks and crystal boundaries adjacent to the commonly corroded and altered radioactive pseudomorphs after uraninite, are evidence that the granitic rocks have likely had corroding fluids passing through them. Radioluxographic photographs of the two-feldspar granite samples (Plate 8-18, 30, 32, 34) shows the nature of disseminated, low-grade radioactivity caused by remobilization.

Allanite, a calcium cerium epidote found in only three thin-sections (16,17,18), is characterized by its very high relief, euhedral hexagonal outline in cross section and has a slight elongation with parallel extinction. The typical appearance of the deep brownish-yellow coloured and weakly anisotropic mineral is seen in Plates 9C and 9D.

Euhedral, wedge-shaped sphene with high relief is always found within biotite grains. Colourless, or light brown in thin section, these grains rarely go to extinction under crossed nicols.

#### Alaskite

Grid-twinned microcline, the major feldspar in the alkali-granite rocks, is never found with myrmekite. String, vein, flame and bleb perthite of albite composition invades most of the K-feldspar blasts which are in graphic granite intergrowth with quartz. The slight alteration of some microcline grains is linked to the cross-cutting perthites of albite composition.



Quartz forms almost invariably as large anhedral undulosed grains and is locally granulated between microcline blasts.

Corroded and intensely chloritized biotite grains up to 7 mm long and 4 mm wide border microcline blasts.

This rock group contains fewer accessories than the other coarse grained pegmatites and migmatites. Zircon and uraninite exist in sample 29, apatite, epidote and possible sphene in sample 25 while garnet is found in sample 2.

#### Quartz-Rich Granitoid and Quartzolite

Plagioclases are often intensely altered, untwinned, anhedral grains in the albite to oligoclase range and with a biaxial negative sign typical for the plagioclases found in the thesis area.

Fine-grained to blastoid, subhedral to anhedral microclines are occasionally the most abundant feldspar. Bleb and string perthites are developed in K-feldspar xenocrysts remaining in the quartz veins.

Abundant, coarse-grained anhedral quartz is always the last mineral phase to crystallize in these rocks. Associated with corroded plagioclase, microcline and biotite grains, the quartz can be strained but is seldomly recrystallized. Crystal boundaries are sharp and angles at triple point junctions approach those of plutonic rocks. In sample 12, pegmatitic quartz is the most abundant mineral.

Biotite grains usually remain as stringers and books which have evidently been corroded by quartz. They are





usually bleached or extensively altered to chlorite, epidote and muscovite. In sample 24, biotites fresher in appearance and presumably recrystallized, border some of the feldspar xenoliths.

Euhedral muscovite plates 6 mm long are found between quartz grains in sample 12 only. Pleochroic from colourless to pale yellow, with low relief and uniform extinction these grains are thought to be a primary mineral constituent. However, smaller less perfectly formed muscovite grains in sample 12 are likely pseudomorphic after biotite.

Zircon, apatite, uraninite, molybdenite and iron opaques are commonly associated together in feldspar-biotite xenoliths surrounded by unstrained quartz. Plate 9B shows part of an elongated xenolith containing a large, zoned zircon, which extends off the picture to the right, and is intergrown with highly altered and cracked, cubic uraninite grains 1 mm wide.

#### Trondhjemite

Plagioclases are the principal feldspar in these rocks. They are of oligoclase composition with biaxial negative sign. The plagioclases are commonly albite twinned, euhedral to anhedral grains that are free of alteration and antiperthitization.

Small corroded microclines are found as xenocrysts or parts of xenoliths surrounded by a plagioclase-quartz matrix.

Large anhedral quartz grains are often strained but



rarely sutured or granulated.

Two generations of biotite are apparent in these rocks. Older chloritized biotite stringers frequently border xenoliths found in samples 8 and 10 (Plate 11). Younger or recrystallized biotites found in samples 14 and D9 (Plates 9G, 9H, 12A, 12C and 12G) are recognized by their euhedral outlines.

Muscovite may appear following the alteration of biotite but most often it is of primary origin. In the latter case, euhedral muscovite plates are found with unaltered biotite (samples 14 and D9), but as seen in Plates 12F and 12G, they appear to be younger than the associated micas.

Zircon, uraninite and iron opaques are the most common accessory minerals in these plagioclase-quartz-biotite rocks.

Two zircon populations are observed in these rocks. Larger zoned and cracked metamict zircons are frequently enclosed in biotite or later forming quartz (Plates 9A, 9G). An abundance of small, unzoned zircons associated with uraninite and fresh biotite are distinctive in samples 14 and D9 (Plates 9H, 12G, 12H).

Uraninite crystals are often larger (up to 1.0 mm), more abundant and less corroded in the trondhjemitic rocks than in the other rock types in the Grease River area. They usually occur with reaction rims (Plates 12B, 12D), but grains are found that are unrimmed (Plates 12A, 12C, 12F,



12H). These uraninites are found with zircon and occasionally, Th-minerals (confirmed by electron microprobe analyses) (see Plate 11).

#### Summary of Petrological Results

The significant mineralogical and textural features observed in the various rocks encountered in the study area are summarized in Table 4. The characteristics of plagioclase, myrmekite, microcline, quartz, biotite and the common secondary minerals are indicated. Points requiring explanation include:

1. Although the extent of plagioclase alteration is easily determined, the secondary products are rarely identified. Saussuritization and sericitization are assumed to be important alterations since occasionally coarser-grained epidote and white mica (sericite) are observed. Clay minerals possibly formed by weathering are also thought to contribute to the cloudiness of the plagioclases.
2. The relative abundance of myrmekite in each sample is determined by comparing the samples with each other.
3. The relative abundance of microcline in each sample reflects the proportion of microcline to total feldspar.

The prominent igneous and metamorphic textures in each thin-section are classified as strongly (3), moderately (2) or weakly (1) developed. Samples containing mild cataclastic





Table 4: Characteristic features of the essential minerals, secondary minerals, and predominant microtextures observed in rocks from the theses area.

rock type, sample no.	plagioclase					myr	microcline			qtz	biotite		sec. min				textures			
	shape	composition	twinning	alteration	antiperthite	abundance	abundance	shape	poikilitic perthite	undulosed	recrystallized	shape	alteration	epidote	chlorite	clay	muscovite	igneous	metamorphic	sheared
biotite gneiss	4 9 13 19	sub an eu,sub	al A ab,ol	A A A	1 1 1 2		1	6l		x x x x		pl,bo pl,pl fl,pl pl				x x x		1 1 1 2	2 3 2 1	
two-feldspar granite	3 5 6 7 11 16 17 18 19 20 22 23 27 28 30 32 33 34	an an an an an sub an an an an an an an eu sub an an	ab,ol A A A.C. ab,ol ol ab ab,ol ol ab ol ab ol an an	A,C A A A A A A A A A A A A A A A	3 3 3 3 3 3 3 3 3 3 3 3 3 3 3 3 3	2 1 2 1 1 3 3 3 3 3 2 1 1 2 2 1	2 3 1 3 2 3 3 3 3 2 2 3 1 2 2 2	an,eu bl an bl bl an bl,an bl bl bl,an bl,an an bl,an an bl bl	x x x x x x x x x x x x x x x x	x x x x x x x x x x x x x x x x	x x x x x x x x x x x x x x x	st st,fl st st st st,bo st fl,pl st st st st st st st	3 3 3 3 3 3 3 1 3 2 3 3 3 3 3 3		x x x x x x x x x x x x x x x		2 2 1 2 2 2 2 2 2 2 2 2 2 2 2 2	1 1 2 1 1 1 1 1 1 1 1 1 1 1 1 1	s s s s s s s s s s s s s s s s	
alkali-feld granite	2 25 26 29						3 3 3 3	bl bl bl bl	x x x x		x x x	st st st st	3 3 3 3		x x x x			3 3 3 3		
granitoid	15 21 24				3 3 3	1	3 2 2	sub sub bl,an			x x x	st st pl	3 3 1	x x x	x x x			3 3 1	2	
quartzolite	12	sub		A	2							st,pl	2	x	x	x		3		
trondhjemite	1 8 10 14 31 D9	sub sub eu sub an sub	ol	A A A A A A	1 1 1 1 0 0		1	an		x x x x x x	x x x x x	bo pl st st pl	3 1 3 3 0	x x x x x	x x x x x	x x x x x		3 3 3 3 3 3		s

Note: relative abundance - 1 - low  
                                   2 - moderate  
                                   3 - high

degree of alteration - 1 - slight  
                                   2 - moderate  
                                   3 - extensive

Symbols used

A - albite twins	C - Carlsbad twins	pl - plate of biotite
ab - albite	eu - euhedral	qtz - quartz
an - anhedral	fl - flakes of biotite	st - stringer of biotite
bla - blastoid	myr - myrmekite	sub - subhedral
bo - books of biotite	ol - oligoclase	



shearing textures are indicated in Table 4.

The biotite gneisses are distinctly free of granitization processes since metamorphic layering is preserved. The presence of only slightly altered plagioclase and biotite coupled with the notable lack of microcline, are further evidence that these rocks have remained essentially undisturbed following crystallization.

The granitized gneisses differ from the biotite gneisses in that they contain extensively altered plagioclases, an abundance of myrmekite and microcline grains and a predominance of strongly chloritized biotite stringers.

The character of the two-feldspar granites is generally igneous with only a few metamorphic features remaining. As seen in Table 4, these rocks are often sheared as evidenced by the granulation of plagioclase, microcline and quartz.

The alkali-feldspar granites are distinguished by having only potassic feldspars. These microcline grains are always perthitic blasts, enclosing quartz and chloritized biotite. Only igneous textures are observed in these coarse-grained pegmatites.

The outstanding characteristic of the granitoid and quartzolite rocks (Table 4) is the abundance of quartz which is observed to corrode plagioclase, microcline and biotite. Pegmatitic appearance is common except in migmatite sample 24.

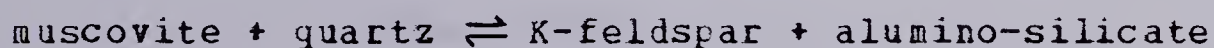
The trondhjemitic rock samples are equally distinctive



for their high concentration of unaltered subhedral plagioclases and nearly complete lack of myrmekite and microcline grains. The shape and extent of alteration of the biotites are variable in this rock group. Their igneous textures are not disturbed by shearing.

### B. Petrogenesis

The biotite gneisses in the Grease River area consist of plagioclase + quartz + biotite + muscovite. According to Winkler (1974), this mineral assemblage is typical of pelites (or clays) metamorphosed to only medium metamorphic grade (see Figure 8a). The mineral reaction which sets the upper limit of medium grade metamorphism is taken from Winkler (1974):



The noticeable lack of anatexis and K-feldspar development in these biotite gneisses further implies that if they formed from prograde metamorphism, high grade conditions could not have prevailed at that time.

According to the metamorphic facies diagram (Figure 8b), the biotite gneisses plot in the lower to medium amphibolite facies range. Although, none of the aluminum silicate minerals such as kyanite, sillimanite, andalusite and staurolite occur in the metapelites, this criteria should not apply for facies determination since these rocks





FIG. 8a : DIAGRAM OF METAMORPHIC GRADE (from Winkler, 1974 ).

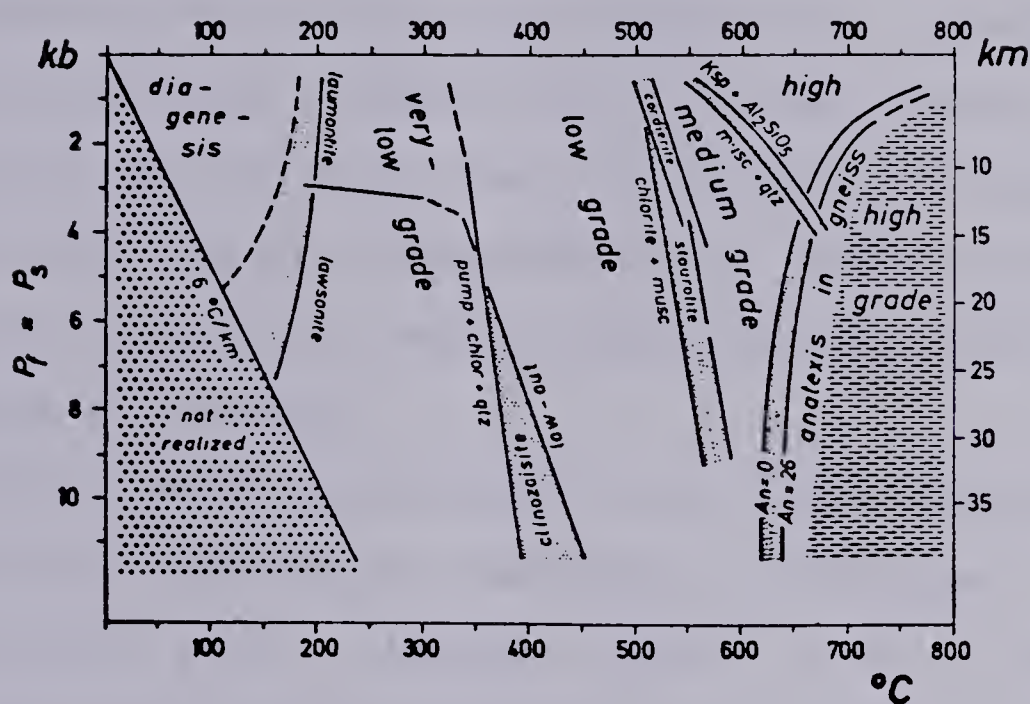
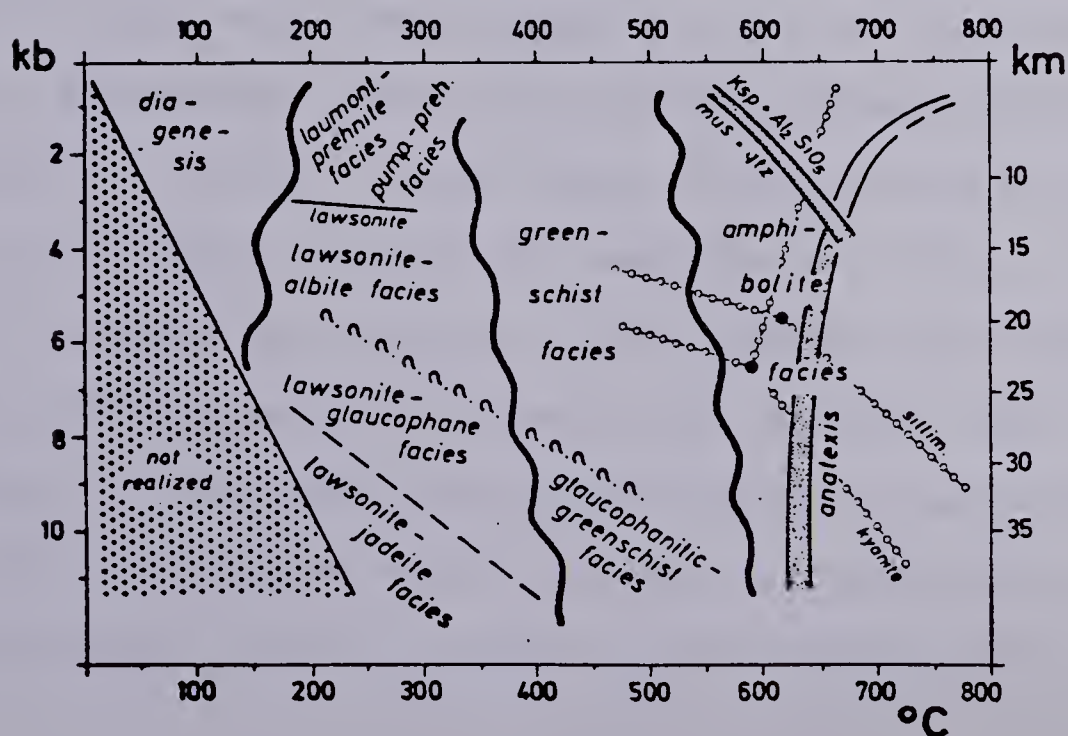


FIG. 8b : DIAGRAM OF METAMORPHIC FACIES ( from Winkler, 1974 ).





are low-Al metasediments.

These interpretations are in agreement with the Grease River mapping by Colborne et al. (1963) and Baer (1968). However, petrological evidences establishing whether the biotite gneisses are a result of amphibolite facies prograde or granulite facies retrograde metamorphism are still lacking. According to Munday (1977) who has studied similar gneisses in the Mudjatic Domain (see Figure 2), these biotite rich rocks are considered to be relict portions of high grade metamorphic amphibolites and granulites subjected to extensive anatexis.

Pink to white pegmatitic granite rocks occurring on the Grease River property are comprised of K-feldspar + plagioclase + quartz + biotite. Figures 8a and 8b show that this assemblage is characteristic of high grade metamorphic rocks in the upper amphibolite facies range.

These pinkish granites have a faint gneissosity that parallels that of the biotite gneisses. This implies that the more felsic rocks were emplaced prior to or during the regional metamorphic event which produced the metapelites. The contact existing between these units implies that a felsic melt formed at depth and ascended in order to intruded the biotite gneisses at the present erosional surface. The distance travelled by the granitic melt is considered to have been significant since it was generated under high metamorphic grade (anatectic) conditions, yet it was consolidated within a zone of only medium grade



metamorphic rocks.

The P,T conditions required for a gneiss to melt are determined by the abundance of low melting minerals and the amount of formation water available at the time (Carmichael et al. 1974; Winkler, 1974). Figure 8a illustrates that for pressures from 6 to 8 kilobars (kb), an average gneiss will commence melting at temperatures ranging from 660 to 625°C, depending on the plagioclase composition. In this case, plagioclase, K-feldspar, quartz, muscovite and biotite will melt once anatexis begins. However, should there be a deficiency of formation water, melting will be delayed until the time that the hydrous minerals, namely, muscovite biotite and hornblende have started melting at temperatures above 700°C (Carmichael et al. 1974).

The source of the pink granitic pegmatites is thought to be similar to that of the biotite gneiss. This is assumed since the overall mineral constituents in each lithology are surprising similar: it is only the mineral proportions which differentiate the two. As mentioned earlier, the Tazin Group basement complex in the area appear to originate from low-Al and high-Fe, Mg, Na, K clays (Bayly, 1968).

The white pegmatites in the Grease River area are composed of plagioclase + K-feldspar + quartz + biotite which developed during three distinct periods of mineral growth. Their crystallization histories have been traced by examining the textural and mineralogical changes that have





occurred with each successive intrusive period.

First, a plagioclase + quartz + biotite assemblage is thought to have crystallized from a silicate melt of trondhjemitic composition. As seen in Table 4, these trondhjemite pegmatites that have not been disturbed by later events are characterized by (1) containing essentially unaltered plagioclases (2) lacking myrmekite and K-feldspar and (3) having igneous-plutonic textures.

In the second intrusive period, K-feldspar + quartz transformed many of the trondhjemitic rocks into the two-feldspar and alkali-feldspar granites. Here the extensive alteration and antiperthitization of the pre-existing plagioclases are related to the appearance of poikilitic microcline blasts and myrmekite intergrowths. The microclines have in turn been perthitized by albite which probably formed from circulating Na-rich solutions generated from the breakdown of plagioclase (Augustithis, 1973).

During the third intrusive phase, hydrothermally crystallized quartz + muscovite produced the quartz-rich granitoid and quartzolite pegmatites. Quartz-veins averaging 2 mm wide cross-cut many of the earlier formed pegmatites and migmatites. These veins appear to be of two origins. First, a dilation type is clearly evident in cases where veins are bounded by sharp edges usually through porphyritic feldspars. Second, a replacement type is suggested since quartz is noticeably lacking in the adjacent wall rocks. Both types were probably derived from a aqueous fluid of



hydrothermal origin.

The white pegmatites in the Grease River area are of syntectonic origin. Only slight tectonic activity was associated with the crystallization of the initial magma as evidenced by the occasional broken plagioclase or kinked biotite in the trondhjemite pegmatites. However, more extensive shearing and alteration occurred during and following the period of K-feldspathization. According to Meyer's et al. (1967) classification, both propylitic and intermediate argillic alteration assemblages developed in the affected rocks. Evidence that shearing of the pegmatites occurred during infiltration of hydrothermal solutions is observed in the two-feldspar granitic pegmatites. Here, even the microcline blasts can be rounded in the slightly mylonitized rocks. Also, the presence of myrmekite and epidote are suggestive of tectonism since they are commonly developed in regions that have undergone considerable shearing (Augustithis, 1973).

The P,T conditions existing during the development of the pegmatites probably decreased from the time of intrusion of the trondhjemitic pegmatites until the hydrothermal period of quartz enrichment. According to Winkler (1974), melts of plagioclase + quartz + biotite composition are formed at temperatures between 686 and 730°C at respective pressures of 7 to 2 kb. However, at the time of intrusion, lower temperatures are believed to have existed since the melt would have cooled in moving upwards through the biotite



gneisses. However, according to Figure 8, temperatures higher than 620°C are implied since locally, portions of the biotite gneiss have been melted or thermally metamorphosed to the almandine garnet isograd.

K-metasomatism likely occurred once the pegmatitic rocks started cooling. Winkler (1974) suggests that microcline + quartz assemblages developed in this period crystallize out at temperatures below 685°C. In restricted zones of the pegmatites, graphic granite intergrowths developed in the alaskite pegmatites have resulted from eutectic crystallization of blastic microcline and quartz.

The overburden pressures that existed when the white pegmatites developed were considerably lower than those during the regional metamorphic formation of the gneisses. Several factors implying this are:

1. no gneissosity occurs in the white pegmatites.
2. the fracturing and shearing of the white pegmatites are typical of rocks emplaced in shallow environments.

Deeper portions of the underlying pink to white granite gneisses are thought to be the source of the white pegmatites (see Map 1). Proofs that suggest the trondhjemitic melt formed from relatively local melting of the felsic gneisses, rather than having developed from mantle or extremely deep crustal sources are listed here:

1. the relatively small size of the pegmatites are typical of anatectic melts developed locally.





2. the discontinuous nature of the white pegmatites in a narrow zone approximately 500 m long suggest that the source of the anomalous pegmatites extends for at least an equal distance in the subsurface.
3. the underlying pink leucocratic gneisses show evidence of having been extensively altered and sheared.
4. the mineral constituents in both the granite gneiss and white pegmatite are comparable to each other.
5. anatexis of the felsic gneisses could well have proceeded at P,T conditions that would not have extensively recrystallized the biotite gneisses.

### C. Oxygen Stable Isotope Analysis

The mineral oxygen isotope analyses of white pegmatite samples from the Grease River area were conducted by Dr. K. Hattori at the University of Alberta. The bromine penta-fluoride extraction technique followed has been described by Clayton et al. 1963. This method of extracting oxygen is suitable for silicate and oxide minerals. Although a brief description of the methodology employed shall be given, the reader is referred to the original paper for more detail.

#### Analytical Procedures

Purified biotite, quartz, K-feldspar, plagioclase and zircon were obtained by heavy liquid separation. Powdered silicate samples weighing approximately 20 mg were reacted



with BrF<sub>5</sub> in nickel reaction vessels at temperatures close to 600°C for 14 hours. The oxygen gas liberated was converted to CO<sub>2</sub> over heated carbon.

Measurement of the oxygen isotopic abundances were made with a 602C Micromass mass spectrometer. The O<sup>18</sup>/O<sup>16</sup> ratios (R) calculated for the mineral samples and the standard were expressed as follows:

$$\delta O^{18} = \left[ \frac{R \text{ sample}}{R \text{ standard}} - 1 \right] 1000$$

where  $\delta$  = the permil deviation of the sample from that of the standard.

The standard used was the SMOW scale defined by Craig, 1961.

### Geological Applications of Oxygen Stable Isotope Analyses

Three stable isotopes of oxygen exist in nature, O<sup>16</sup>, O<sup>17</sup> and O<sup>18</sup> known relative proportions in oxygen air at 99.76, .0374 and .2039, respectively (Taylor, 1967). Because of their slightly different physio-chemical properties, natural geological processes cause the oxygen isotopic abundances to deviate from those quoted above.

Oxygen isotope studies of geological materials involve obtaining and comparing the O<sup>16</sup>, O<sup>18</sup> and  $\delta O^{18}$  values (Taylor, 1968; Taylor et al. 1962). Igneous, metamorphic and sedimentary rock types each have a characteristic range of whole rock and mineral oxygen isotopic compositions. Varied



isotopic compositions can result from the assimilation of rock masses with differing isotope values. Similarly, fluids originating from these geological formations have distinctive  $O^{18}/O^{16}$  ratios, and are capable of re-equilibrating with other fluids and rock masses.

The objectives for determining the mineral  $\delta O^{18}$  compositions of white pegmatites found in the Grease River area are:

1. To establish what igneous petrographic rock type (or source rock) they isotopically resemble.
2. To determine if the white pegmatites formed in equilibrium by comparing the mineral isotopic sequences of each sample analyzed.

### Results

The  $\delta O^{18}$  values for the minerals analyzed are given in Table 5. The minerals analyzed are arranged in order of increasing  $\delta O^{18}$  permil (‰) content: biotite (4.1-4.9 ‰), zircon (5.5-6.4 ‰), plagioclase (7.9-8.0 ‰), k-feldspar (8.5-8.7 ‰), quartz (9.2-10.04 ‰).

The  $\delta O^{18}$  values are plotted in Figure 9. Samples 3 and 30, both white pegmatites of granitic composition have similar biotite, plagioclase, K-feldspar and quartz  $O^{18}/O^{16}$  ratios. The trend of  $\delta O^{18}$  values for biotite and quartz from trondhjemitic pegmatite samples 14 and 27 differ slightly with each other and with the granitic pegmatites. The lowest  $O^{18}/O^{16}$  ratios for quartz occurred in quartzolite sample 12.





Table 5:  $\delta O^{18}$  values in ‰ of minerals from the Grease River area pegmatites and from granitoids of igneous and metamorphic origin.

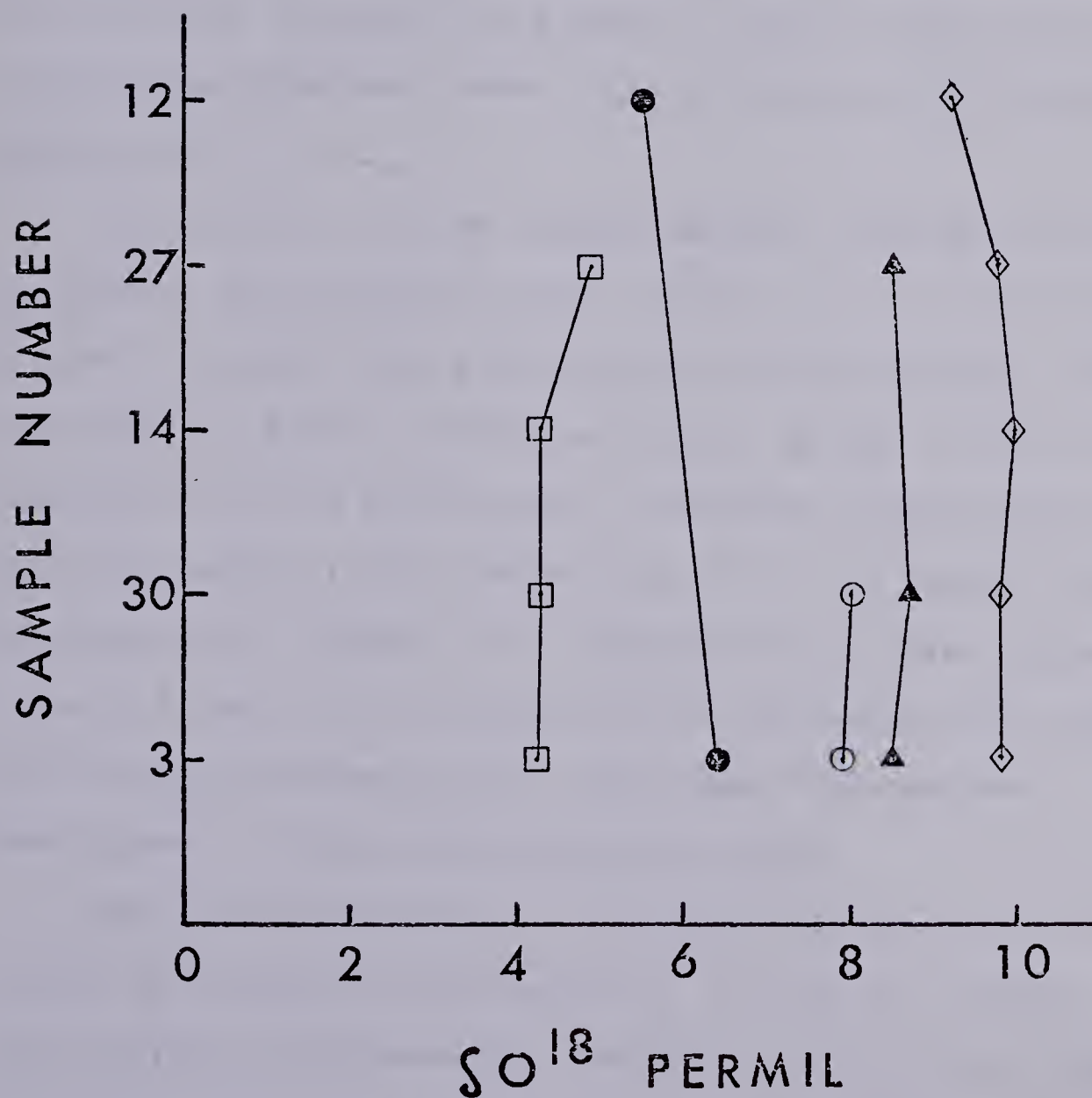
mineral	granite				trondhjemitic	quartz-rich	granitoid range <sup>1</sup> .
	3	30	14	27			
quartz	9.8	9.8	10.0	9.7	9.2	8.9 - 10.3	
microcline	8.5	8.7	n.d. <sup>2</sup>	8.5	n.d.	7.0 - 9.1	
plagioclase	7.9	8.0	n.d.	n.d.	n.d.	6.5 - 9.1	
zircon	6.4	n.d.	n.d.	n.d.	5.5	n.d.	
biotite	4.1, 4.2	4.3	4.3	4.9	n.d.	4.4 - 6.6	

Notes: 1. data from Taylor, 1967. 2. n.d. denotes not determined.



FIG. 9 :  $\delta O^{18}$  MINERAL RESULTS FOR  
PEGMATITES, GREASE RIVER AREA

- |   |             |   |            |
|---|-------------|---|------------|
| □ | biotite     | ▲ | microcline |
| ● | zircon      | ◇ | quartz     |
| ○ | plagioclase |   |            |





## Interpretations of the Results

The mineral  $\delta O^{18}$  value found for all of the samples analyzed fall within the range commonly observed in granitoids and migmatites of igneous and high-grade metamorphic origin (Longstaffe, 1979; Taylor, 1968; Taylor et al. 1962; Viswanathan, 1974). Most of the isotopic results tend towards the low end of the mineral  $\delta O^{18}$  ranges.

Mineral equilibrium is apparent from the sequence of  $O^{18}/O^{16}$  ratios obtained for the five white pegmatite samples analyzed. A progressive enrichment of  $O^{18}$  content in going from biotite to quartz in Figure 9, implies that the mineral assemblages developed under oxygen isotopic equilibrium conditions.

Although all of the results signify pegmatitic-magmatic intrusion, the slightly lower  $O^{18}/O^{16}$  ratio in quartz from sample 12 suggest the possibility of hydrothermal activity. According to Taylor (1967) and Taylor et al. (1979), quartz precipitated from hydrothermal solutions contaminated with meteoric waters ( $\delta O^{18}$  range from -10 to -4 permil) would have lower  $O^{18}$  content as a consequence of lower magmatic values. Indeed, this interpretation correlates with the petrological evidence for a late-stage hydrothermal development of the quartz-enriched rocks.

The same hydrothermal event likely lowered the  $O^{18}/O^{16}$  ratios of biotites from samples 3, 14 and 30. Because of their crystal structure and chemistry, biotites are known to exchange isotopically with formation fluids even in the





hydrothermal range from 200 to 500°C (Taylor, 1967). This suggests that the pegmatites were open systems at the time that quartz precipitating solutions were emplaced. The often severely chloritized biotites observed in the more potassic pegmatites at the main showing support these oxygen isotope results and interpretations.



## V. Geochronology

### A. U-Th-Pb Dating Method

#### Introduction

The choice of the U-Th-Pb method in dating the Grease River rocks was made for two reasons. First, the presence of uranium and thorium bearing minerals in these rocks. Second, because U and Th have long half lives, the U-Th-Pb system would be appropriate for Precambrian research (Baadsgaard, 1964).

The minerals best suited for dating rocks sampled for this study are zircon and uraninite. Zircon is especially useful since it is ubiquitous in both the metamorphic and pegmatitic assemblages. The uraninite grains are not as useful as zircon because they are concentrated only in the pegmatites and the intensely migmatized biotite gneiss.

The composition and crystal structure of zircon and uraninite greatly influence their physiochemical behaviors during geological processes. The chemical and mechanical stabilities of zircon persist until extreme temperatures and pressures are attained (Bibikova, 1977). However, uraninite is disturbed under much less intense temperature and pressure conditions because of the thermodynamic properties of the uranium atom (Langmuir, 1978). The tetravalent ( $U^{+4}$ ) form found in pegmatitic uraninite crystals is readily oxidized to the highly mobile hexavalent ( $U^{+6}$ ) state under slightly oxidizing conditions (Berman, 1957; Grandstaff,



1976).

In districts such as the Grease River area where several metamorphic and igneous events are known to have occurred (Colborne et al. 1963), mineral dating studies will frequently record these events. Zircons tend to date the older magmatic events while uraninites tend to reflect ages of younger events.

### Theory of Radioisotope Dating

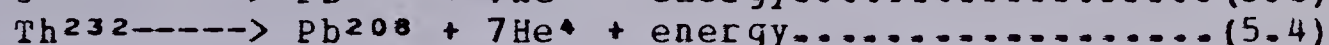
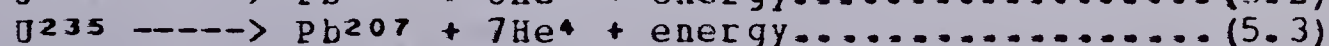
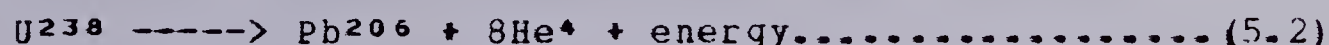
A brief introduction to the theory and practicalities of radioisotopic dating is given here to help the reader understand the analytical procedures used to date the events in the Grease River area. The theory is a brief discussion based on the work by Baadsgaard (1964) and Moorbath (1970).

When a radioactive parent nuclide breaks down to give a daughter nucleide it does so according to the Law of Radioactive Decay

$$N_d = N_p (e^{\lambda t} - 1) \dots \dots \dots (5.1)$$

where  $N_d$  = number of atoms of daughter nuclide  
 $N_p$  = number of atoms of parent nuclide  
 $\lambda$  = decay constant for a particular parent nuclide  
 $t$  = time since formation of the mineral

In the U and Th bearing minerals, three radioactive parents decay via unstable intermediates to give stable radiogenic Pb isotopes plus helium and energy according to the following reactions:



The decay of  $U^{238}$ ,  $U^{235}$  and  $Th^{232}$  atoms proceeds at rates





determined by their decay constants ( $\lambda$ ):

where  $U^{238} = 1.5513 \times 10^{-10} \text{yr}^{-1}$  (Jaffey et al. 1971)  
 $U^{235} = 9.8485 \times 10^{-10} \text{yr}^{-1}$  (Jaffey et al. 1971)  
 $Th^{232} = .4948 \times 10^{-10} \text{yr}^{-1}$  (Le Roux et al. 1963)

The abundances and relative proportions of the parent and daughter nucleides co-existing in mineral samples are obtained through isotopic mass spectrometric analysis. Substitution of the isotope concentrations (in weight percent) and the corresponding decay constants into Eq. 5.1 yields three geologic ages ( $t$ ):

where

$$t_{206} = \frac{1}{\lambda_{U^{238}}} \ln \left[ \frac{Pb^{206}}{U^{238}} + 1 \right] \dots \dots \dots (5.5)$$

$$t_{207} = \frac{1}{\lambda_{U^{235}}} \ln \left[ \frac{Pb^{207}}{U^{235}} + 1 \right] \dots \dots \dots (5.6)$$

$$t_{208} = \frac{1}{\lambda_{Th^{232}}} \ln \left[ \frac{Pb^{208}}{Th^{232}} + 1 \right] \dots \dots \dots (5.7)$$

Since the relative isotopic proportions of natural uranium are known ( $U^{235} / U^{238} = 137.88$ ) and are assumed to have remained constant over geologic time, the ratio of the  $U^{235} / U^{238}$  radioactive decay equations (ie. 5.6/5.5) results in another particularly useful age equivalent to  $t_{207} / t_{206}$ :

$$\frac{Pb^{207}}{Pb^{206}} = \frac{U^{235} (e^{\lambda_{235} t_{207}} - 1)}{137.9 U^{238} (e^{\lambda_{238} t_{206}} - 1)} \dots \dots \dots (5.8)$$

Ideally, a mineral system should not incorporate contaminant daughter atoms at the time of its formation. However, since this is rarely the case, the amount of primordial (contaminant) lead isotopes are determined and



subsequently subtracted from the total isotopic concentrations. This is done by assuming all  $Pb^{204}$ , a non-radiogenic lead isotope, is primordial. Since the natural proportions of  $Pb^{208}$ ,  $Pb^{207}$ ,  $Pb^{206}$ ,  $Pb^{204}$  are known and the amount of  $Pb^{204}$  determined, the concentration of contaminant  $Pb^{208}$ ,  $Pb^{207}$  and  $Pb^{206}$  may be calculated.

Another assumption made in geochronology is that once a geologic system has formed it remains closed (no parent or daughter nuclides may be gained or lost). Plots of daughter / parent ratios for any two decay series such as  $Pb^{206}/U^{238}$ ,  $Pb^{207}/U^{235}$  and  $Pb^{208}/Th^{232}$  showing up the ideal behavior, have been drawn. The most frequently used U-Th-Pb evolution diagram is a Concordia curve of  $Pb^{206}/U^{238}$  versus  $Pb^{207}/U^{235}$  (Wetherill, 1956). However, plots of present day daughter/parent ratios of typical U and Th minerals normally depart from the ideal curve. Such departures are recognized as age discordancies in the specimens analyzed. Theories accounting for the age differences include episodic disturbances (Wetherill, 1956) and diffusion effects (Tilton, 1960).

## B. Analytical Procedures

Samples selected for geochronological study were chosen on the basis of rock type, location in the field and presence of accessory minerals datable with the U-Th-Pb system. The quantity and quality of zircon and uraninite were initially determined by radioluxographic and petrologic



examinations.

The rock samples chosen for dating include samples of biotite gneiss (3B), migmatized biotite gneiss and granofels (11,17,18,32,34), trondhjemite pegmatite (3G, 14, 27), quartz-rich granitoid (15,24) and quartzolite (12).

The chosen samples were processed by methods outlined in Appendix C. Very briefly, the rocks were crushed, separated with heavy liquids, chemically treated to extract U, Th and Pb, and isotopically analyzed.

### C. U-Th-Pb Isotope Results and Mineral Dates

Judging from the U and Pb isotope concentrations in the zircons (Table 6), the samples dated fall into two groups. The biotite gneiss (3B) and pink gneissic pegmatite (17) samples contain less than .06 percent total U and less than .02 percent total Pb. On the other hand, zircons analyzed from the white pegmatites have elevated U and Pb values and more variable isotope compositions. These pegmatitic U-rich zircons contain from .32 to .78 percent total U and .09 to .21 percent total Pb.

The U-Th-Pb isotopic results for uraninite are also listed in Table 6. In both samples analyzed,  $U^{238}$ ,  $U^{235}$  and  $Th^{232}$  values vary inversely to the accumulations of their respective daughter isotopes,  $Pb^{206}$ ,  $Pb^{207}$  and  $Pb^{208}$ . However, the uraninites dated are isotopically dissimilar in that sample 14 contains higher U and Th and lower Pb values than sample 32.





Table 6: U-Th-Pb isotopic results for zircons and uraninites dated

sample no.	Mineral	isotopic concentration (weight percent)				
		U <sup>238</sup>	U <sup>235</sup>	Pb <sup>206</sup>	Pb <sup>207</sup>	Pb <sup>208</sup> Th <sup>232</sup>
3G	zircon	.5474	.0039	.1626	.0196	.0247 n.d. <sup>1</sup>
3B	"	.0476	.0003	.0145	.0020	.0012 n.d.
12	"	.7744	.0056	.1256	.0114	.0099 n.d.
15	"	.3204	.0023	.0738	.0078	.0051 n.d.
17	"	.0569	.0004	.0162	.0022	.0012 n.d.
14	uraninite	62.3334	.4464	7.4982	.6913	.3424 7.7901
32	"	56.6621	.4058	10.7310	1.1841	.3913 7.5382

Note: 1. n.d. denotes not determined.

Table 7: U-Pb, Pb-Pb, Th-Pb dates, Grease River Area, N. Saskatchewan

sample no.	rock type	mineral	ages Ma			
			Pb <sup>206</sup> U <sup>238</sup>	Pb <sup>207</sup> U <sup>235</sup>	Pb <sup>207</sup> Pb <sup>206</sup>	Pb <sup>208</sup> Th <sup>232</sup>
3G	tonalitic pegmatite	zircon	1902	1927	1950	n.d. <sup>1</sup>
3B	biotite gneiss	zircon	1941	2072	2200	n.d.
12	quartzolitic pegmatite	zircon	1107	1224	1430	n.d.
15	granitoid migmatite	zircon	1521	1609	1720	n.d.
17	granitic migmatite	zircon	1829	2001	2180	n.d.
14	tonalitic granofels	uraninite	839	1030	1460	967
32	granitic granofels	uraninite	1276	1494	1800	1138

Note: 1. n.d. denotes not determined.



The U-Th-Pb zircon and uraninite ages are listed in Table 7. The data appears on a  $Pb^{207}/U^{235}$  versus  $Pb^{206}/U^{238}$  concordia curve for zircon and uraninite (Figure 10) as well as on a  $Pb^{208}/Th^{232}$  versus  $Pb^{206}/U^{238}$  evolution curve for uraninite (Figure 11). The U and Th decay constants and uranium atomic ratios used to calculate the ages are as given in the introductory note of Chapter V.

The distribution of points on the concordia plot suggests that the minerals dated fall into two groups. Because of the close proximity of the strongly discordant zircon (12,15) and uraninite (14,32) samples from white pegmatite, petrological evidence has been used to decipher the results. The best fitting lines intercept the concordia curve to give a distinctly older date of 2250 Ma. and two younger dates of 1970 and 1845 Ma.

The two zircon samples yielding the older date are representative of biotite gneiss. Although their  $Pb^{206}/U^{238}$  and  $Pb^{207}/U^{235}$  ages (Table 7) are moderately discordant, their  $Pb^{207}/Pb^{206}$  dates are closer to the ages projected from the concordia plot.

The younger ages (1970 and 1845 Ma) are from the quartz-rich and the quartz-feldspar white pegmatites found in the study area. One nearly concordant zircon (3G) and two highly discordant uraninite samples are interpreted as dating the same event while two zircon samples (12 and 15) date the last igneous event in the mineralized zone.



FIG. 10 : CONCORDIA CURVE FOR ZIRCONS (◊) AND URANINITES (⊙)  
FROM THE GREASE RIVER AREA.

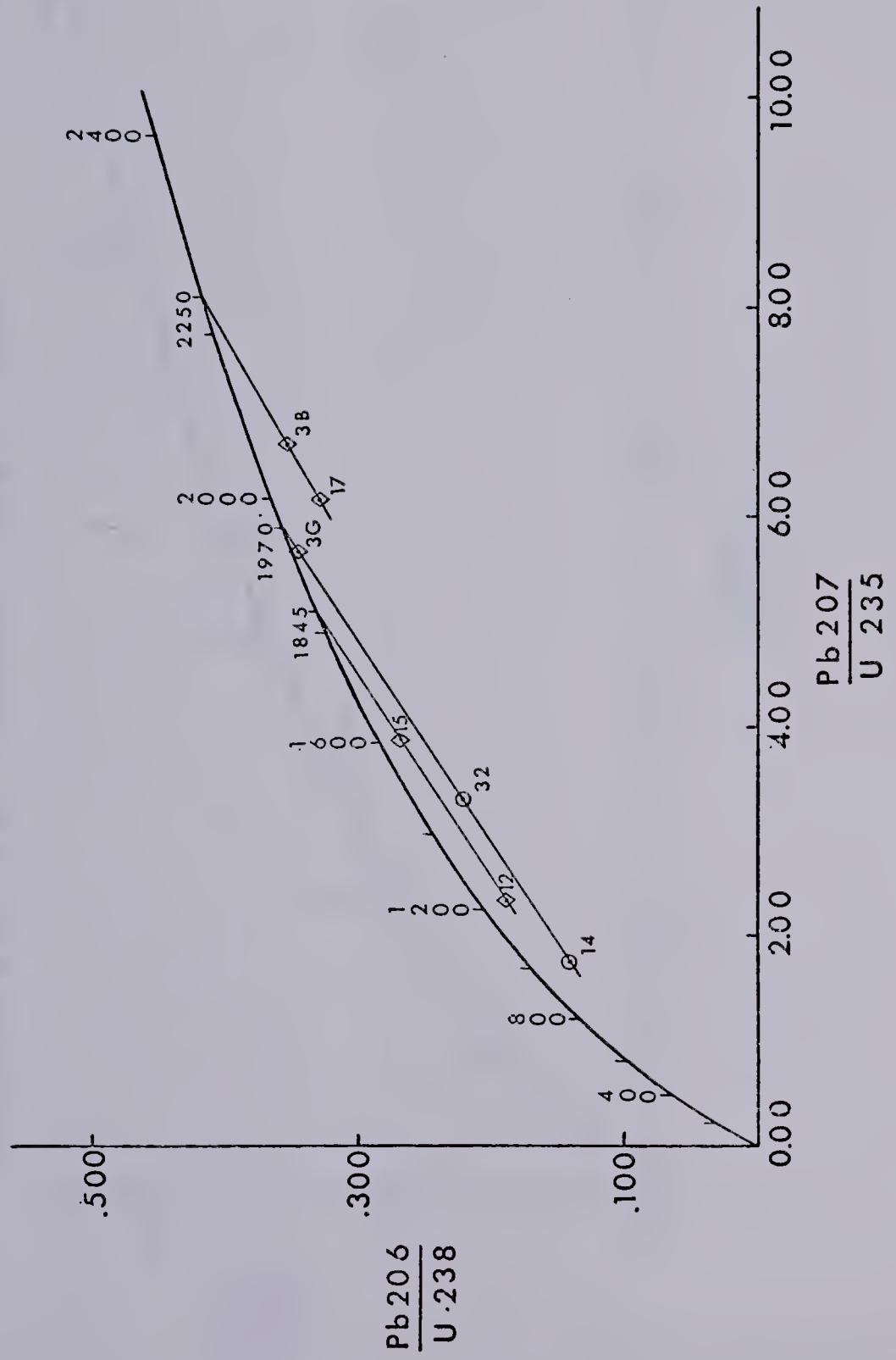
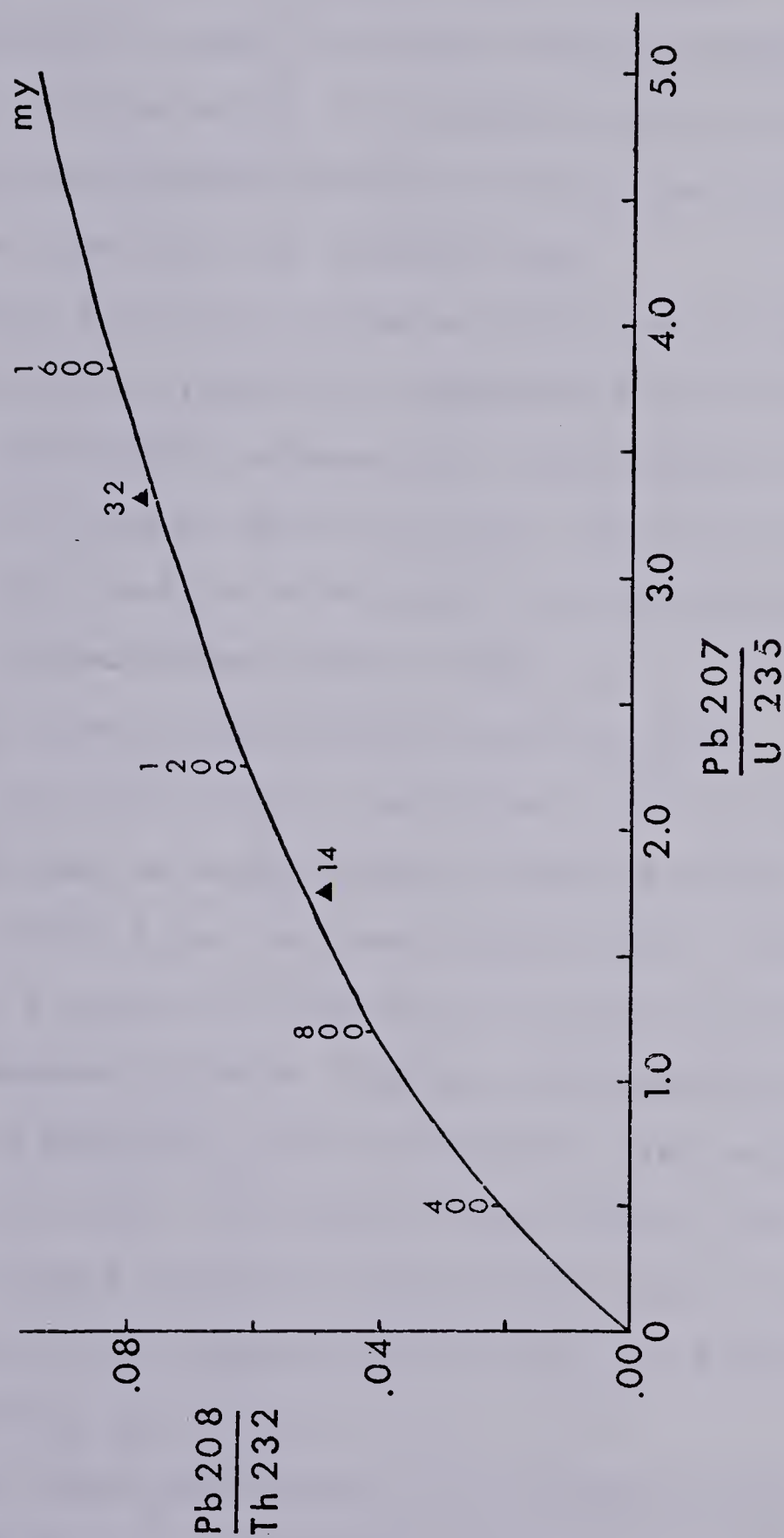






FIG. 11 : U-Th-Pb EVOLUTION DIAGRAM FOR URANINITES  
DATED FROM THE GREASE RIVER AREA





#### D. Interpretation of Results

The biotite gneisses in the study area have been dated at 2250 Ma by U-Pb zircon samples. Since no known magmatic-metamorphic events occurring during mid-Aphebian time have been recognized in the Canadian Shield, this age for the Tazin Group metasediments is interpreted as an Archean (older than 2500 Ma) survival date.

The younger ages date intrusive events of the Hudsonian orogeny. Two distinct phases are interpreted from isotope results and petrological evidence. The emplacement of the trondhjemite to alaskite series of white pegmatites (1975 Ma) slightly pre-dates the development of quartz-enriched pegmatites which have been dated at 1845 Ma.

The Grease River area results correlate with geochronological data acquired for Archean, Tazin Group complexes occurring in Saskatchewan, Alberta and the adjoining portions of the Northwest Territories. Table 8 shows that the 8 mineral and whole rock samples dated are grouped into Kenoran (2530 to 2450 Ma), mid-Aphebian (2360 to 2200 Ma) and Hudsonian (2070 to 1600 Ma) time periods. The clustering of dates obtained in this part of the Churchill structural province is due to the varying extent of reactivation of the Archean crust during the Hudsonian orogeny (Burwash et al. 1962).

The oldest dates discovered in the Western Craton of northern Saskatchewan occur in the Tazin Lake area. Kenoran ages retained in the granodioritic and granitic gneisses



Table 8: K-Ar, Rb-Sr, U-Pb mineral and whole rock ages (Ma) from the Western Craton of Saskatchewan, Alberta and the Northwest Territories.

location, formation	rock type	material dated	ages, Ma.			analyst
			K-Ar	Rb-Sr	U-Pb	
<u>Saskatchewan</u>						
Grease River	biotite gneiss	zircon			2250	
Tazin Group	trondhjemitic pegmatite	zircon, uraninite			1970	
	quartz-rich	zircon			1845	
Fontaine Lake Tazin Group	pegmatite	muscovite	1740			Burwash <i>et al.</i> 1962
Straight River	muscovite granite	whole rock		1820 <sup>±</sup> 100		Beck, 1967
Stony Rapids Tazin Group	porphyritic biotite granite	biotite	1720			Burwash <i>et al.</i> 1962
	pyroxene-hornblende granulite	hornblende	2350			
Beaverlodge Area	syngenetic pegmatite	uraninite, monazite			1930 <sup>±</sup> 40	Koeppel, 1968
	epigenetic veins	biotite	1780 <sup>±</sup> 20			
Fond-du-Lac	biotite gneiss	biotite	1740			Beck, 1967
Tazin Lake	granodiorite, granite gneisses	whole rock		2530 <sup>±</sup> 15		Baadsgaard, per. Comm.
		biotite		2360		Beck's (1967) values updated by Baadsgaard (per. comm.)
		hornblende				
<u>Alberta</u>		zircon uraninite, allanite			1900-2440	Baadsgaard <i>et al.</i> 1967
		mica	1800			
		whole rock		1900, 2250		
Andrew Lake		biotite	1740, 1830			Burwash <i>et al.</i> 1962
Northeast Alberta			←	2550	→	Burwash <i>et al.</i> 1972
<u>Northwest Territories</u>						
Armit Lake block	gneisses		1600-1800	-	-	Heywood <i>et al.</i> 1978
		zircon	-	2070-3100	-	
		biotite	2460		2000	London, 1963
		hornblende whole rock		2650		Baadsgaard, per. comm.
	low Rb pegmatite			2400		
Hill Island Lake Area	granitic, granodioritic gneisses	biotite	2200			C. Banks, per. comm.
		hornblende	2450			





from the Northern Stable Block (see Beck, 1969) imply that this segment of the crust was not significantly affected by later dynamothermal events. A continuation of the stable block into the Hill Island Lake area (N.W.T.) is confirmed by 2450 million year old hornblende (K-Ar) bearing gneisses (Banks, per. comm.).

In the Beaverlodge and Stony Rapids linear belts where the Hudsonian reworking has been intense, mid-Aphebian and Hudsonian dates are observed (Table 8). As the U-Pb and Rb-Sr dates are older than the K-Ar ages, it is assumed that the rocks were only partially recrystallized in most cases.

The geochronological evidence for the Grease River area suggests Tazin Group biotite gneisses were thermally affected, and quite possible, partially recrystallized during the Hudsonian orogeny. The zircon concordia plot age of 2250 Ma for the 'Archean' gneisses from the main showing is low probably as a result of episodic Pb-loss (Wetherill, 1956). Since the zircon U-Pb radioisotope clock was reset, it is inferred that the K-Ar age for biotite would be Hudsonian rather than mid-Aphebian.

These conclusions imply that the biotite gneisses may have partially recrystallized during the Hudsonian. But as pointed out in Chapter 4, the thin, parallel banding recognized in thin-sections is evidence that these rocks were affected by essentially one metamorphic event. However, the close association of biotite with minor muscovite in several gneissic samples may have resulted from the



degradation of biotite subjected to lower amphibolite facies conditions. It is noteworthy that the muscovite in the biotite gneisses was previously interpreted as a prograde metamorphic mineral.

Heavy mineral results on the zircon fractions from the biotite gneiss show that only one population of exceedingly uniform stubby, hyacinth zircons has been isolated. Petrological examinations show these grains to be devoid of optically distinct zones, cores and overgrowths. These findings indicate that zircons in the biotite gneisses developed primarily during one phase of crystal growth. And as the U-Pb date is mid-Aphebian, this necessitates that the gneisses had formed during the Kenoran orogeny. In summary then, it does not appear likely from petrological, heavy mineral and geochronological information available, that the biotite gneisses in the Grease River area were significantly recrystallized during Hudsonian regional metamorphism.

The dating results shed light on other geological events that occurred at the Grease River property. Although the pink granite gneiss plots on the same isochron as the biotite gneiss (3B), it is possible that the felsic gneiss was recrystallized during the Hudsonian event. The best solution to this problem comes from the zircon mineral analyses of granite gneiss and the white pegmatitic rocks.

Two distinct populations of zircons are found in the pegmatitic rocks from the main showing. One type which is best exemplified in the sheared pink granite gneiss (sample





18) is described as large, rounded, stubby zircons, often dark reddish brown in colour. The surfaces of these grains are frequently etched. These zircons are found in the granitic gneisses and white pegmatites, though their concentrations in the latter rock type are variable. The character of these large zircons is sufficiently similar in both rock type so as to suggest that they have a common source. This implies that the pink coloured felsic gneisses were partially melted during the Hudsonian Orogeny.

The second zircon type occurs as elongated tetragonal, bipyramidal forms that are invariably pale yellow or honey coloured. The interesting point is that the elongated yellow coloured zircon population exists exclusively in the white pegmatite examples.

The source of the elongated, yellow zircons is more enigmatic than that of the large stubby type. Two theories are possible. First, the yellow zircons could have formed from a zirconium rich solution derived during the anatexis of the granite gneisses. Second, these elongated euhedral zircons could have been intruded from depth into the Grease River metasedimentary belt.

Two important points given below infer with reasonable certainty that the population of yellow zircons was intruded from depth:

1. A striking resemblance in the shapes of zircons from the Grease River trondhjemitic and related pegmatites to those found in granite rocks





(Bibikova, 1977; Poldervaart, 1956).

2. These zircons are anomalously enriched in uranium compared to the gneissic zircons. The occurrence of such radioactive rocks and minerals is known to be a normal process during granitization processes associated with regional metamorphic events

(Yeliseyeva et al. 1974; Yermolayev et al. 1976).

Equally convincing evidence that a magma intruded the Tazin Group gneisses at the Grease River property is established by these findings. The highly uraniferous yellow zircons which occur in the white pegmatites are accessory minerals to primary uraninite grains. Also, the mineralization is confined to the pegmatites rather than to the granite or biotite gneisses. These results strongly infer that the source of uranium was derived at depth rather than 'sweated out' of the granitic gneisses exposed at the present erosional surface.

A conceptual model of the events occurring at the time the pegmatites intruded are summarized here. Major faulting following the regional strike and dip and intersecting the granitic and biotite gneisses at the main showing, was likely the first significant development during early Hudsonian. The fault(s) acted as a channel way for the granitoid melt to travel up. The pink granitic gneiss were probably open to fluids migrating through the metasedimentary units.



## VI. Mineral Geochemistry of the Mineralized Zone

This chapter deals exclusively with the electron microprobe (EMP) study of minerals from the Grease River area. In section A, the methods used will be outlined. In section B on minerals analyses, the petrology, compositional results and interpretations are given. The significant geochemical findings are summarized in section C.

A geochemical approach to this study was undertaken for the following reasons:

1. to determine the composition of the primary radioactive minerals in the Grease River area, and
2. to determine if compositional analyses of biotite, zircon and uraninite could help explain the origin of the discontinuous white pegmatites hosting the uranium mineralization.

### A. Analytical Approach

#### Sample Selection

Fourteen radioactive samples were chosen for probe analysis. Of these, only two samples (17 and 18) were pink pegmatite. The remaining samples were different compositional varieties of white pegmatite as follows: quartz-enriched granitoids (12, 15, 24, and 32); trondhjemitic rocks (10, 14, 27, 31 and D9); and two feldspar granite pegmatites (30, 32, 34 and D7).

#### Location of Grains for Analysis





The locations of all the minerals to be probed on each polished mount were mapped, using various techniques on page-size diagrams. The purpose of this was to help in locating grains while probing. The positions of the radioactive grains were determined by radioluxography. These ore minerals and all other readily identifiable marks such as cracks and pits on the surface of the mounts were also seen under reflected light. The transparent silicate minerals found in EMP - thin sections were mapped by transmitted light optics. Finally, reflected light polaroid photomicrographs located most of the better quality zircon and uraninite grains.

#### Instrumentation and Operating Conditions

Compositional analyses of the minerals were obtained with an Applied Research Laboratories (ARL - EMX) electron microprobe that has three wavelength dispersive spectrometers (WDS) and an Ortec energy dispersive spectrometer (EDS). The heavier elements were analyzed with two WDS using EDDT, LiF or ADP crystals and the lighter elements with a WDS using an RbAP crystal.

#### Methodology

Quantitative chemical analysis have been obtained on silicates (biotite and zircon) and uranium oxides from the study area. The energy dispersive analysis (EDA) techniques employed for biotite and zircon analysis are summarized in Appendix D. The wavelength dispersive analysis (WDA) approach followed for uraninite analysis is also outlined in





Appendix D. For detailed information regarding techniques and instrumentation, the reader is referred to Rucklidge (1976) and Smith (1976).

## **B. Minerals Analyzed by the Electron Microprobe**

### Biotite Analyses

The biotite books, flakes and stringers analyzed ranged from 0.5 to 5 mm in length. All grains showed marked pleochroism in shades of either reddish-brown or olive-green. Only those grains exhibiting uniform physical and optical properties as well as perfect polished surfaces have been probed. Biotites not selected for analysis were discarded for the following reasons: the appearance of opaques or dark spots (usually an indication of either Fe-bearing or radioactive inclusions); close association with muscovite, epidote, sphene or rutile; advanced chloritization; evidence of strain, bending or breaking of the mica grains.

Chemical Results Biotite compositional analyses (in weight percent oxides) are given in Table 9. Total Fe has been calculated as  $\text{Fe}^{+2}$ , since the  $\text{Fe}^{+2}/\text{Fe}^{+3}$  ratios are usually high in biotites from igneous-metamorphic granitoids (Deer et al. 1962).  $\text{H}_2\text{O}$  values are by difference as mentioned in Appendix D.

The average oxide concentrations (Table 9) have been calculated for three groups of biotites: the strongly chloritized biotites (samples 12 and 32); the low  $\text{Al}_2\text{O}_3$  -



Table 9: Chemical analyses<sup>1</sup> in weight percentages of biotites from the Grease River Area, N. Saskatchewan

Sample	Na <sub>2</sub> O	MgO	Al <sub>2</sub> O <sub>3</sub>	SiO <sub>2</sub>	K <sub>2</sub> O	CaO	TiO	MnO	FeO <sup>2</sup>	H <sub>2</sub> O <sup>3</sup>
01-A	-	6.16	18.28	34.79	9.61	-	3.26	.32	24.21	3.34
B	-	6.68	18.25	33.53	7.80	-	3.00	.30	24.68	5.77
C	-	5.91	17.95	34.80	9.43	-	3.66	.32	23.69	4.24
10-A	-	6.21	17.99	34.72	9.31	-	3.67	.35	24.01	3.75
B	-	6.24	17.85	34.16	8.48	.06	3.34	.36	24.72	4.80
C	-	6.82	18.17	32.10	5.93	.81	3.58	.33	25.84	6.42
D	-	6.54	18.52	33.74	8.04	.11	2.77	.30	24.97	5.02
12-A	-	8.25	19.17	31.72	5.16	.08	3.06	.33	24.59	7.64
B	.04	7.46	19.45	31.65	4.99	.13	2.58	.25	25.83	7.61
C	-	7.69	19.44	31.98	5.35	.06	2.60	.34	25.11	7.44
D	-	8.77	19.14	31.69	5.41	.11	3.39	.26	23.33	7.90
14-A	-	7.02	18.36	34.60	9.35	-	3.14	.24	22.46	4.83
B	-	7.56	18.81	33.66	8.11	-	2.66	.34	23.47	5.40
C	-	6.84	18.60	34.95	9.62	-	3.49	.31	22.51	3.69
D	-	6.85	18.62	34.48	9.46	-	3.14	.26	22.14	5.04
E	-	7.03	18.61	35.14	9.53	-	3.29	.26	22.53	3.62
F	-	6.89	18.82	35.16	9.39	-	3.19	.28	22.35	3.93
15-A	-	7.49	18.05	35.11	8.53	-	2.76	.37	22.77	4.92
B	-	7.11	17.78	35.53	9.41	-	3.19	.42	22.37	4.20
C	-	7.43	17.43	35.44	9.30	-	3.16	.38	22.68	4.18
D	-	7.13	17.63	35.50	9.22	-	3.32	.38	22.58	4.24
17-B	-	5.81	16.10	33.63	7.77	.56	3.48	.51	27.33	4.82
C	-	5.64	15.84	34.44	8.33	.21	3.45	.55	26.75	4.81
D	-	5.66	15.85	34.72	8.62	.24	3.53	.53	26.61	4.26
E	-	5.44	15.99	34.27	8.67	.22	3.29	.57	27.01	4.54
F	-	5.57	15.91	34.38	8.41	.34	3.44	.54	26.54	4.87
24-A	-	7.96	16.46	34.10	8.52	.18	3.54	.33	23.12	5.80
B	-	7.74	16.30	34.89	9.28	.19	3.31	.29	23.01	4.99
C	-	7.93	16.23	35.16	8.68	.16	3.41	.29	23.37	4.78
30-B	-	7.37	17.76	34.95	9.52	.19	3.35	.33	21.88	4.66
C	-	7.37	17.80	35.05	9.36	.18	3.16	.29	21.86	4.92
F	-	7.36	17.64	35.15	9.57	.12	3.28	.35	22.58	3.96
31-A	-	7.82	18.19	34.16	7.15	-	2.85	.42	25.26	4.17
C	-	7.39	17.94	35.62	9.15	-	3.13	.41	24.18	2.19
D	-	7.33	17.94	35.42	9.32	-	3.04	.37	24.21	2.37
E	.06	7.01	17.96	35.72	9.69	-	3.42	.40	23.69	2.05
H	-	7.09	18.46	36.27	9.94	-	3.28	.44	24.31	0.24
32-A	-	7.94	18.53	34.46	5.83	.22	2.38	.48	23.59	6.59
D7-H	-	5.26	18.34	34.76	8.78	-	3.97	.46	26.18	2.24
D9-A	.05	7.80	18.90	35.46	9.33	-	2.61	.22	23.54	1.09
C	-	7.46	19.28	36.02	10.07	-	3.01	.17	23.53	0.38
I	.10	7.60	19.49	35.70	10.00	-	3.01	.25	24.03	0.28
Aver <sup>4</sup>	.01	7.18	18.09	34.86	8.93	.07	3.28	.33	23.52	3.88
Aver <sup>5</sup>	-	5.62	15.94	34.29	8.36	.31	3.44	.54	26.91	4.66

notes: 1. Biotite analyses were obtained using EMP-EDA methods. 2. Total Fe as FeO. 3. H<sub>2</sub>O by difference of calculated oxides and 100%. 4. Average weight percentage of oxides excluding samples 12 and 17. 5. Average weight percentage of oxides in sample 17. 6. A (-) denotes not detected.



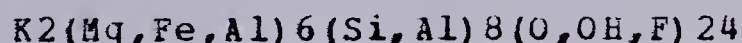


high FeO biotites in sample 17; and the remaining white pegmatite biotites.

Arranged in order of decreasing abundance, the oxides detected in the biotites are: SiO<sub>2</sub>, FeO, Al<sub>2</sub>O<sub>3</sub>, K<sub>2</sub>O, MgO, TiO<sub>2</sub>, MnO, CaO and Na<sub>2</sub>O. Compared with compositional analyses of biotites from plutonic and high-grade metamorphic rocks of similar composition (Deer et al. 1962; Engel et al. 1960; Nockolds, 1947; Stephenson, 1977) the results obtained in this study are only slightly different.

The geochemical features which characterize the biotites from the Grease River area are slightly lower concentrations of SiO<sub>2</sub>, MgO, MnO, CaO and Na<sub>2</sub>O. Although the other oxides fluctuate considerably, their concentrations fall within the normal biotite range.

The stoichiometric equivalents of the analyzed biotites have been calculated on the basis of 24 O atoms and the following formula unit taken from Deer et al. 1962;



where

Si, Al fill 8 tetrahedral (Z) sites

Ti, Mg, Mn, Fe fill 4 - 6 octahedral (Y) sites

Ka, Ca, Na fill 0 - 2 interplanar (X) sites

H<sub>2</sub>O, OH, F, Cl fill 2 - 4 interplanar

The biotite stoichiometric results obtained in this study are given in Table 10. Sub-totals for the four groups of elements are also included. A comparison of these atomic





Table 10: Structural formulae of biotites from the Grease River Area, N. Saskatchewan

sample	Structural formulae (based on 24 oxygens per formula unit)											Sub Totals				C <sup>4</sup>
	Si	Al	Al	Ti	Mg	Mn	Fe	K	Ca	Na	OH	Z <sup>1</sup>	Y <sup>2</sup>	X <sup>3</sup>	H <sub>2</sub> O	
01-A	5.43	2.57	0.76	.38	1.43	.04	3.16	1.92	-	-	3.50	8.00	5.77	1.92	3.50	C
B	5.06	2.94	0.27	.34	1.50	.04	3.12	1.50	-	-	5.82	8.00	5.27	1.50	5.82	
C	5.36	2.64	0.59	.42	1.36	.04	3.05	1.86	-	-	4.36	8.00	5.46	1.86	4.36	
10-A	5.38	2.52	0.63	.43	1.43	.05	3.11	1.84	-	-	3.88	8.00	5.65	1.84	3.88	C
B	5.23	2.77	0.42	.38	1.42	.05	3.17	1.66	.01	-	4.90	8.00	5.44	1.67	4.90	
C	4.82	3.18	0.01	.40	1.53	.04	3.24	1.14	.13	-	6.42	8.00	5.22	1.27	6.42	
D	5.15	2.85	0.46	.32	1.49	.04	3.19	1.56	.02	-	5.10	8.00	5.50	1.58	5.10	C
12-A	4.64	3.27	-	.34	1.80	.04	3.01	0.96	.01	-	7.46	7.91	5.19	0.97	7.46	
B	4.65	3.35	-	.29	1.63	.03	3.18	0.94	.02	.02	7.46	8.00	5.13	0.98	7.46	
C	4.70	3.30	0.03	.29	1.68	.04	3.09	1.00	.01	-	7.30	8.00	5.13	1.01	7.30	C
D	4.61	3.25	-	.37	1.90	.03	2.84	1.00	.02	-	7.66	7.86	5.14	1.02	7.66	
14-A	5.26	2.75	0.51	.36	1.59	.03	2.85	1.82	-	-	4.90	8.00	5.34	1.82	4.90	
B	5.08	2.92	0.39	.30	1.70	.04	2.96	1.56	-	-	5.44	8.00	5.39	1.56	5.44	C
C	5.39	2.61	0.74	.40	1.57	.04	2.90	1.90	-	-	3.80	8.00	5.65	1.90	3.80	
D	5.22	2.78	0.51	.36	1.55	.03	2.81	1.82	-	-	5.10	8.00	5.26	1.82	5.10	
E	5.41	2.59	0.76	.38	1.61	.03	2.90	1.88	-	-	3.72	8.00	5.68	1.88	3.72	C
F	5.40	2.60	0.74	.37	1.58	.04	2.87	1.84	-	-	4.02	8.00	5.60	1.84	4.02	
15-A	5.31	2.69	0.50	.31	1.69	.05	2.88	1.64	-	-	4.96	8.00	5.43	1.64	4.96	
B	5.43	2.57	0.60	.37	1.62	.05	2.86	1.84	-	-	4.28	8.00	5.50	1.84	4.28	C
C	5.43	2.57	0.54	.36	1.70	.05	2.91	1.82	-	-	4.28	8.00	5.56	1.82	4.28	
D	5.43	2.57	0.58	.38	1.62	.05	2.89	1.80	-	-	4.32	8.00	5.52	1.80	4.32	
17-B	5.22	2.78	0.13	.41	1.35	.07	3.55	1.54	.09	-	5.00	8.00	5.51	1.63	5.00	C
C	5.35	2.65	0.22	.40	1.25	.07	3.48	1.66	.04	-	4.98	8.00	5.42	1.70	4.98	
D	5.42	2.58	0.31	.41	1.32	.07	3.47	1.72	.04	-	4.42	8.00	5.58	1.76	4.42	
E	5.35	2.65	0.26	.39	1.26	.08	3.52	1.72	.04	-	4.72	8.00	5.51	1.76	4.72	C
F	5.32	2.68	0.19	.40	1.29	.07	3.44	1.66	.06	-	5.02	8.00	5.39	1.72	5.02	
24-A	5.14	2.86	0.03	.40	1.79	.04	2.92	1.64	.03	-	5.84	8.00	5.18	1.67	5.84	
B	5.32	2.68	0.23	.38	1.76	.04	2.93	1.80	.03	-	5.08	8.00	5.34	1.83	5.08	C
C	5.36	2.64	0.25	.39	1.80	.04	2.98	1.68	.03	-	4.86	8.00	5.46	1.71	4.86	
30-B	5.32	2.68	0.47	.38	1.67	.04	2.78	1.84	.03	-	4.74	8.00	5.34	1.87	4.74	
C	5.31	2.59	0.46	.36	1.66	.04	2.77	1.80	.03	-	4.98	8.00	5.29	1.83	4.98	C
F	5.41	2.59	0.58	.38	1.69	.05	2.91	1.88	.02	-	4.06	8.00	5.61	1.90	4.06	
31-A	5.24	2.56	0.51	.33	1.79	.05	3.24	1.40	-	-	4.26	8.00	5.92	1.40	4.26	
C	5.61	2.39	0.92	.37	1.73	.05	3.18	1.84	-	-	2.30	8.00	6.25	1.84	2.30	C
D	5.58	2.42	0.87	.36	1.72	.05	3.19	1.88	-	-	2.48	8.00	6.19	1.88	2.48	
E	5.64	2.35	0.95	.41	1.65	.05	3.13	1.96	-	.02	2.16	8.00	6.19	1.98	2.16	
H	5.83	2.17	1.30	.40	1.70	.06	3.27	2.04	-	-	0.48	8.00	6.73	2.04	0.48	C
32-A	5.07	2.93	0.26	.26	1.74	.06	2.90	1.10	.03	-	6.46	8.00	5.22	1.13	6.46	
D7-H	5.52	2.48	0.93	.47	1.25	.06	3.48	1.78	-	-	2.38	8.00	6.19	1.78	2.38	
D9-A	5.57	2.43	1.04	.31	1.83	.03	3.09	1.88	-	.02	2.18	8.00	6.30	1.90	2.18	C
C	5.46	2.24	1.36	.36	1.78	.02	3.15	2.06	-	-	0.76	8.00	6.67	2.06	0.76	
I	5.70	2.30	1.15	.36	1.81	.03	3.21	2.04	-	.04	0.56	8.00	6.56	2.08	0.56	
range	4.61-5.76	2.17-3.35	0-1.36	.26-.47	1.25-1.83	.02-.08	2.77-3.55	0.94-2.06	0-.13	0-.04	0.48-7.66	7.86-8.00	5.13-6.73	0.97-2.08	0.48-7.66	

notes: 1. Z sites include Si, Al. 2. Y sites include Al, Ti, Mg, Mn, Fe. 3. X sites include K, Ca, Na.

4. C denotes biotites affected by chloritization. 5. A (-) denotes note detected.



proportions with the literature (Deer et al. 1962; Nockolds, 1947) reveals that although many of the biotites from the thesis area are hydrated, they are within the biotite range.

The eight tetrahedral (Z) sites are fully occupied by Si and Al in all the biotites except those in samples 12 and 32 which are chloritized. [Any excess of Al has been included with the octahedral (Y) group of elements.] The supersaturation of tetrahedral elements is particularly marked in the fresh, unhydrated trondhjemitic biotites from samples 31 and D9.

Ti, Mg, Mn, Fe and excess Al atoms filling the octahedral (Y) sites total between 5.13 and 6.73 atomic equivalents (Table 10). The minimum value is expected since Deer et al. (1962) state that this group rarely falls below 5.0 equivalents. The maximum octahedral site sub-totals occur in the trondhjemitic biotites whose tetrahedral Si and Al sites are also supersaturated.

The larger K, Ca and Na cations occurring between the tetrahedral (Si, Al) and octahedral (Fe, Mg, Ti, Mn, Al) sheets total from .97 to 2.08 atomic equivalences in the biotites from the thesis area. The lowest values are found in the chloritized biotites and the highest values in the D9 biotites. It is noteworthy that all of the biotites from the study area are anomalously low in Ca and Na content.

The alteration of biotite is nearly always accompanied by an increase in water content. The H<sub>2</sub>O stoichiometric equivalences range from .48 in the trondhjemitic biotites to





7.66 in the chloritized biotites. This range is unusual for biotite which theoretically should contain from 2 to 4 percent equivalences of H<sub>2</sub>O (Deer et al. 1962) . It is interesting that those biotites deficient in H<sub>2</sub>O are supersaturated with elements occupying the Z, Y and X sites. This finding holds for the optically fresh biotites occurring in samples 31 and D9.

The chemical and stoichiometric results presented above show that biotites from the thesis area are of three types: partially chloritized biotites (samples 12 and 32); hydrated biotites (the majority of the samples); low H<sub>2</sub>O, optically fresh biotites (samples 31 and D9).

Although biotites analyzed in this study vary in their degree of alteration and hydration, information regarding their origin is still lacking. For this reason, the subtle chemical variations were more closely examined.

Interpretation of Results A chemical variation diagram (Figure 12) shows the correlation existing between the major oxides detected in the biotites. Chloritization and hydration effects are believed to be the cause of several of the observed trends. In particular, decreasing concentrations of SiO<sub>2</sub> and K<sub>2</sub>O (Figures 13a, 13b) are paralleled by increasing contents of FeO, Al<sub>2</sub>O<sub>3</sub>, MgO and H<sub>2</sub>O in the chloritized samples (1-B, 1-O-C, 12(A-D), 14-B, 24-A and 32-A). However, not all the mineral chemical variations found can be explained by such alteration processes.

In Figure 14, the SiO<sub>2</sub> and Al<sub>2</sub>O<sub>3</sub> contents of





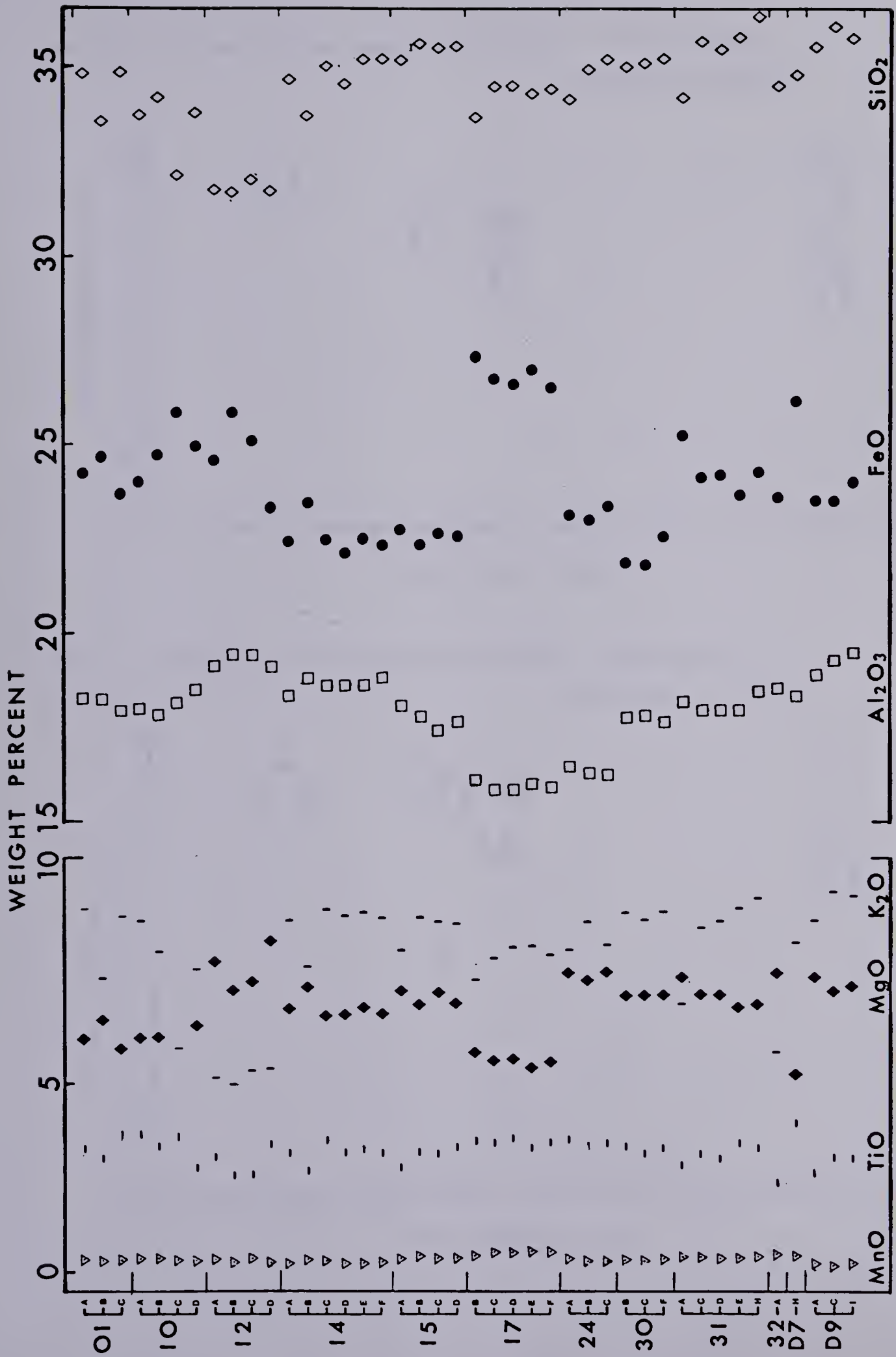


FIG. 12 : DISTRIBUTION OF OXIDES FOUND IN BIOTITES FROM THE GREASE RIVER AREA



FIG. 13a : PLOT OF  $\text{SiO}_2$  VS  $\text{H}_2\text{O}$  IN UNALTERED AND PARTIALLY  
CHLORITIZED BIOTITES

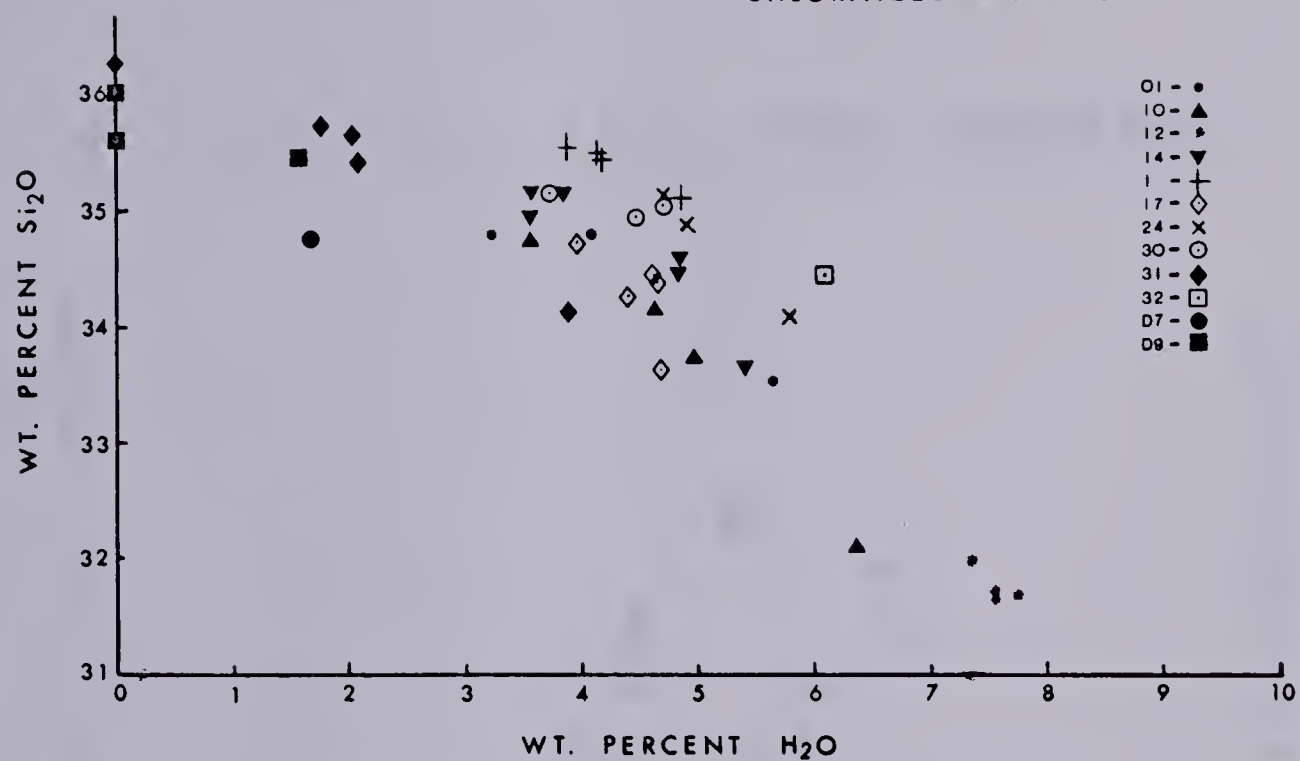


FIG. 13b : PLOT OF  $\text{K}_2\text{O}$  VS  $\text{H}_2\text{O}$  IN UNALTERED AND PARTIALLY  
CHLORITIZED BIOTITES

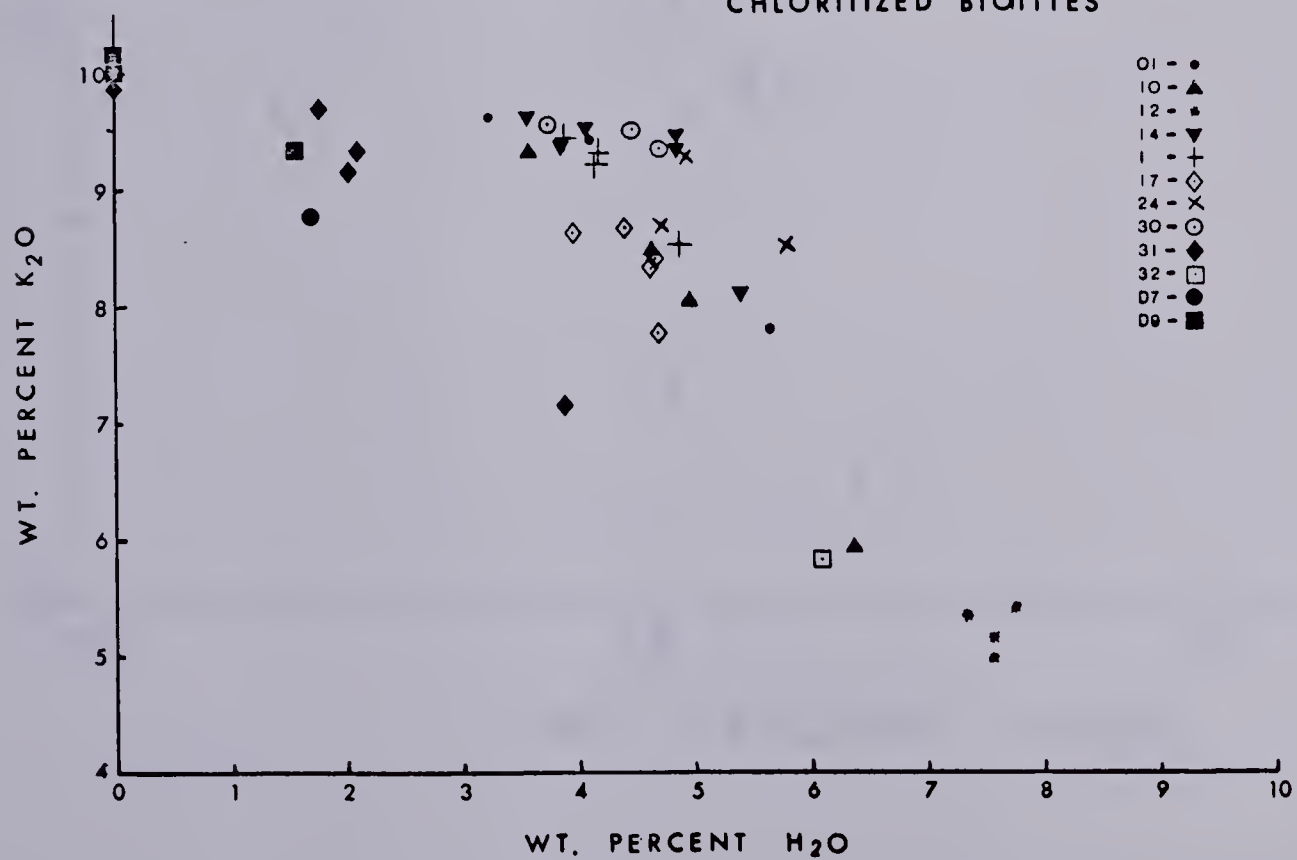
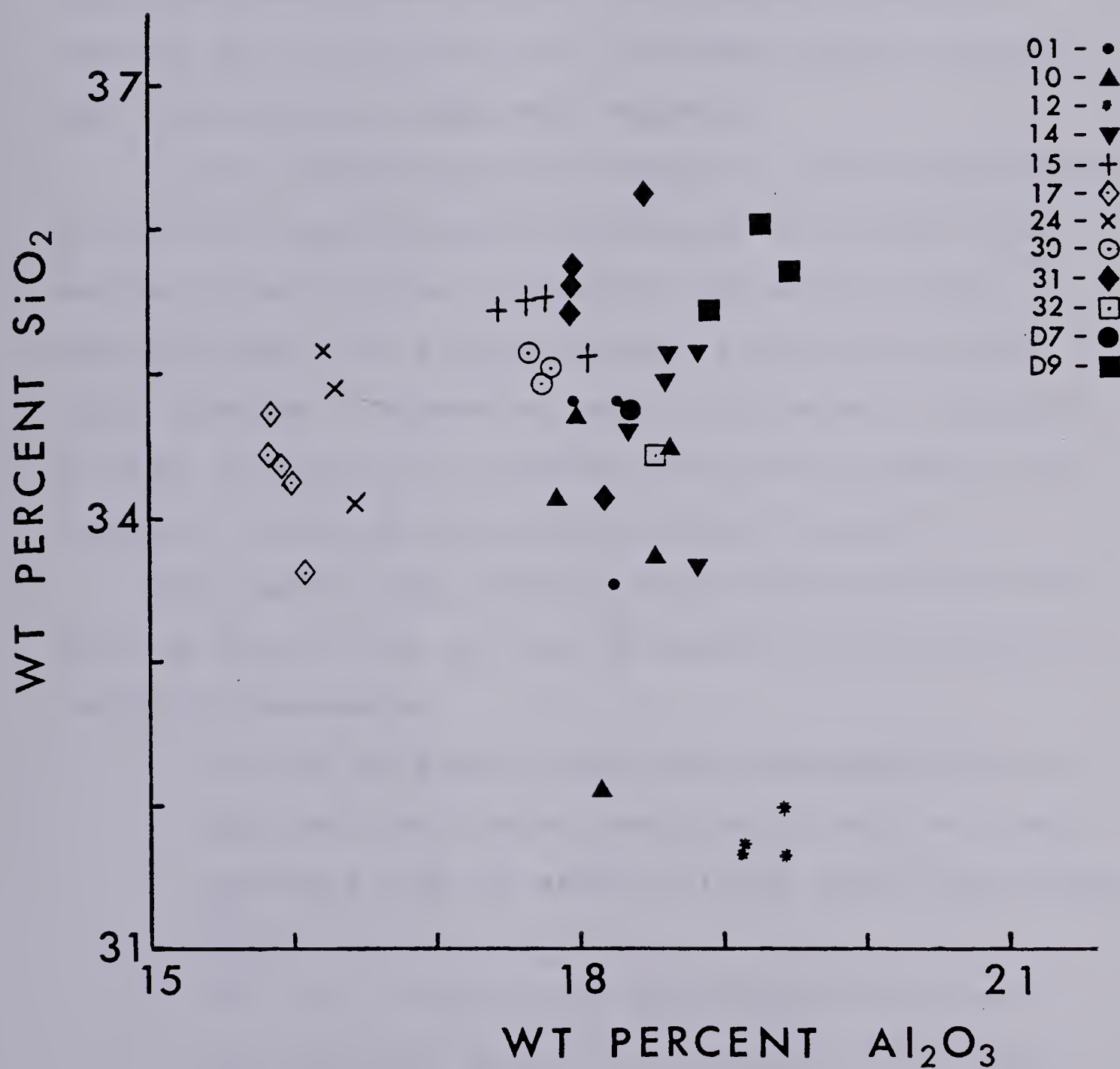




FIG. 14 :  $\text{SiO}_2$  VS  $\text{Al}_2\text{O}_3$  FOR BIOTITES





unchloritized biotites are seen to correlate positively. The  $Al_2O_3$  concentrations are more variable and the majority of the data points plot between the low Al (samples 17 and 24) and high Al (sample D9) biotites. This spread implies that a chemical correlation exists between biotites from the entire migmatized zone. Nevertheless, the distinct clustering observed for biotites from the individual samples suggests that their origins differ only slightly.

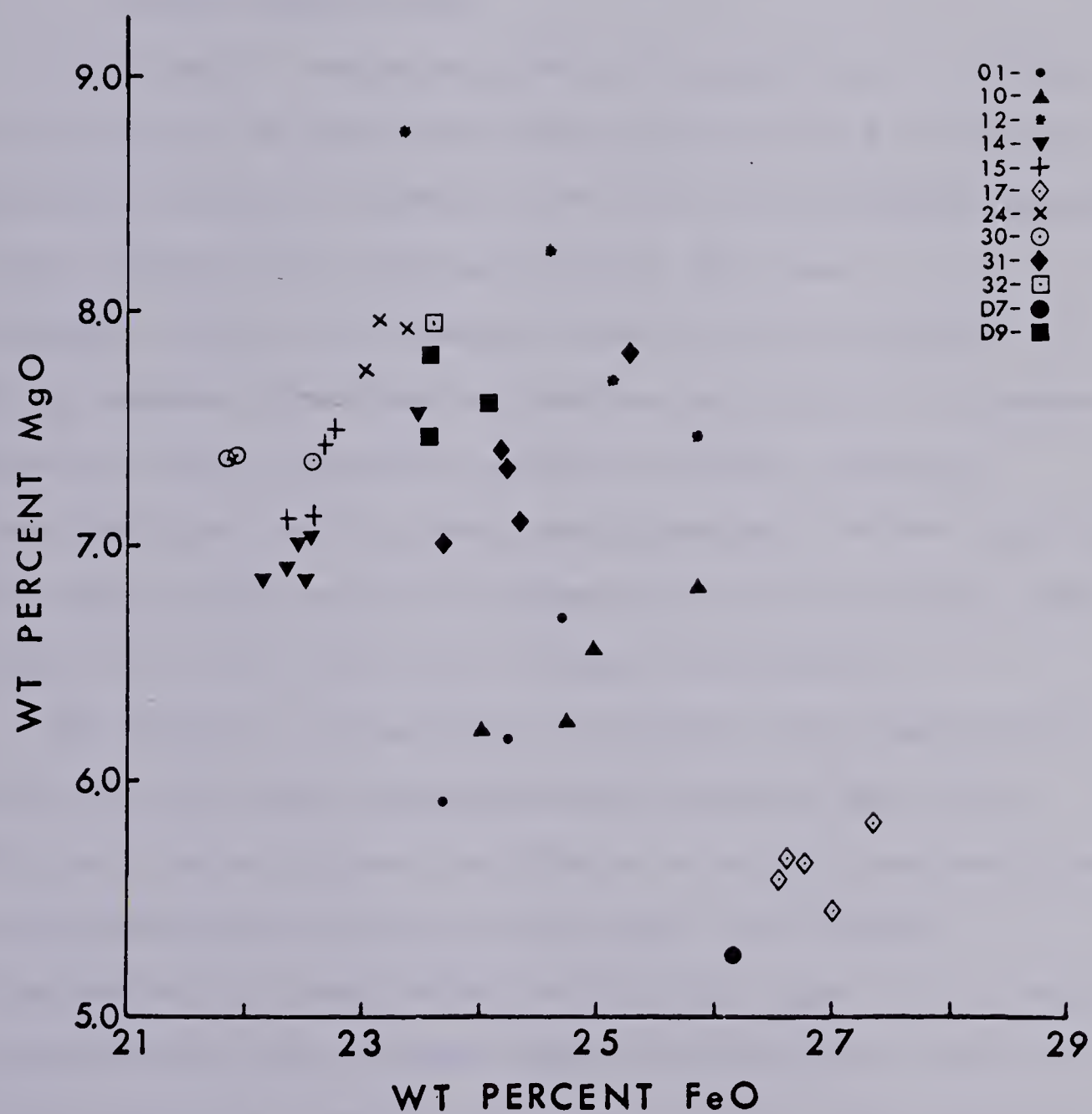
A plot of MgO versus FeO (Figure 15) shows these oxides to correlate negatively. The separation of biotites from samples 17 and D9 with a noticeable clustering of the remaining data points between them, is analagous to the trend observed in Figure 14. Despite the general similarity of these two plots, the relative positions of some of the individual groups of biotites has shifted somewhat.

These major oxide chemical trends existing in biotites from the Grease River area may be evidence of the following geological phenomena:

1. biotites originating from the metamorphic biotite gneisses, the igneous trondhjemitic melt or a melt resulting from the assimilation of both these source rocks.
2. biotites of metamorphic origin which have been recrystallized during the intrusion of the white pegmatites.
3. biotites of igneous origin which have been re-equilibrated with late-stage K-metasomatizing



FIG.15 : MgO VS FeO FOR BIOTITES





solutions associated with the emplacement of the white pegmatites.

4. biotites originating by any of the above processes and later re-equilibrating with Si-rich solutions circulating during the formation of the quartz-rich granitoid rocks dated as the youngest igneous event in the thesis area.

Petrological evidence exists to support all of these possibilities. By comparison with biotites from a granitic pegmatite studied by Vernon, 1977, the microtextures present in the Grease River biotites suggest that some recrystallization has occurred. Several of the samples (17, 24, D7) contain xenoliths of biotite and altered feldspars which are unquestionably corroded by either quartz or quartz-feldspar matrix. Here, the appearance of the biotites often vary enough so as to suggest that even biotites found in the same probe mount have formed differently.

The chemical variability of biotites from the Grease River area has been interpreted as resulting from their original chemistry plus the effects of having recrystallized or re-equilibrated at some later time. The chemical inhomogeneity is proof that the biotites found in the white pegmatites have not reached chemical equilibrium. This is likely caused by biotite resistance to melt below magmatic temperatures of 700°C (Winkler, 1974). However, biotites do readily exchange with circulating ground waters at much lower temperatures, but rarely do they attain chemical





equilibrium (Deer et al. 1962).

Geological conditions existing during the emplacement of the white pegmatites in the Grease River area may be deduced from the biotite analysis. A triangular diagram for the FeO + MnO, TiO<sub>2</sub> and MgO contents (Figure 16) shows that the biotites are a FeO + MnO rich variety typical of igneous differentiates in the granite to pegmatite region (Nockolds, 1947).

In order to determine if some of the biotites were of hydrothermal origin, their MgO and FeO contents were more closely examined. According to Kesler (1975), biotites with MgO/MgO + FeO ratios greater than .47 have formed hydrothermally. MgO/MgO + FeO ratios for biotites from the thesis area range from .17 to .27 and clearly are not indicative of hydrothermal origin. However, it is interesting that the values greater than .24 are from rocks containing a high proportion of quartz veining (samples 12, 14, 15, 24, 30, 32 and D9). This suggests that these biotites may have re-equilibrated with hydrothermal solutions during the silicification of the rocks. This quartz-enrichment would have taken place at temperatures tending towards the hypothermal range of 300 to 500°C (Park et al. 1964), following the cooling of the trondhjemitic and granitic pegmatites.

The rock type and associated mineral parageneses are also reflected in the biotite compositional analyses. In a MgO-FeO-Al<sub>2</sub>O<sub>3</sub> triangular diagram (Figure 17) the biotites



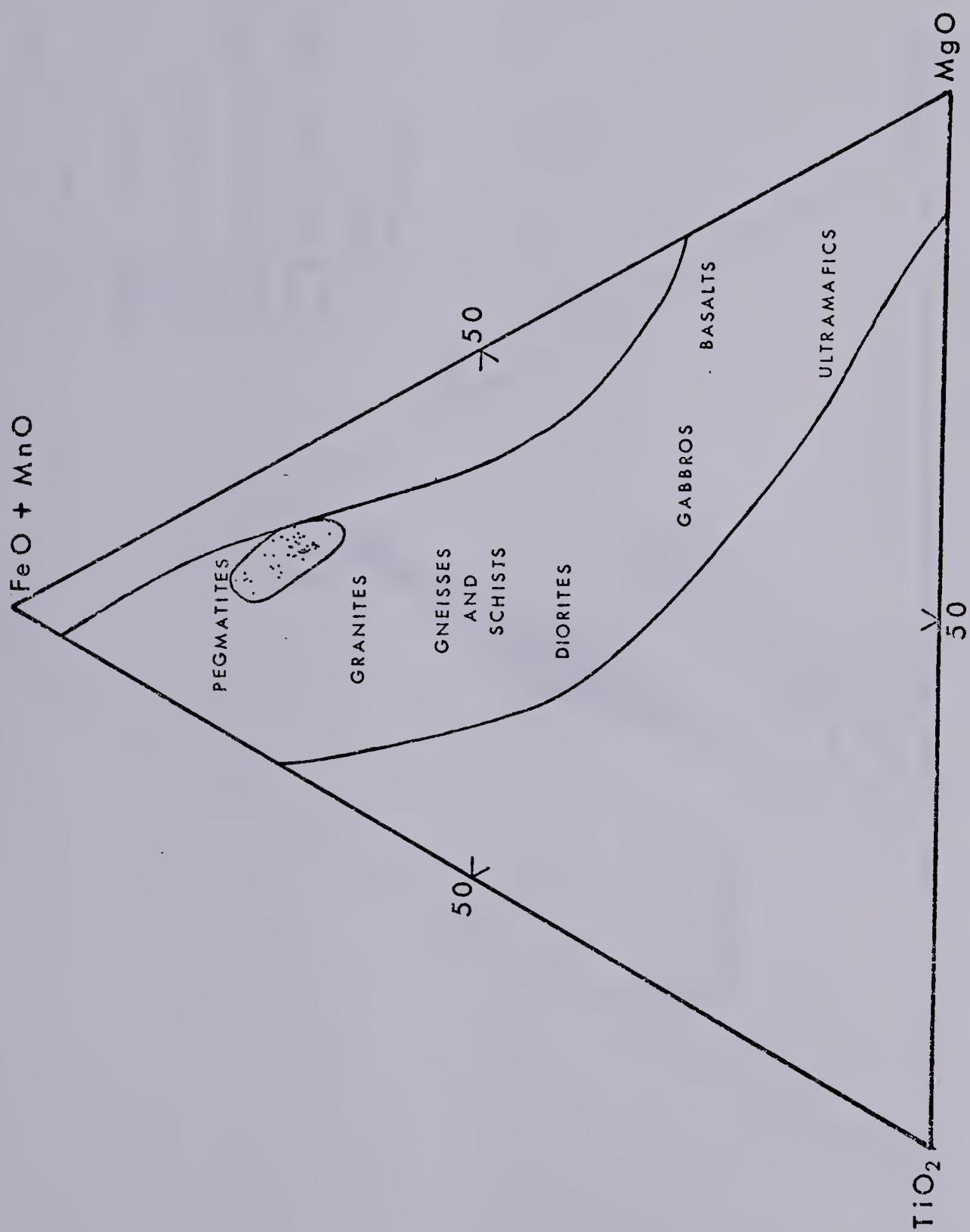


FIG.16 :  $(\text{FeO} + \text{MnO}) - \text{TiO}_2 - \text{MgO}$  PLOT FOR BIOTITES FROM THE GREASE RIVER AREA (.)



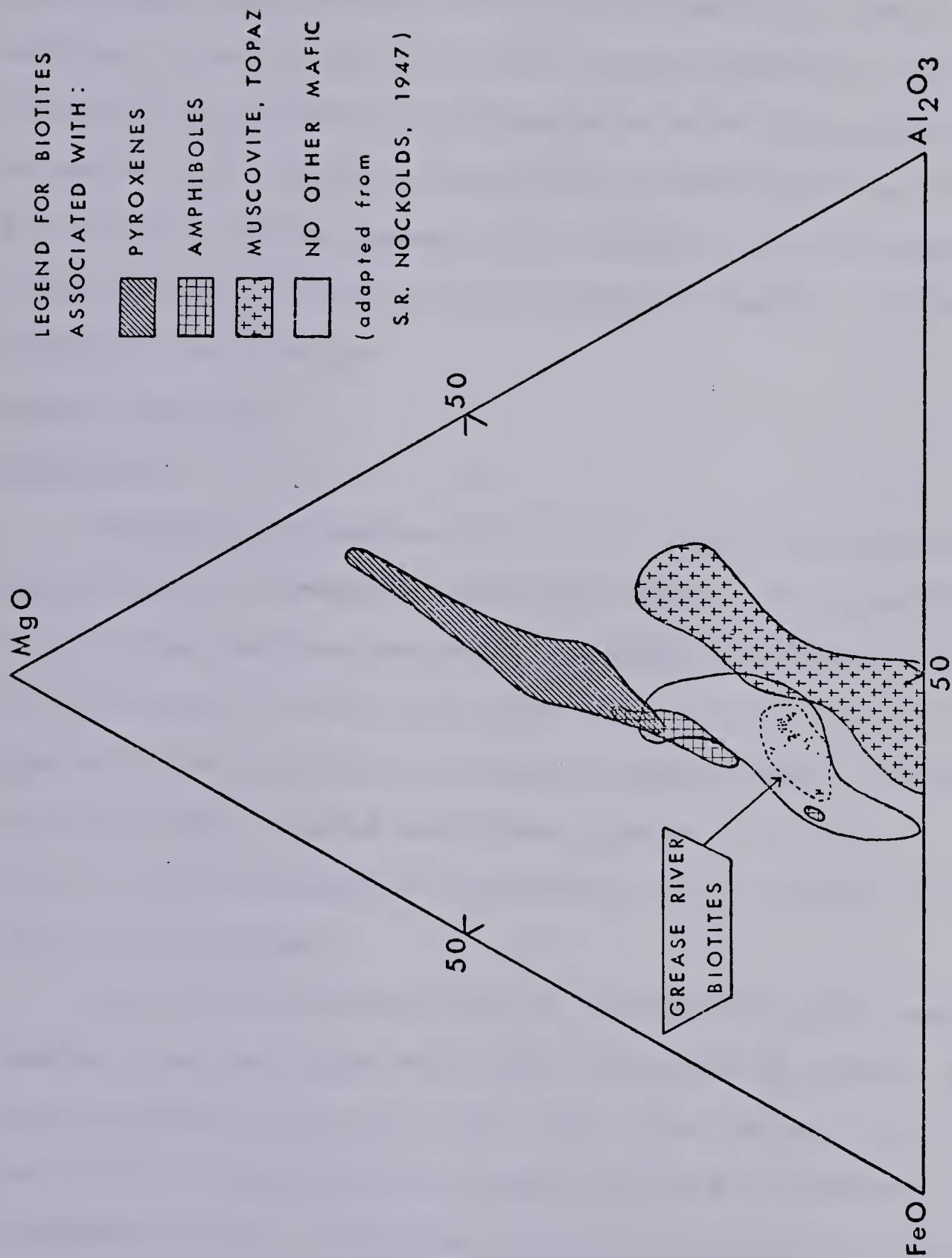


FIG. 17 : TRIANGULAR DIAGRAM FOR CONTENTS OF  $\text{MgO}$ ,  $\text{FeO}$ ,  $\text{Al}_2\text{O}_3$  FOR BIOTITES IN THE GREASE RIVER AREA (•)





from the Grease River area plot in the region for biotites occurring with no other mafics. Although the majority of the data points tend towards the biotite-muscovite field, samples 17 and D7 approach the biotite-amphibole. This distribution pattern is substantiated with petrological evidence. For example, rocks with biotites plotting closer to the  $Al_2O_3$  vertex (sample D9) contain some muscovite while those plotting closer to the FeO vertex contain a higher proportion of biotite.

### Zircon Analyses

#### Petrology

Zircons from samples 14, 15, 30, and D9 have similar morphological characteristics: bipyramidal or pyramidal in longitudinal section and equidimensional tetragonal forms in cross section. On the other hand most of the zircons in samples 18 and 32 are fragments of large zircons obtained from the heavy mineral separates. Plates 9, 10 and 11 contain photomicrographs revealing the usual appearance of the zircons probed.

All the zircons examined in transmitted light have biaxial negative signs and highly variable 2V angles. They are colourless or tinted brown when iron stained. Many of the grains contain microfractures and dark inclusions of irregular shapes. The larger zircons in samples 15 and D9 are distinctly zoned. The coarse banding parallels the crystal outlines. The zircons probed are weakly anisotropic, displaying interference colours ranging from black to medium



grey. Occasionally, patches of first order red and blue are found in some of the coarser zones. Many of the optical properties determined indicate that these zircons are metamict.

Observed under an ore microscope, the zircons are light grey and slightly reflective. Occasionally, highly reflective radioactive ore minerals are intergrown with or proximal to the zircons (Plates 9B, 9G, 11, 12G, 12H).

### Chemical Results

The compositional analyses (in weight percentages) of zircons from the Grease River area are listed in Table 11. The difference between the oxides detected and 100% is shown as weight percent H<sub>2</sub>O. Total Fe appears as Fe<sub>2</sub>O<sub>3</sub> and total S as SO<sub>4</sub> since their presence in zircon is likely secondary and therefore in an oxidized form.

ZrO<sub>2</sub> is the principal oxide in the zircons, ranging in concentration from 42.87 to 60.15 weight percent. These values are extremely low compared to those of Deer et al. (1962) who show their lowest ZrO<sub>2</sub> concentrations at 52 percent. It is interesting that the D9 specimens have consistently lower ZrO<sub>2</sub> concentrations than the other zircons probed.

The SiO<sub>2</sub> values fall within a much narrower range, from 28.18 to 32.48 weight percent. According to Deer et al. (1962) these concentrations are normal.

A plot of ZrO<sub>2</sub> versus SiO<sub>2</sub> contents (Figure 18) reveals a positive correlation between these major oxides. Zircons



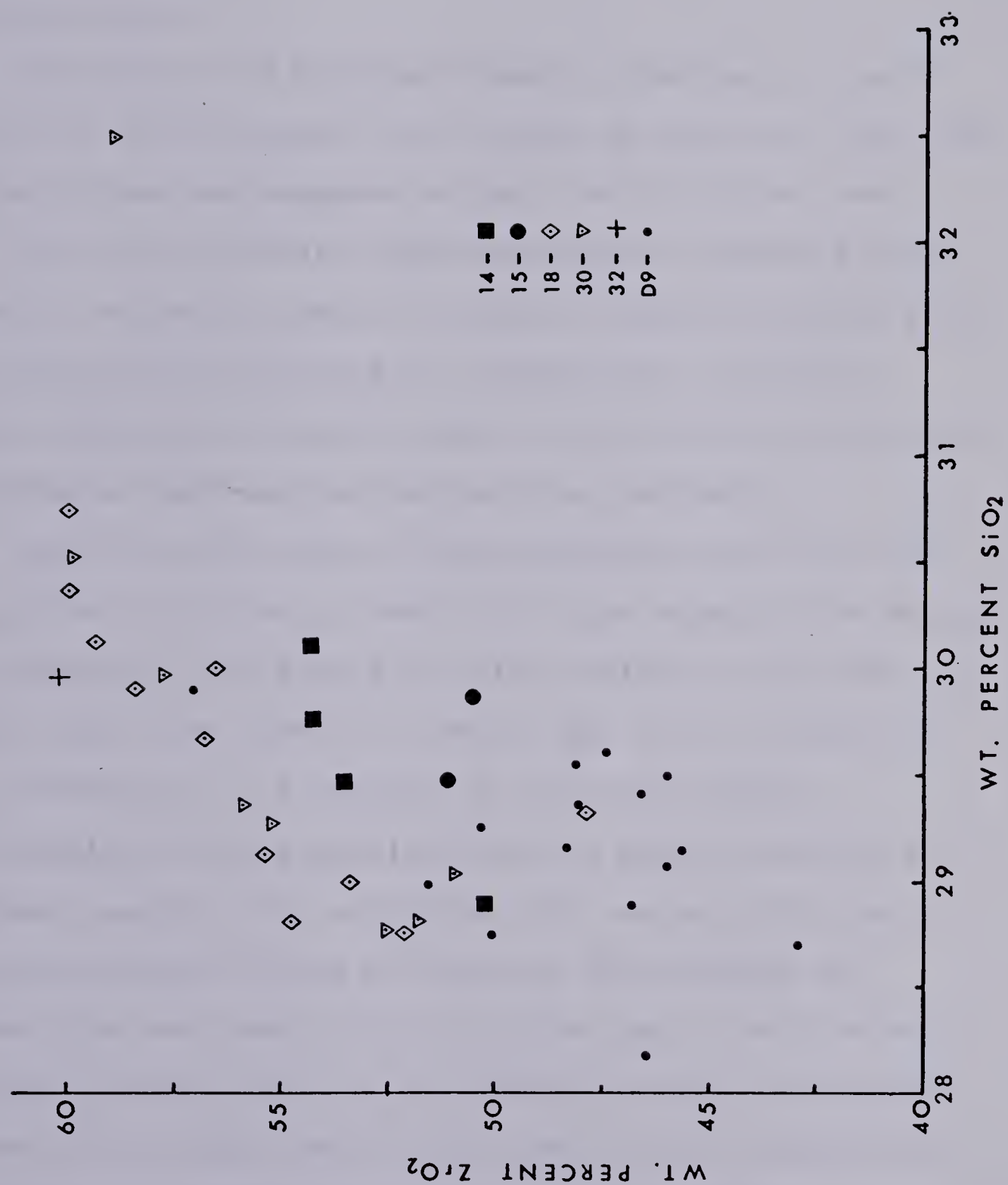
Table 11: Chemical analyses<sup>1</sup>. in weight percentages of zircons from the Grease River area, N. Saskatchewan

Sample	Na <sub>2</sub> O	MgO	Al <sub>2</sub> O <sub>3</sub>	SiO <sub>2</sub>	P <sub>2</sub> O <sub>5</sub>	SO <sub>4</sub>	Cl	K <sub>2</sub> O	CaO	TiO <sub>2</sub>	MnO	Fe <sub>2</sub> O <sub>3</sub> <sup>2</sup>	ZrO <sub>2</sub>	H <sub>2</sub> O <sup>3</sup>
14-DD	-	-	0.81	29.77	0.80	-	.20	.16	3.09	-	.28	1.32	54.22	9.35
14-G2	-	-	1.53	28.89	0.82	4.26	.11	.23	2.68	.08	.21	2.25	50.24	8.69
14-G3	-	-	0.93	30.10	1.21	0.15	-	.11	1.41	-	.12	4.45	54.27	7.24
14-ZZ-	0.18	-	1.02	29.47	0.70	0.11	.22	.16	2.87	-	.23	1.57	53.49	9.99
15-1--	0.60	-	1.72	29.48	0.62	0.25	.35	.15	4.22	-	.24	0.98	51.07	10.32
15-2	0.29	-	1.94	29.86	0.96	0.63	.21	.19	3.36	-	.11	1.37	50.46	10.67
18-A1	0.54	-	0.43	28.76	0.09	0.24	.25	.26	3.71	-	.05	0.17	52.08	13.43
18-B1	0.62	-	1.40	29.33	0.24	0.27	.35	.36	4.79	.07	.28	0.37	47.78	14.16
18-B2	0.51	-	0.07	30.36	-	0.15	.15	-	1.96	-	.22	0.52	59.88	6.19
18-B3	0.54	-	0.54	28.99	-	0.16	.20	.10	2.74	-	.24	2.50	53.32	10.68
18-B4	0.68	-	0.64	29.13	-	0.16	.22	.08	3.19	-	.25	0.63	55.30	9.71
18-B5	0.52	-	0.28	30.00	0.87	0.37	.06	.25	2.89	-	-	0.06	56.55	8.17
18-C1	1.08	-	1.08	28.81	0.18	0.22	.26	.18	4.19	-	.20	0.71	54.74	8.91
18-C2	0.12	-	-	30.12	-	0.26	.25	-	2.48	-	.34	0.67	59.28	6.50
18-C3	0.37	-	0.28	29.90	-	0.25	.23	.19	2.84	-	.18	0.59	58.39	6.78
18-C4	0.13	-	0.18	30.74	-	0.44	.13	.11	2.37	-	.07	0.65	59.97	5.22
18-CA	0.44	-	0.52	29.67	-	0.21	.27	.12	2.98	-	.19	0.69	56.73	8.19
30-1	0.57	.05	1.87	29.03	0.55	0.40	.27	.15	3.88	.12	.36	1.24	50.85	10.66
30-2A	0.64	.06	1.29	28.77	0.39	0.21	.25	.16	3.96	-	.40	0.97	52.50	10.38
30-2B	-	-	0.79	32.48	1.02	0.09	.07	.19	1.49	.18	.14	0.98	58.89	3.70
30-3	0.62	-	1.50	28.81	0.20	-	.23	.16	4.00	-	.36	1.02	51.73	11.40
30-4	0.43	-	0.90	29.27	0.61	0.48	.26	.14	2.92	-	.26	1.04	55.18	8.52
30-5	0.16	-	0.29	29.96	0.74	1.19	.27	.14	2.61	-	.12	0.99	57.72	5.81
30-6	0.51	-	0.56	29.35	0.49	-	.15	.11	2.94	.09	.34	1.13	55.87	8.47
30-6	0.33	-	0.32	30.52	0.43	-	.08	.08	1.77	-	.28	0.87	59.81	5.50
32-1	0.34	-	0.19	29.95	-	0.29	.09	.08	1.30	-	.09	0.17	60.15	7.37
D9-1R	0.49	-	2.36	29.36	0.88	0.29	.26	.39	4.38	-	.20	1.01	48.06	12.34
D9-1C	0.36	-	3.16	29.07	0.66	0.43	.32	.40	4.84	-	.16	0.95	46.00	13.66
D9-2	0.35	-	2.94	29.61	-	0.34	.20	.39	4.30	-	.16	1.14	47.40	12.99
D9-3R	0.58	.05	2.00	28.75	0.10	0.39	.30	.26	4.38	-	.24	1.08	50.06	11.81
D9-3C	0.54	-	2.87	28.18	0.10	0.60	.40	.35	4.99	.07	.18	1.12	46.50	14.11
D9-4	0.43	-	0.80	29.89	0.35	0.32	.09	.26	2.09	-	.21	1.26	57.01	7.30
D9-5	0.46	.19	3.00	29.16	-	0.42	.23	.44	3.94	.35	.17	1.60	48.31	11.73
D9-6	0.59	-	2.25	28.89	0.34	0.40	.28	.34	4.63	-	.15	0.89	46.79	14.47
D9-7R	0.54	-	3.08	29.55	0.18	0.46	.23	.35	4.06	-	.20	1.26	48.11	11.98
D9-7C	0.36	.16	3.62	29.50	0.41	0.53	.16	.57	3.93	-	.13	1.43	45.91	13.30
D9-8	0.55	-	1.88	28.98	-	0.37	.31	.24	4.00	-	.21	0.92	51.54	11.00
D9-9	0.65	-	3.14	29.15	1.10	0.50	.23	.33	4.76	.19	.16	1.17	45.65	12.97
D9-10	0.75	-	3.22	29.41	0.86	0.47	.20	.39	4.38	-	.13	1.15	46.58	12.48
D9-11	0.58	-	1.75	29.25	1.01	0.57	.13	.39	3.36	-	.18	1.05	50.27	11.47
D9-12	0.38	-	2.39	28.70	1.36	1.50	.19	.63	4.34	-	.21	1.24	42.87	16.17

notes: 1. Zircon analyses were obtained using EMP-EDA methods. 2. Total Fe as Fe<sub>2</sub>O<sub>3</sub>. 3. H<sub>2</sub>O by difference of calculated oxides and 100%.





FIG. 18 :  $ZrO_2$  VS  $SiO_2$  IN MIGMATITIC AND PEGMATITIC ZIRCONS



from the trondhjemite (14 and D9) and quartz-rich (15) white pegmatites have both low  $ZrO_2$  and  $SiO_2$  contents. On the other hand, zircons occurring in the K-feldspathized rocks (namely 18, 30 and 32) have distinctly higher  $ZrO_2$  concentrations.

The presence of internal chemical zonation in the D9 zircons is also suggested from Figure 18 since  $ZrO_2$  and  $SiO_2$  concentrations are enhanced in the rims of zircons D9-1, D9-3 and D9-7. Although, these findings are expected since Zr and Si concentrations are known to increase sharply with increasing differentiation of igneous melts (Bibikova, 1977), they are puzzling in light of the overall low Zr and Si contents discussed in the preceding paragraph.

The  $CaO$ ,  $Al_2O_3$ ,  $K_2O$  and  $Na_2O$  concentrations found in the zircons are given in Table 11. These oxides often change sympathetically and amount to totals which are unmistakably higher than those quoted in Deer *et al.* (1962). Together, they comprise up to 8 percent of the zircon weight. Individually, their concentrations are highly variable and somewhat abnormal. In particular, the readers attention is directed to the D9 group of zircons. They contain the highest and most consistent  $CaO$  values (up to 4.99 percent). Similarly, their  $Al_2O_3$  and  $K_2O$  concentrations are elevated. However, it is important to note that the  $K_2O$  contents are believed to be caused in part by an undetermined concentration of uranium (generally less than 1 percent) in the anomalous zircons. This interference is likely to occur



because of K and U peak overlaps.

The other components detected in the zircons probed are:  $\text{Fe}_2\text{O}_3$ ,  $\text{SO}_4$ ,  $\text{MnO}$ ,  $\text{Cl}$ ,  $\text{MgO}$  and  $\text{TiO}_2$ . The  $\text{Fe}_2\text{O}_3$  and  $\text{SO}_4$  contents range from .06 to 4.45 and up to 4.26 weight percent, respectively.  $\text{MnO}$  and  $\text{Cl}^-$  each form up to .40 weight percent and although their concentrations are low, they are steady.  $\text{MgO}$  and  $\text{TiO}_2$  concentrations are usually too low for detection by EDA methods.

The zircons from the Grease River area are abnormally hydrated, with  $\text{H}_2\text{O}$  contents as high as 16.17 weight percent. The highest values are found in the D9 zircons.

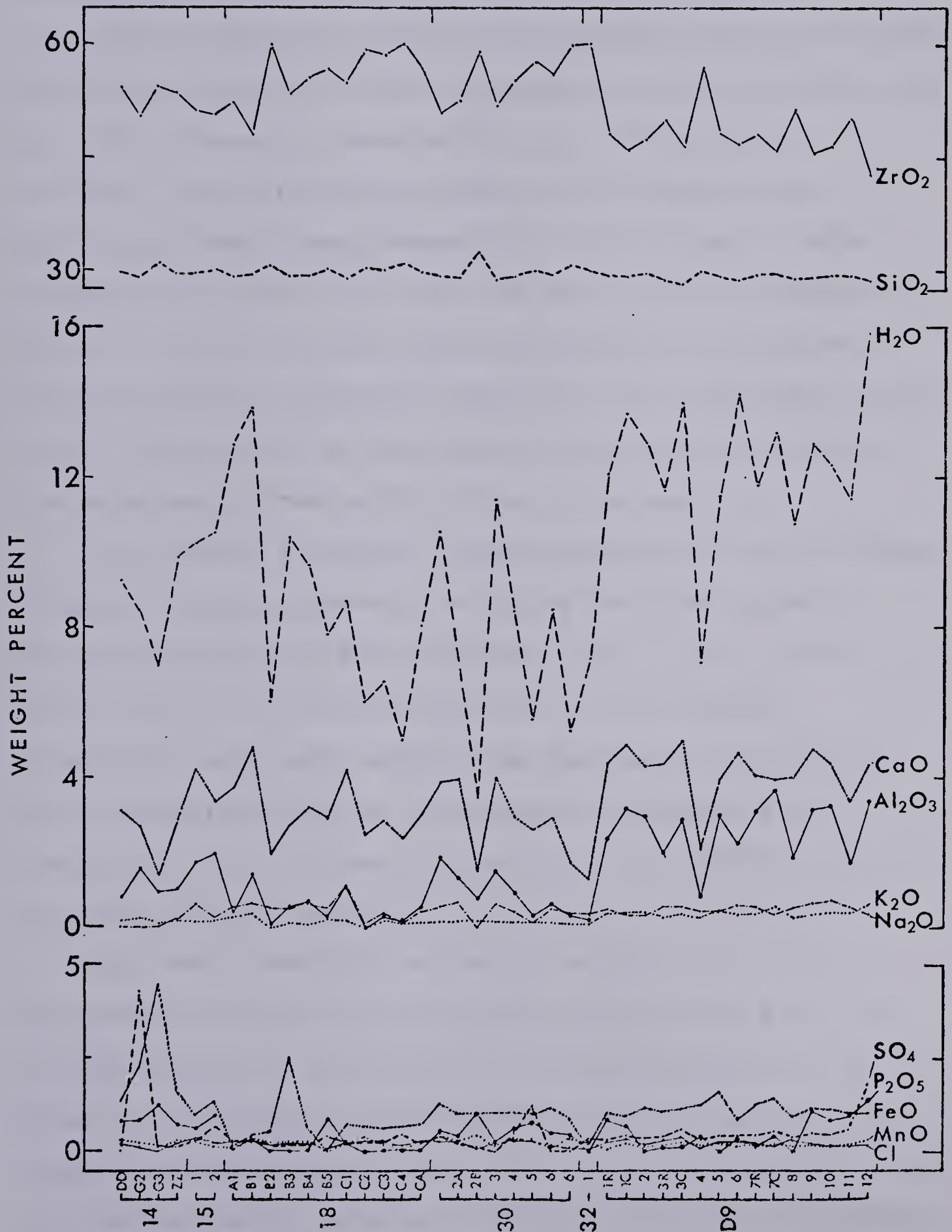
The chemical variations existing between the zircons probed from the Grease River area are illustrated in Figure 19.  $\text{ZrO}_2$  and  $\text{SiO}_2$  correlate positively, while each in turn is seen to correlate negatively to the  $\text{H}_2\text{O}$ ,  $\text{CaO}$ ,  $\text{Al}_2\text{O}_3$ ,  $\text{K}_2\text{O}$  and  $\text{Na}_2\text{O}$  in most grains. Conversely, the  $\text{Cl}^-$  content appears to parallel changes in the  $\text{ZrO}_2$  concentrations in several zircons.

Interpretation of Results The foregoing petrological and chemical results suggest that the zircons from the Grease River area are severely metamict and consequently inhomogenous due to related alteration processes. The zircons probed depart from the ideal formula unit of  $\text{ZrSiO}_4$  in two significant ways. First, a tremendous decrease in the Zr content is indicated. The Si/Zr atomic proportion (atomic weight divided by element weight percent) ratios approximated at .48/.38 for the D9 zircons and at .49/.45





FIG. 19: PLOT OF THE CHEMICAL VARIATIONS IN ZIRCONS FROM THE GREASE RIVER AREA





for the other grains, are a verification of the low Zr values. Second, abnormally high H<sub>2</sub>O totals are inversely proportional to the combined ZrO<sub>2</sub> and SiO<sub>2</sub> contents.

Similar chemical trends have frequently been attributed to metamictization processes (Deer et al. 1962; Medenbach et al. 1978). Recently, Medenbach et al. (1978) probed hydrated, metamict zircons collected from world-wide localities. Their study showed that: (1) Zr and Si were replaced by Fe, Ca, Al, P and REE and (2) H<sub>2</sub>O is present in order to compensate for charge imbalances in extensively altered zircons. Analogous trends have been observed in this study, with the low Si and especially Zr being balanced by the substitution of Ca, Al, K (or U), Na and H<sub>2</sub>O.

The secondary chemical trends established by the author have been further investigated using the photographic facility of the electron microprobe. Zr, Si, Ca, Al, Na, K, Fe, Mn, Hf, U and Th characteristic x-ray emission photographs have been obtained on zircons 30-1, 30-2 and D9-6. Interpretations of the elemental photograph are compatible with the compositional and petrological findings presented in this section.

The subtle chemical variations existing in D9-6, a moderately hydrated zircon are displayed in Plate 10. The crystal outline of zircon D9-6 is clearly evident in the Zr elemental photograph. The concentration of Zr and Si atoms appear to vary sympathetically as well as individually. The Ca distribution is variable, with gradual changes evidenced



over the entire grain. Al and Na are slightly concentrated in a band crossing the zircon. Although the concentrations of the major (Zr and Si) and minor secondary (Ca, Al, Na) atoms do fluctuate on a micron scale, distinct chemical zonation is lacking even though this zircon is optically zoned.

The causes of metamictization (loss of crystal state) of zircons have been researched by the following persons: Bursill et al. 1966; Deer et al. 1965; Krasnobayer et al. 1974; Mitchell, 1973; Pyatenko, 1970. Their findings show that an amorphous state commonly develops because of crystal defects caused by:

1. radioactive damage to the crystal bonds
2. numerous ionic substitutions for Zr and Si
3. internal zoning
4. fast crystallization rates
5. presence of inclusions

Radioactive damage is likely the principal cause of the metamictization of zircons from the Grease River area. Not only do these zircons occur in a radioactive zone, they contain considerable quantities of U and Th. Up to 0.78 percent U was measured in some zircons analyzed by the mass spectrometer (see Table 6).

Internal zoning observed in many of these metamict zircons is also thought to have contributed to their physical and chemical deterioration. Although the results are only semi-qualitative, chemical inhomogeneities similar to





those seen in Plate 10 have been observed in most of the optically zoned and metamict zircons.

Mineral inclusions are present in many of the zircons analyzed in this study. Most are of highly radioactive opaques (Plates 9B, 9E, 10 and 11), but the presence of transparent mineral inclusions has been confirmed as well.

For example, the Th, U, Fe and Ca x-ray emission photographs in Plate 10 demonstrate the presence of two inclusions in zircon D9-6. In one inclusion, Fe is associated with a thorium mineral? which contains two zones of U enrichment. The region defined by the Th atoms is possibly pseudomorphic after uraninite, since the bulk of the U atoms appear to have been mobilized to the crystal boundaries. The position of the second inclusion is indicated by the accumulation of Ca atoms just next to the thorium phase. Incidentally, this Ca-bearing inclusion which has been verified as apatite, is optically invisible.

Fast crystallization rates could also have produced the extreme metamictization of the zircons studied. Recalling that these zircons occur in syntectonic pegmatites emplaced during the Hudsonian orogeny, tectonic movements would certainly have disturbed their crystallization rates. Minerals crystallizing during faulting conditions would likely form at accelerated rates due to rapid cooling.

It is still questionable whether these anomalous zircon compositions are due solely to later alteration processes or whether significant ionic substitutions occurred when the



zircons were forming. Intrinsic chemical dissimilarity may account for the unique D9 group of zircons which have consistently higher  $Al_2O_3$  and  $CaO$  concentrations and lower  $ZrO_2$  concentrations than the zircons analyzed from the main showing

### Uraninite Analyses

#### Petrology

Although all of the fifteen EMP mounts prepared for this study were of rock samples containing anomalous radioactivity, only six had uraninite grains of quality good enough for quantitative analysis. Altogether, fourteen uraninites from samples 14, 24, 30, 31, 32 and D9 were probed using WDA methods.

The uraninites exhibit cubic forms or variations such as triangular and rectangular shapes when cut oblique to their crystallographic axes. The typical morphological forms of uraninites are seen in Plate 12. Their edges are often rounded or rough due to secondary processes. Grain sizes range from 0.2 to 1.2 mm in length. Twinning on the {111} plane occurs rarely.

Under the ore microscope, the uraninites are highly reflective, white to cream coloured grains. They are only moderately hard with VHN 100: 265-345 values falling well below the range of VHN 50-100: 625-925 quoted for uraninites (Morton et al. 1972).



Red and yellow coloured stains generally surround the uraninites and extend along cracks and crystal boundaries of the host minerals. Radioluxographs of the ore mounts (Plate 8) show that much of the alteration coating grains in samples 12, 15, 76.15 and 32 is highly radioactive and probably secondary  $U^6$  mineralization.

### Chemical Results

The oxide and element weight percents for uraninites analyzed from the Grease River area are listed in Table 12. The amount of  $U^4$  occurring in  $UO_2-3$  has been determined from the total Pb content since  $U^4$  is the principal radioactive parent decaying to Pb. Total Fe has been calculated as  $Fe^3$  since iron is believed to be secondary. Sulfur (S) has been calculated as  $PbS$  rather than  $FeS$  since Pb is more abundant and readily combined with S than is Fe.  $H_2O$  has been calculated by difference.

Uraninites from the Grease River area contain from 66.77 to 74.11 weight percent  $UO_2-3$ . These concentrations are comparable to those quoted for uraninites from granitoid rocks (Cameron-Schimann, 1978; Lang et al. 1962; Morton et al. 1972).

$ThO_2$  is the second major oxide with concentrations from 7.91 to 13.00 weight percent. According to Lang's et al. (1962) classification of uraninites, two types are found in the thesis area: normal uraninites with up to 10 percent  $ThO_2$  and thorian uraninites with greater than 10 percent  $ThO_2$ . These concentrations of thorium are typical of





Table 12: Chemical analyses<sup>1.</sup> in weight percentages of uraninites from the Grease River area, N. Saskatchewan

Sample	Na <sub>2</sub> O	Al <sub>2</sub> O <sub>3</sub>	SiO <sub>2</sub>	K <sub>2</sub> O	CaO	Fe <sub>2</sub> O <sub>3</sub> <sup>2.</sup>	PbS	PbO	ThO <sub>2</sub>	UO <sub>2-3</sub> <sup>3.</sup>	Total
14-A	.35	.11	0.43	1.05	2.34	0.26	-	7.03	9.08	72.69	93.34
14-H	.60	.07	0.26	0.97	1.24	0.20	-	8.36	10.55	70.15	92.40
14-O	.57	-	0.18	0.96	2.90	0.07	-	7.92	8.42	72.28	93.30
14-R	.46	.16	0.29	0.97	2.03	0.79	-	8.38	12.10	66.92	92.10
14-S	-	-	0.26	1.02	2.17	0.23	-	7.10	10.67	70.51	91.96
24-D	.11	.24	0.50	0.91	0.56	2.73	0.56	11.60	7.91	69.43	94.55
30-1	.35	-	0.47	0.97	1.09	0.81	1.22	9.40	8.44	71.36	94.11
31-1	.36	.06	0.49	0.92	1.07	0.21	-	8.93	8.47	71.57	92.08
32-A	.18	.14	0.34	0.90	0.58	0.14	-	12.56	8.04	69.71	92.59
D9-1	.21	-	0.25	0.96	0.70	0.19	1.08	9.13	13.00	69.70	95.22
D9-2	.21	.15	1.23	1.02	1.33	0.24	0.40	12.07	7.91	71.53	96.09
D9-3	.19	.17	0.69	0.91	0.35	0.13	0.76	14.47	12.30	63.77	93.74
D9-4	.35	.10	0.55	0.94	0.19	0.29	0.31	16.88	10.91	66.22	96.74
D9-7	.26	.12	0.68	1.01	0.79	0.33	0.99	8.49	8.53	74.11	95.31

	Na	Al	Si	K	Ca	Fe	S	Pb	Th	U	O <sup>4.</sup>
14-A	.26	.06	.20	.87	1.67	0.18	-	6.52	7.98	63.80	18.46
14-H	.44	.04	.12	.81	0.89	0.14	-	7.76	9.27	61.51	19.03
14-O	.42	-	.09	.80	2.07	0.05	-	7.35	7.40	63.40	18.43
14-R	.34	.08	.14	.80	1.45	0.55	-	7.78	10.63	58.68	19.55
14-S	-	-	.12	.85	1.55	0.16	-	6.59	9.38	61.88	19.48
24-D	.08	.13	.23	.75	0.40	1.91	.08	11.25	6.96	60.74	17.49
30-1	.26	-	.22	.81	0.78	0.57	.16	9.79	7.42	62.49	17.51
31-1	.26	.03	.23	.76	0.77	0.15	-	8.29	7.45	62.74	19.32
32-A	.13	.07	.16	.74	0.42	0.10	-	11.66	7.07	60.97	18.68
D9-1	.15	-	.12	.80	0.50	0.13	.14	9.41	11.43	61.05	16.28
D9-2	.16	.08	.57	.06	0.85	0.17	-	11.60	6.95	62.56	16.07
D9-3	.14	.09	.32	.76	0.25	0.09	.10	14.09	10.81	55.68	17.67
D9-4	.26	.05	.26	.78	0.13	0.20	.04	15.94	9.59	57.75	15.00
D9-7	.20	.06	.32	.84	0.57	0.23	.13	8.74	7.50	64.94	16.48

notes: 1. Uraninite analyses were obtained using EMP-WDA methods. 2. Total Fe as Fe<sub>2</sub>O<sub>3</sub>. 3. The UO<sub>2</sub>/UO<sub>3</sub> ratio was calculated assuming that Pb is produced from UO<sub>2</sub>. 4. O calculated by difference.



uraninites crystallized at magmatic temperatures (Kimberley, 1978; Steacy et al. 1978).

PbO concentrations range from 7.03 to 16.88 weight percent in the uraninites probed. The values are highly variable even in grains occurring in the same rock sample (Table 12).

The non-essential minor constituents detected in uraninites from the Grease River area (Tables 12 and 13) total from 2.11 to 5.13 weight percent. Listed in order of decreasing abundance, these minor components are: CaO, K<sub>2</sub>O, SiO<sub>2</sub>, Fe<sub>2</sub>O<sub>3</sub>, PbS, Na<sub>2</sub>O and Al<sub>2</sub>O<sub>3</sub>. Individually, these constituents are often spurious and probably a result of alteration processes which have also been documented by Cameron-Schimann (1978).

A range of 3.26 to 8.04 weight percent H<sub>2</sub>O and possibly helium is calculated in the uraninites from the Grease River area. Helium would be generated by the radioactive decay of U and Th atoms. The lowest values are observed in the D9 uraninites.

Figure 20 shows the compositional variations existing in the uraninites from the Grease River area. The UO<sub>2</sub>-3 contents appear to correlate negatively with the ThO<sub>2</sub> contents. The relationships between PbO and both UO<sub>2</sub>-3 and ThO<sub>2</sub> are less distinct. The CaO, SiO<sub>2</sub>, Fe<sub>2</sub>O<sub>3</sub> and Na<sub>2</sub>O values show wide fluctuations and frequent paralld trends, while the K<sub>2</sub>O and Al<sub>2</sub>O<sub>3</sub> concentrations are less variable.

Three X-Y diagrams of the major chemical components of



Table 13: Subtotals, ratios and chemical ages calculated for uraninites from the Grease River area, N. Saskatchewan.

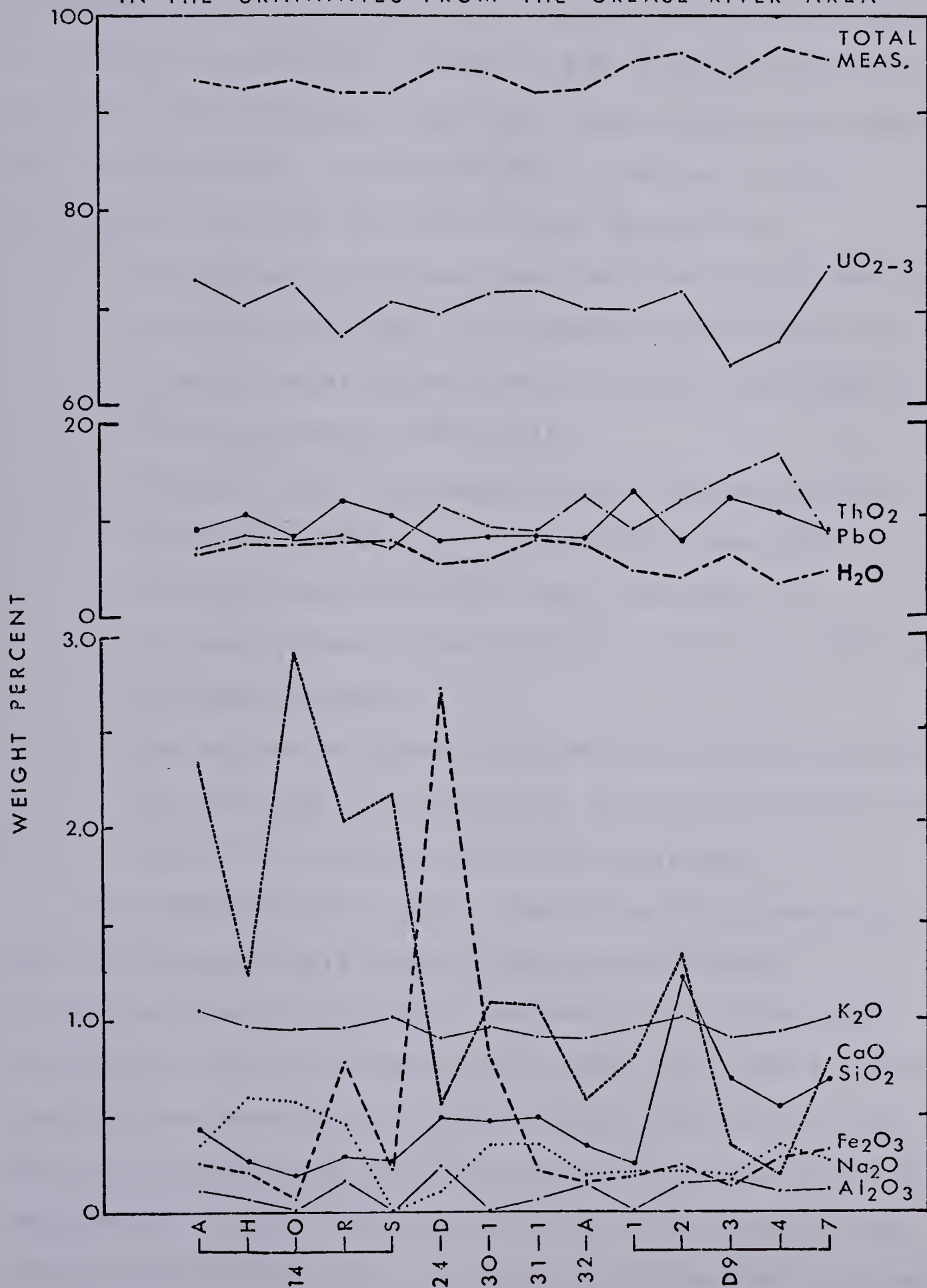
sample	H <sub>2</sub> O <sup>1</sup>	S ext <sup>2</sup>	S main <sup>3</sup>	Pb/U	Pb/Th	age (Ma)
14-A	6.66	4.54	88.80	.10	0.82	611
14-H	7.60	3.34	89.06	.13	0.84	748
14-O	6.70	4.68	88.62	.12	0.99	694
14-R	7.90	4.70	87.40	.13	0.73	779
14-S	8.04	3.68	88.28	.11	0.70	631
24-D	5.45	5.13	89.50	.19	1.62	1110
30-1	5.89	3.85	90.42	.16	1.32	938
31-1	7.92	3.11	88.97	.13	1.11	791
32-A	7.41	2.28	90.31	.19	1.65	1146
D9-1	4.78	2.45	92.91	.15	0.82	904
D9-2	3.91	4.18	91.91	.19	1.67	1112
D9-3	6.26	2.54	91.30	.25	1.30	1481
D9-4	5.68	2.11	94.32	.28	1.66	1629
D9-7	4.69	3.32	92.12	.14	1.17	806

- notes: 1. H<sub>2</sub>O by difference of calculated oxides and 100%  
2. Subtotal of the extrenous oxides Na<sub>2</sub>O, Al<sub>2</sub>O<sub>3</sub>, SiO<sub>2</sub>, K<sub>2</sub>O, CaO, Fe<sub>2</sub>O<sub>3</sub> plus S  
3. Subtotal of the main oxides UO<sub>2-3</sub>, ThO, PbO





FIG. 20: DISTRIBUTION OF MAJOR AND MINOR OXIDES FOUND IN THE URANINITES FROM THE GREASE RIVER AREA





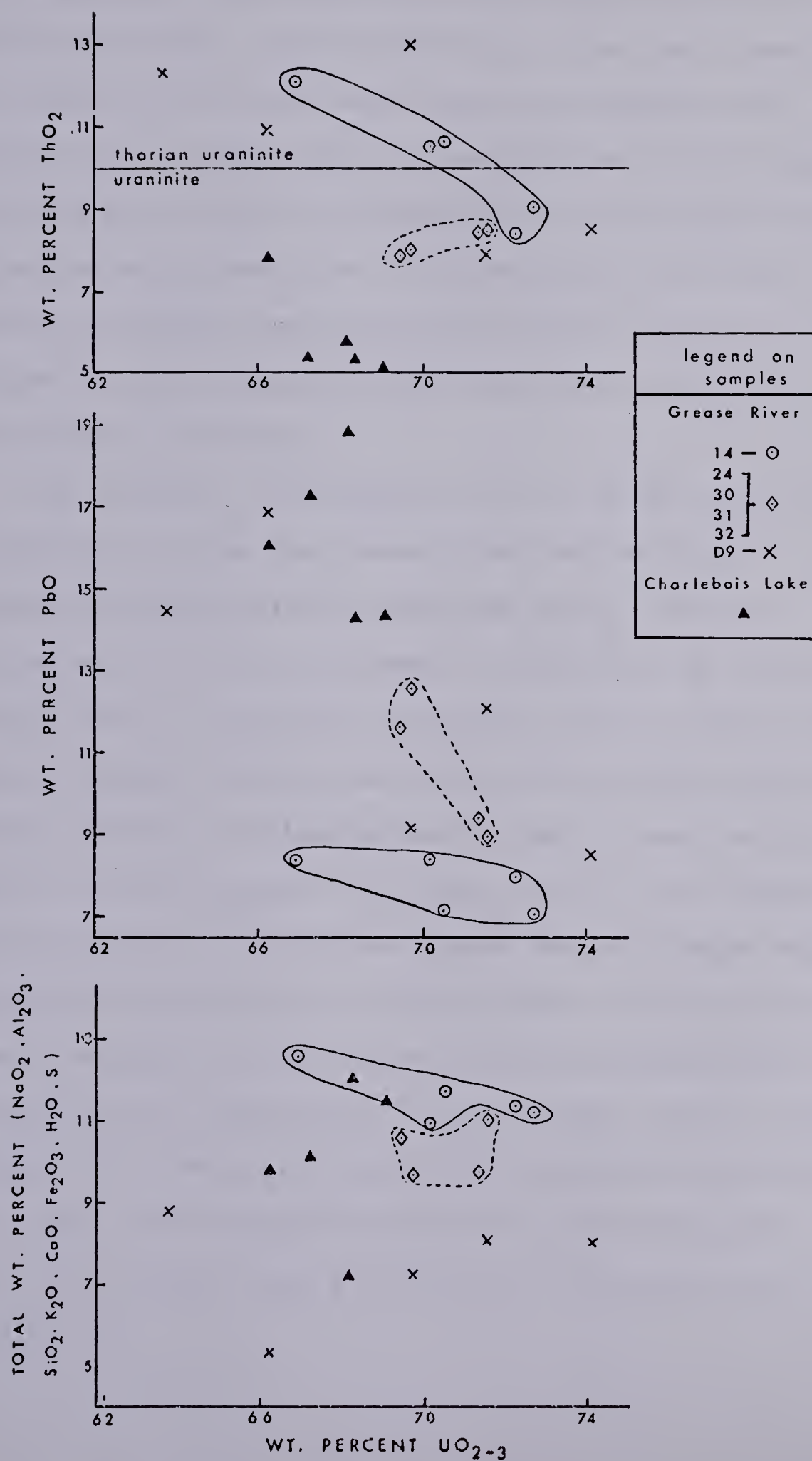
uraninites from the study area serve to categorize the uraninites probed. The plots of  $UO_2-3$  versus  $ThO_2$ ,  $PbO$ , and combined minor constituents plus  $H_2O$  are shown in Figures 21 a, b and c, respectively. Based on the distribution pattern obtained, the uraninites fall into three groups: (1) sample 14; (2) samples 24, 30, 31 and 32; (3) sample D9. The distinctive features of each of these groups are:

1. The sample 14 specimens are moderately high  $ThO_2$  and low  $PbO$  uraninites. The elevated Th contents are understandable since thorium minerals are found with these uraninites (Plate 11).
2. Reverse trends are indicated for uraninites from samples 24, 30, 31 and 32. Whereas their  $ThO_2$  concentrations are lower than the sample 14 specimens, they contain moderate amounts of  $PbO$  and secondary oxides.
3. The scatter of points obtained for the D9 uraninites are puzzling. No correlation is observed between the major U, Th and Pb oxide concentrations.

For comparative purposes, uraninites from chemically and geochronologically similar pegmatites from the Charlebois Lake area (Cameron-Schimann, 1978) have been plotted on Figure 21. These grains have lower  $ThO_2$  and  $UO_2-3$  contents than most of the uraninites from the thesis area. But more surprisingly, uraninites from Charlebois Lake have considerably higher  $PbO$  concentrations. These results are interpreted to mean that (1) radiogenic Pb has not migrated



FIG. 21: CHEMICAL TRENDS OF URANINITES IN  
PEGMATITES FROM GREASE RIVER AND  
CHARLEBOIS LAKE AREAS







out of the uraninites, or (2) initial contaminant Pb concentrations were higher in the samples from Clarlebois Lake. Conversely, the low PbO values for the Grease River area could imply that these grains have been more extensively altered. This is exemplified by the sample 14 uraninites that have unusually low PbO and high secondary oxide concentrations. The close proximity of trench 14 with zones of extensive silicification lends support to the suggestion that uraninite may have been disturbed by hydrothermal solutions.

The chemical inhomogeneity of U, Th and especially Pb in uraninites from the Grease River and elsewhere (Cameron-Schimann, 1978; Pavshukov et al. 1975) is recognized on the micron scale. Examination of the raw data accumulated by the author using WDA methods, shows that these elements can vary as much as 50 percent simply by moving the electron beam a few microns (these results do not appear in the chemical analyses). Proof of the density variability of U and Th atoms over the uraninite surface is provided in Plates 13, 14 and 15. The mobilization of uranium appears to be a major factor contributing to the alteration and breakdown of the uraninite grains. Despite evidence that Th-rich uraninites are chemically more stable than those with lower Th concentrations (Granstaff, 1976), this relationship does not hold for uraninites from the thesis area.



### C. Summary of Chapter VI

The origin of the uraniferous pegmatites at the main showing can be deduced from the mineral compositional analyses. The biotite chemical variability suggests that biotites in the discontinuous zone of pegmatites at the main showing have formed in several ways. The more Fe-rich grains are believed to be relict biotites from the pelitic gneisses. On the other hand, it appears that the Si and Al enriched biotites crystallized from the intruding trondhjemitic melt. The strong chloritization of the biotites at the main showing is evidence of hydrothermal alteration processes of the pegmatites and migmatites.

Zircon and uraninite analyses from pegmatites at the main showing reflect the same events. The extensively hydrated zircons coupled with severally altered uraninites are shown to be the result of alteration.

Conversely, the D9 pegmatite mineral analyses show that alteration processes have been minimal in that region of the Grease River property. The fresh biotites are closely associated with zircons low in zirconium and high in CaO and H<sub>2</sub>O. The uraninites found here are the least altered grains probed by the author. These results imply that the trondhjemitic melt enriched in uranium, was consolidated and left essentially undisturbed by later corroding solutions.



## **VII. Uranium Mineralization in the Grease River Area**

Since their discovery in the 1950's, the pegmatitic uranium occurrences in the Grease River area have been prospected a number of times. As outlined in Chapter I, radiometric surveys and U3O8 assay tests were carried out by the following: Al Hemingson, Fosago Limited, Geological Survey of Canada and Urangesellschaft. The radiometric surveys conducted on the property have included airborne spectrometer as well as ground scintillometer and spectrometer measurements.

Inasmuch as Urangesellschaft's involvement in the thesis area produced the most detailed evaluation of the uranium mineralization on the Grease River property, their results released in Beesley's 1977 report will be reviewed in part A of this chapter. In part B, Urangesellschaft's exploration findings and economic assessment of the property will be interpreted in regards to the petrology and geology of the area. In part C, similar uraniferous pegmatite occurrences throughout the world will be discussed.

### **A. Radiometric Survey, Ore Grades and Economic Potential of the Grease River Property**

Urangesellschaft's airborne spectrometer survey of 1976 indicated numerous radiometric anomalies at the Grease River property main showing. The follow-up geologic and radiometric field work run the same season included these





methods: 1. a grid-pattern scintillometric survey of the main showing; 2. a spectrometer survey of the trenches; 3. collection of trench chip samples for U308 assay.

The scintillometric survey was conducted with a BGL-1SL scintillometer. Readings were taken every three meters along the 040 and 025 baselines and the perpendicular secondary lines. The scintillometer responses represent the total gamma radiation in counts per second (c.p.s.) emitted predominantly from K + U + Th atoms in the various rock types. The anomalies discovered were categorized as follows: weak (500-1000 c.p.s.), moderate (1000-2000 c.p.s.), and strong (2000-4000 c.p.s.).

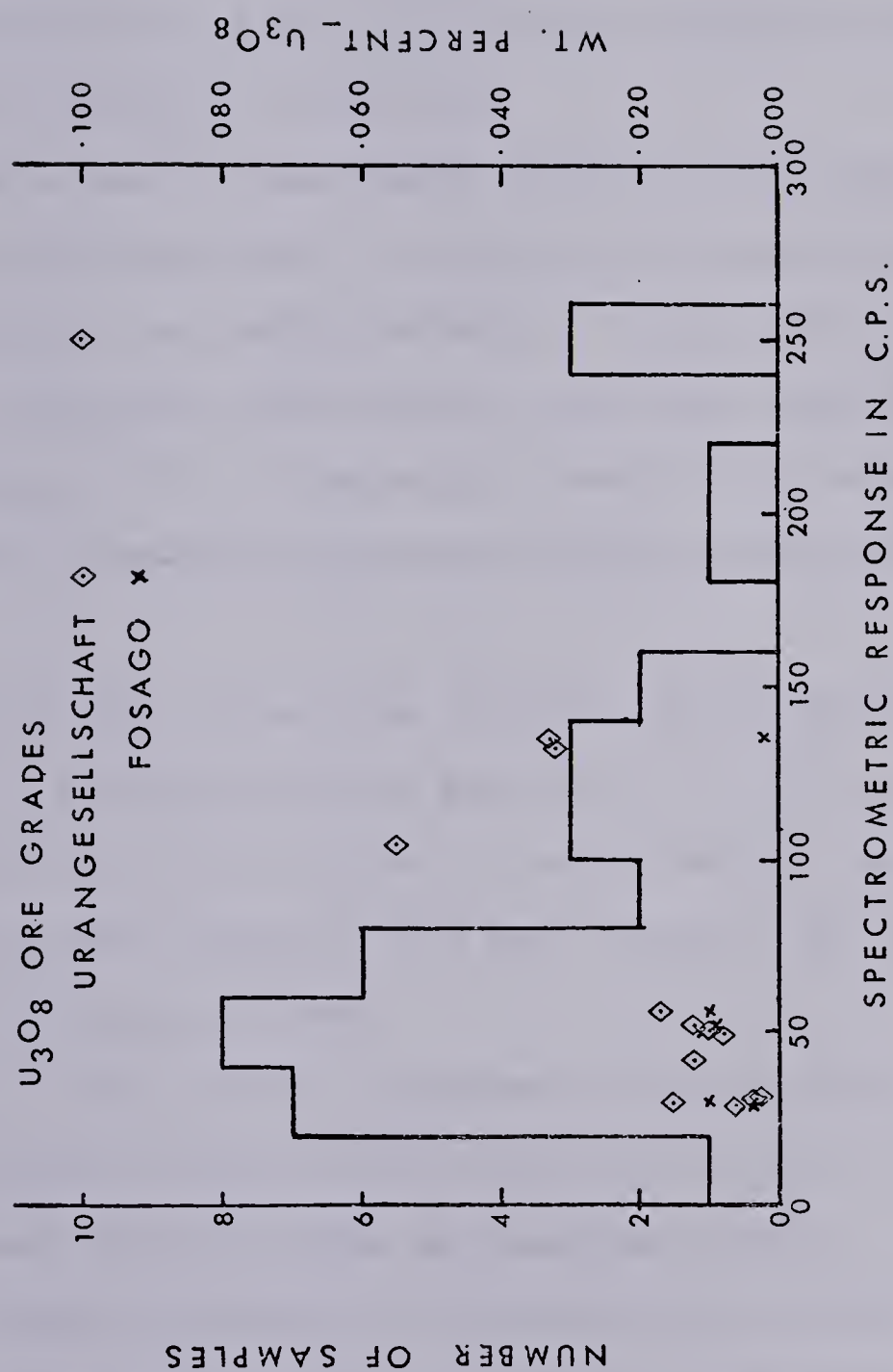
Subsequent to the grid survey of the main showing, a total of 279 scintillometric anomalies have been discovered (Map 3). The proportion of weak, moderate and strong responses are 70, 26 and 4 percent, respectively. Although the moderate and strong responses occur over the entire length of exposed bedrock at the main showing, they do appear to be slightly concentrated in the central portion along the 040 baseline.

Results from Urangesellschaft's (Beesley, 1977) spectrometer survey of the trenches on the Grease River property are also indicated in Map 3. The spectrometer responses (in c.p.s.) are an average of the gamma radiation emitted from only U + Th atoms over a given interval.

A histogram of the spectrometer results (Figure 22) denotes a range of values from 10 to 251 c.p.s. with the



FIG. 22 : HISTOGRAM OF THE SPECTROMETRIC RESULTS AND  $U_3O_8$  ASSAYS FOR TRENCHES SURVEYED, GREASE RIVER PROPERTY





distribution of responses skewed to the lower end. A comparison of Figure 22 and Map 3 reveals that the majority of trenches with values less than 100 c.p.s. are adjacent to the 040 baseline. In contrast, trenches with spectrometer readings greater than 100 c.p.s. are predominantly located along the southeastern margin of the main showing in the vicinities of locations 12 and 27.

Urangesellschaft's U308 assay results determined on chip samples collected from 15 trenches are indicated in Map 3. The ore grades are listed in Table 14 along with the spectrometer responses and Fosago's U308 assay results (Folinsbee et al. 1974). Geochemical results for trenches sampled by both companies correlate closely except for location C.

U308 ore grades range from .003 to .099 percent and calculate to a weighted average ore grade of .0157 percent U308. Trenches 12, 15, C, 21 and 27 all of which are located on the southeastern margin of the main showing (see Map 3) have above .022 percent U308.

Beesley's 1977 economic assessment of the Grease River property includes an estimate of the U308 reserves minable on the property. The principal mineralized zone as determined through radiometric and geochemical surveys is approximately 500 meters long and 66 meters wide and comprised of less than 50 percent of anomalous white pegmatite (Maps 1 and 3).

Using an average ore grade of .0157 percent U308, an





Table 14: Average grade (%  $U_3O_8$ ) and spectrometric results for trenches in white pegmatite

trench	sample length feet	average grade % $U_3O_8$ <sup>1</sup> ( ) <sup>2</sup>	spectrometer reading U + Th c.p.s.
1	18	.012 (.009)	52
2	17	.008 (.011)	50
3	62	.017 (.010)	56
A	7	.003	32
7	25	.012	42
B	5	n.d. <sup>3</sup> (.004)	29
8	4	.006	29
12	7	.099	251
14	10	n.d.	123
15	7	.055	106
16	7	n.d.	197
16	6	n.d.	190
18	28	.015 (.010)	30
C	7	.033 (.002)	135
D	8	n.d.	246
19	52	.003	31
21	29	.022	140
23	40	.010	51
27	13	.032	132
E	4	n.d.	107
29	5	n.d.	241
30	5	n.d.	145
32	5	n.d.	118
33	10	.007	39
34	6	n.d.	209
assay range		.003-.099 (.004-.011)	
average grade		.0157	

Notes: 1. Results from Urangesellschaft (Beesley, 1977). 2. Results from Fosago (Donaghy, 1976) 3. n.d. denotes not determined.



estimated 2386 kilograms (2.63 short tons) of ore per vertical .305 meter (1 foot) are projected from a total  $6.6 \times 10^7$  kilograms (15,000 tons) of rock. Thus, if the property were developed to a depth of 61 meters (200 feet) by conventional open pit mining, Urangesellschaft proposes that a total of  $.43 \times 10^6$  kilograms (471 tons) U<sub>3</sub>O<sub>8</sub> would be minable if surface ore grades were reflected in the subsurface. With such low U<sub>3</sub>O<sub>8</sub> grades and estimated tonnages, the Grease River property is sub-economical at today's world prices for uranium [\$43.40 US per .454 kilogram (1 pound) U<sub>3</sub>O<sub>8</sub> : spot price, Northern Miner, July 1978]

## B. Discussion of the Geology and Economic Evaluation of the Grease River Property

Several points are inferred from Urangesellschaft's radiometric and U<sub>3</sub>O<sub>8</sub> assay results. The most significant include:

1. A negative correlation between the scintillometer and spectrometer results, thus implying that zones of K-enrichment do not coincide with zones of U + Th mineralization.
2. The skewed bimodal distribution of spectrometer values is caused by two periods of mineralization.
3. Parallel trends between U<sub>3</sub>O<sub>8</sub> grades and U + Th spectrometer responses suggests that uranium is the major radioactive ore element.
4. Trenches with high ore grades and spectrometer



responses border the southeastern margin of the main showing, and therefore reflected possible structural control of the mineralization.

These exploration findings are in agreement with the geology of the Grease River property. First, the areas characterized with high scintillometric, and low spectrometer responses and U308 contents, are underlain by microcline-rich alaskite and two-feldspar granite pegmatities. Petrological examination shows that these potash-rich white pegmatites are frequently very coarse-grained and containing graphic granite textures, but are seldomly mineralized. Consequently, they contain few of the accessory minerals (zircon, sphene, apatite, thorite, molybdenite) commonly found with uranium-rich phases.

Second, petrological and geochronological findings correlate with the trench spectrometer results (see Figure 22) which have been interpreted as resulting from two periods of mineralization. The lower values (up to 120 c.p.c.) would appear to reflect the uranium occurring in the trondhjemitic pegmatites which were emplaced around 1940 Ma. Proof that uranium did occur in the initial melt is provided by the close relationship observed between the uraninite and the other minerals known to crystallize out both early and at high temperatures during the cooling histories of similar granitoid melts (Berry et al. 1959). The associated minerals include plagioclase, biotite, zircon, allanite, sphene molybdenite, magnetite and ilmenite.





The second period of uranium mineralization is believed to be reflected by the higher spectrometric responses, occurred during the youngest Hudsonian event dated (at 1840 Ma) in the thesis area. At that time, quartz ± muscovite bearing solutions intruded both pegmatitic and migmatitic assemblages, thus producing the quartz-rich granitoid and quartzolite rocks. In these rocks, which incidently have been collected from the most radioactive trenches subsequently surveyed by Urangesellschaft, the following geological findings suggest that the quartz-precipitating solutions were hot, corrosive and U-bearing:

1. surfaces of the zircon phases are extensively etched.
2. zircons, or cyrtolites contain up to 0.78 percent U (see Chapter V) which is believed to have been partially removed from the Si-rich solutions.
3. ubiquitous dark, smoky coloured quartz is evidence of anomalous quantities of radioactivity in the rocks.

The uranium enrichment accompanying this last intrusive phase in the development of the white pegmatites is recognized by Bibikova (1977) and Zhukova *et al.* (1975) as a common occurrence in magmatic rocks of granitoid composition.

In summary, the most radioactive zones have been delineated as several pegmatite lenses probably in the order of 3 to 7 meters in diameter and of irregular shape. Their



apparent distribution on the southeastern flank of the main showing suggests a partial involvement of structural controls. The rocks are generally trondhjemitic or quartz-rich white pegmatites and containing between .022 and .099 percent U<sub>3</sub>O<sub>8</sub>.

A more complete evaluation of the Grease River property is possible following geological research conducted by Donaghy (1975, 1976) and the author. These studies indicate that the uranium in the pegmatitic and migmatitic rocks can be concentrated rather easily. The radioactive minerals (uraninite, uranothorite and zircon) are readily set free by crushing the rock to an average grain size of 0.5 mm. Further concentration of the radioactive phases is accomplished using heavy liquid. Here, even the rock fragments coated with secondary yellow U<sup>6</sup> mineralization are isolated. These results imply that the radioactive rocks in the study area could be up-graded with relatively simple milling procedures, should ever they be mined.

The heavy mineral studies indicate that processing of the uranium ore would be facilitated by the ease with which uranium dissolves in acid solutions. Results indicated that uranium from uraninite and the secondary ore minerals is solubilized in heated 10 N H<sub>2</sub>SO<sub>4</sub>, HNO<sub>3</sub> and HCl solutions. Similarly, it appears that the radioactive zircons, which are metamict and, therefore, susceptible to chemical attack, could be treated with slightly hotter and stronger acid solutions. Uranium extraction processes comparable to those



discussed for the Grease River area pegmatites are presently being used on the Rossing uranium deposit (Berning et al. 1976) .

### C. Comparison with Similar Pegmatitic Uranium Occurrences

Syngenetic uranium occurrences in pegmatitic rocks originate from either primary igneous differentiates or metamorphic, anatectic melts (Bowie, 1970; Little, 1970; McMillan, 1978; Ruzicka 1971, 1975) . The carbonatite and peralkaline syenite deposits occurring at Oka, Gabon, and Ilimaussaq, Greenland, respectively, are examples of the igneous type. On the other hand, deposits of metamorphic origin include large granitic bodies (Baie Johan Beetz, Que.), pegmatites (Bancroft, Ont.), porphyries (Rossing, S.W.A.) and metasomatites (Charlebois Lake, Sask.) .

Many of the pegmatitic uranium occurrences of metamorphic origin have been described by Page (1950), Klepper et al. (1956), Heinrich (1958), Hauseux (1976), Roubault (1958) and Tatsch (1976) . These pegmatites contain higher concentrations of U than normal granitic rocks (2.2 to 15 ppm U: Rich et al. 1977) . The significant features ascribed to most of these mineralized rocks included the following:

1. they are often products of dynamothermal metamorphic events occurring during Precambrian time
2. they frequently intrude metasedimentary assemblages of granulite or amphibolite facies grade





3. they are closely associated with large, potassic or sodic granite bodies which are commonly red in colour
4. they appear as pegmatitic dyke, lense, pod, lit-par-lit and layer forms throughout a metamorphic belt and may be found in both the metamorphic assemblages and igneous differentiates
5. mineralization is variable: U is often the major element but may co-exist with unpredictable quantities of Th, Mo, Ti, Zr, RE, Nb, F, S, Cu, P.
6. uranium is generally disseminated throughout the coarser-grained fractions which are not always mineralized.
7. uraninite is the most common ore mineral but other uraniferous minerals include uranothorite, thorite, thorianite, allanite, zircon (cyrtolite), monazite
8. other characteristic minerals are sphene, apatite, molybdenite, magnetite, quartz, biotite, amphibole and pyroxene.

Parallel trends existing between the typical metamorphic occurrences described above and the Grease River area uraniferous pegmatites studied in this thesis, suggest that they are of similar origins. Although, evidence supporting this statement is given in the preceding chapters, the most important facts will be summarized here:

1. intrusion of the white pegmatites into amphibolite facies biotite gneiss.



2. pink granitic rocks underlying the principal radioactive zone.
3. unzoned granitoid pegmatites of both simple composition and mineralogy.
4. disseminated U-mineralization occurring with variable quantities of Th, Zr, Ti, Fe and Mo.

Numerous pegmatitic uranium occurrences with similar characteristics have been discovered in northern Saskatchewan. Most occur west of the Needle Falls Shear Zone (see Figure 2) in a region which may be termed as a uranium province according to Klepper's 1956 classification. Here, anomalous concentrations of uranium and an abundance of rich U-deposits have been discovered.

In this region underlain by the Western Craton and the Cree Lake Zone, most mineralized pegmatites have been derived by the metamorphic segregation or anatexis of metasediments. According to Beck (1966), Burwash (1979), Koepfel (1968), Tremblay (1972) and Sibbald et al. (1976), uranium (and thorium) were concentrated into anatectic fractions formed during the Kenoran and Hudsonian orogenies. Sibbald et al. (1976) has classified the resulting pegmatites into two types: Archean and Aphebian.

Radioactive pegmatites in the Aphebian Cree Lake zone are concentrated in the Mudjatic Domain, Wollaston Domain and Charlebois Lake area (see Figure 2). The North



Blackstone Lake pegmatites occurring in the Mudjatic Hudsonian mobile zone (Sibbald et al. 1976) are coarse-grained mineralized layers and lenses of biotite granite and leucogranite. They have formed from the large, more calcic and felsic gneisses which host them. Average ore grades are between 15 to 25 ppm U with occasional samples yielding 1100 ppm U (Sibbald et al. 1976).

In the Charlebois Lake area, radioactive granodioritic granofels are associated with Aphebian age amphibolite facies metasediments (Morra, 1977; Mawdsley, 1957). The fourteen deposits discovered are peripheral to large granitic and tonalitic gneissic domes, and are metasomatic in origin. The mineralization occurs primarily as uraninite crystals which are closely associated with large books of biotite. Grades obtained for the granodiorite reach .84 percent U<sub>308</sub>. Other mineralized lithologies adjacent to the principal rock type include: migmatites and biotite gneisses (up to .16 percent U<sub>308</sub>) and granitic gneiss (up to .01 percent U<sub>308</sub>).

In the Western Craton, uraniferous pegmatoids in the Archean basement gneisses are exposed at Cluff Lake (Harper, 1978). These pegmatites are associated with red quartzo-feldspathic gneisses which have even better ore grades (.83 percent U<sub>308</sub> and .24 percent Th) than the pegmatites. Together, these felsic units are analogous to the granitic gneisses and white pegmatites found on the Grease River property. In both areas, the Archean crust was





remobilized and the uranium concentrations were up-graded during the Hudsonian orogeny.

Although many similar granitic and pegmatitic uranium occurrences have been discovered throughout the world (Page, 1950; Heinrich, 1958; Tatsch, 1976), only a few have been economical enough to have been mined. Periodically, the uranium deposits in Madagascar have been worked, but the remaining reserves are not significant (Heinrich, 1958).

Until recently, the uranium deposits in the Bancroft mining district were the only pegmatites to have been mined extensively. A combination of high grades (.11 percent  $U_3O_8$ : Bowie, 1970) and tonnages, and relatively easy mining and milling procedures (facilitated by exceptionally coarse-grained minerals) have been important in the exploitation of these ores (Lang *et al.* 1962).

In 1978, another syngenetic uranium deposit started production. The Rossing deposit in South West Africa is presently the world's largest (Barnaby, 1978) but lowest-grade uranium deposit ever to be mined. The deposit has been described as a porphyry type. The uranium ore is hosted in pegmatitic alaskite lenses which preferentially intrude pyroxene-garnet gneiss, amphibole-biotite schist, and marbles (Bailey *et al.* 1977). The ore mineralogy is typical of uranium deposits of metamorphic origin with accessory monazite, betafite, zircon, apatite and sphene occurring with uraninite. An estimated  $.14 \times 10^9$  kg  $U_3O_8$  equivalent to 150,000 tons at .035 percent  $U_3O_8$  are reported



to be contained within the white pegmatites (Bailey et al. 1977).

In having briefly described the ore grades and tonnages of several uranium occurrences, we see that the Grease River area pegmatites are presently uneconomical.



### VIII. Summary and Conclusion

The geological events recognized in the Grease River area in northern Saskatchewan are indicated in Table 15. The Tazin Group biotite gneiss and pink granitic gneiss occurring in the Grease River linear belt were regionally metamorphosed to middle amphibolite facies. Petrologic evidences and field relationships between the pelitic and felsic gneisses indicate that the felsic component was generated at depth and later intruded into the biotite gneisses. The gneisses give U-Pb dates of 2250 Ma and thus imply that the regional metamorphic event occurred during the Kenoran orogeny.

The white pegmatites which intruded and migmatized the gneisses at the main showing were generated as a result of anatexis in the Archean basement. Three distinct phases of intrusion are recognized on the basis of petrological, geochronological and geochemical results. From the trondhjemitic melt associated with the initial emplacement of the pegmatites, a plagioclase + quartz + biotite mineral assemblage was precipitated. K-metasomatism solutions infiltrated most of the pegmatites, thus transforming them into two-feldspar granite and alaskite granite pegmatites. A quartz enrichment of the pegmatites in several places at the main showing occurred as a result of hydrothermal activity. Extensive propylitic and intermediate argillic alteration of primarily the granitic pegmatites occurred at the time of silification.





Table 15

Time Stratigraphic Sequence of EventsGrease River Area, N. Saskatchewan

<u>Period</u>	<u>Time (Ma)</u>	<u>Geologic Event</u>
Recent	$1000 \times 10^{-3}$	
Paleohelikian	1700	deposition of Athabasca Formation; uplifting, erosion, faulting.
Late Hudsonian	1840	orogenic reactivation associated with silicification and uranium mobilization.
Early Hudsonian	1970	intrusion of radioactive syntectonic white pegmatites and local thermal metamorphism of Tazin Group biotite gneisses; faulting, cataclasis with reactivation of the craton.
Kenoran	2600	metamorphism of Tazin Group meta-sediments with intrusion of granite plutons; possibility of concentration of U + Th into the granitic rocks.



In the Grease River linear belt, extensive faulting and shearing occurred in the Tazin Group complexes during the emplacement of the white pegmatites. Near vertical major faults acted as channel ways in the transport of magma and hydrothermal solutions into the granitic and biotite gneisses presently exposed at the main showing. Critical evidence suggesting some fault control on the emplacement of the white pegmatites is provided by the fact that (1) faults occur in the immediate area and (2) trondhjemitic melt whose minimum temperature was 685°C intruded relatively cool metasediments, thereby implying rapid movement of magma over considerable distances.

The source of the white pegmatites is deduced to be partially magmatic (from anatexis of Archean granitoid rocks occurring at depth) and partially as a result of the local assimilation of gneissic material at a higher structural level (ie. exposed at the main showing).

On the contrary, the principal source of uranium in the mineralized white pegmatites appears to be magmatic and hydrothermal in origin. This is suggested since all of the radioactive anomalies discovered at the Grease River property occur in the trondhjemitic and quartz-rich white pegmatites. Furthermore, the yellow euhedral granite zircons which are associated with uraninite, are enriched in uranium and occur only in the white pegmatites. Similarly, the accessory molybdenite, uranothorianite, blue apatite, sphene and iron minerals found with uraninite and zircon are



restricted to the white pegmatites.

During the Kenoran orogeny (app. 2500 Ma), this portion of the Archean craton is believed to have been regionally metamorphosed. The development of pink felsic gneisses occurred during this time as a result of anatexis of the crust. Later during the Hudsonian orogeny, similar melting occurred in this part of the Churchill structural province. The wide-spread distribution of massive, K-rich pegmatites and migmatites in the metasedimentary rocks is evidence of local anatexis of the basement rocks.









## PHOTOGRAPHIC PLATES

Abbreviations used in the Photographic Plates

ALL - allanite  
BIO - biotite  
bs - backscatter electron  
E.T. - exposure time to radioluxographic film  
KF - potassium feldspar  
MOLY - molybdenite  
PL - plagioclase feldspar  
Q - quartz  
RECRY - recrystallized  
U - uranium rich grains  
URAN - uraninite  
TH - thorium rich grains  
Z - zircon



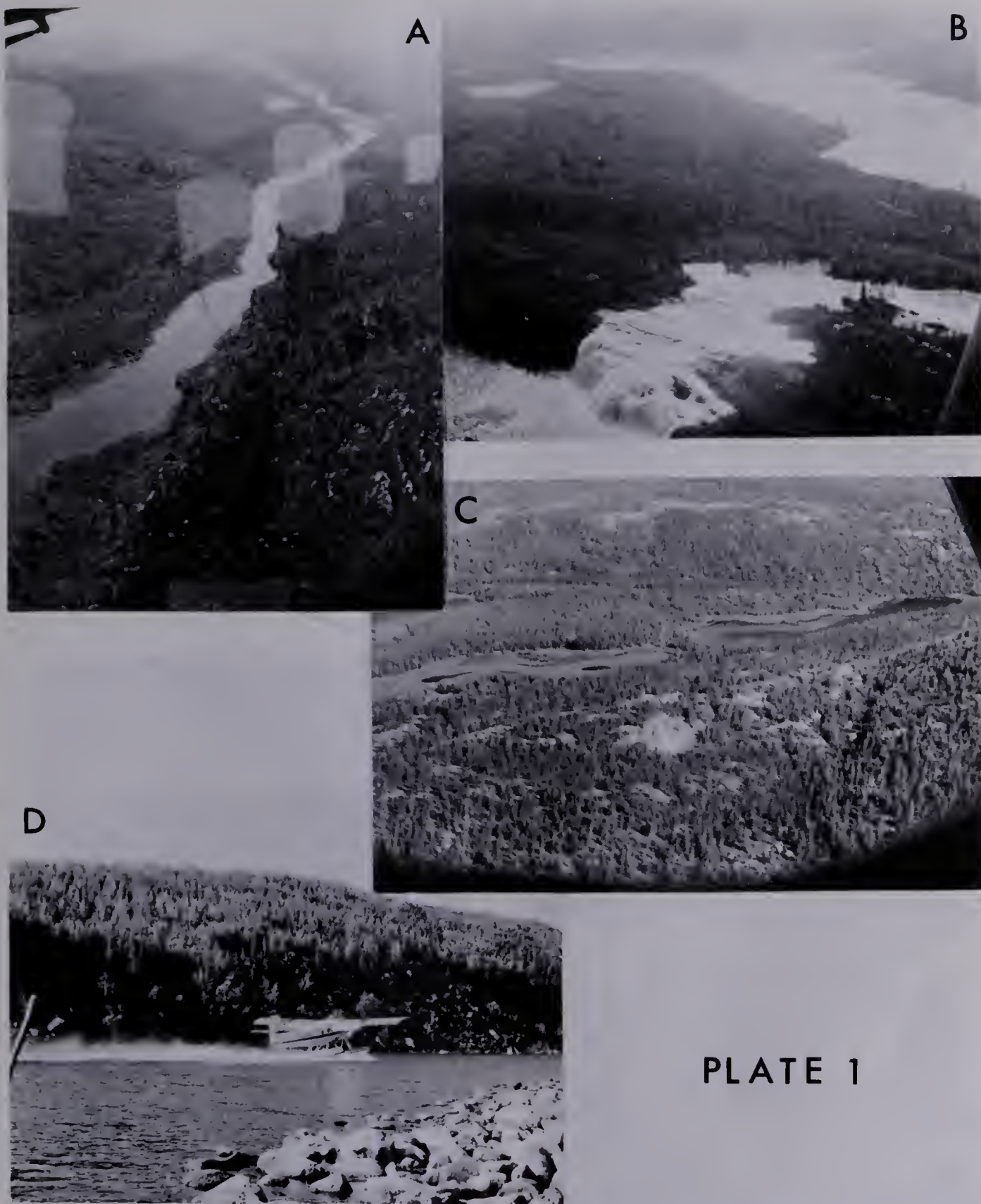


## PLATE 1

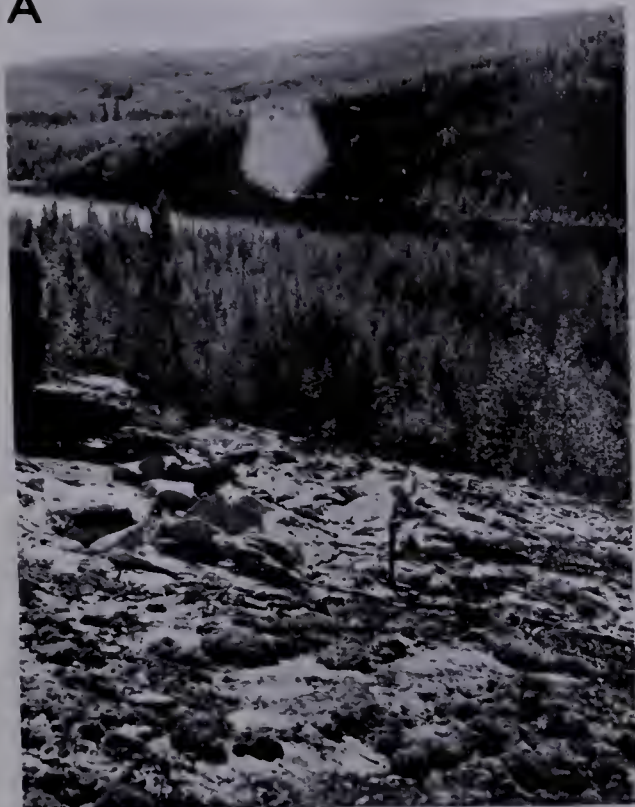
Photographs of the Grease River Area. A. Looking NE along the Grease River fault valley. The main showing occurs in claim blocks CBS 2745 and CBS 5398 (foreground) and the G.S.C. anomaly occurs in claim blocks CBS 3424 (background). B. Looking SW of claim block 2745 at Lefty's Falls. C. Looking SE at the main showing. Trenches 17 and 18 occur in the tree-barren outcrop. D. Looking NW across the Grease River at the relatively steep shoreline formed by the Tazin Group meta-sediments.





## PLATE 2

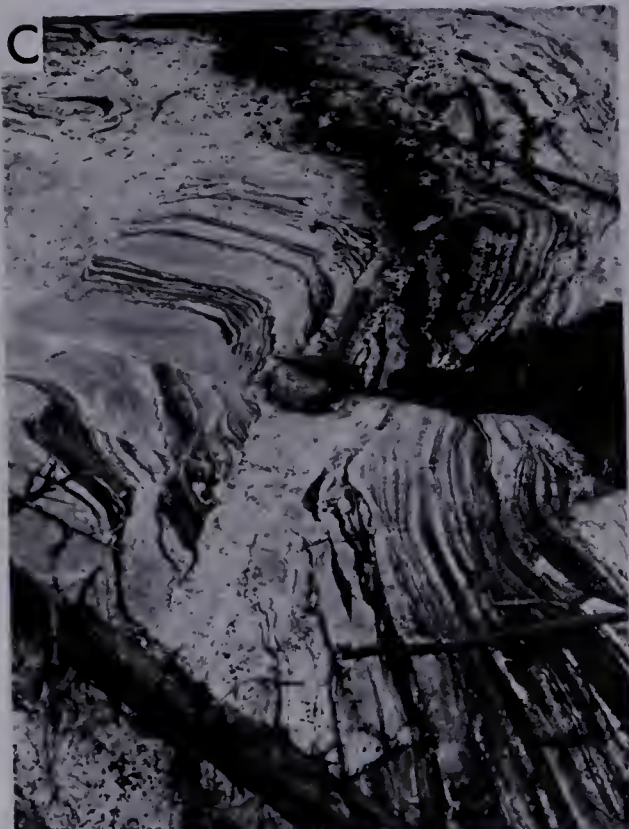
A



B



C



D



Photographs illustrating field relationships. A. Pink to white granitic pegmatite occurring at trench 18. B. The relationship between granitized biotite gneiss and intruding white pegmatite. C. Cross-cutting, white pegmatite mixing with paleosome from the gneissic xenolith blocks. D. Tazin Group biotite gneiss with small parallel felsic stringers related to faulting.





# PLATE 3

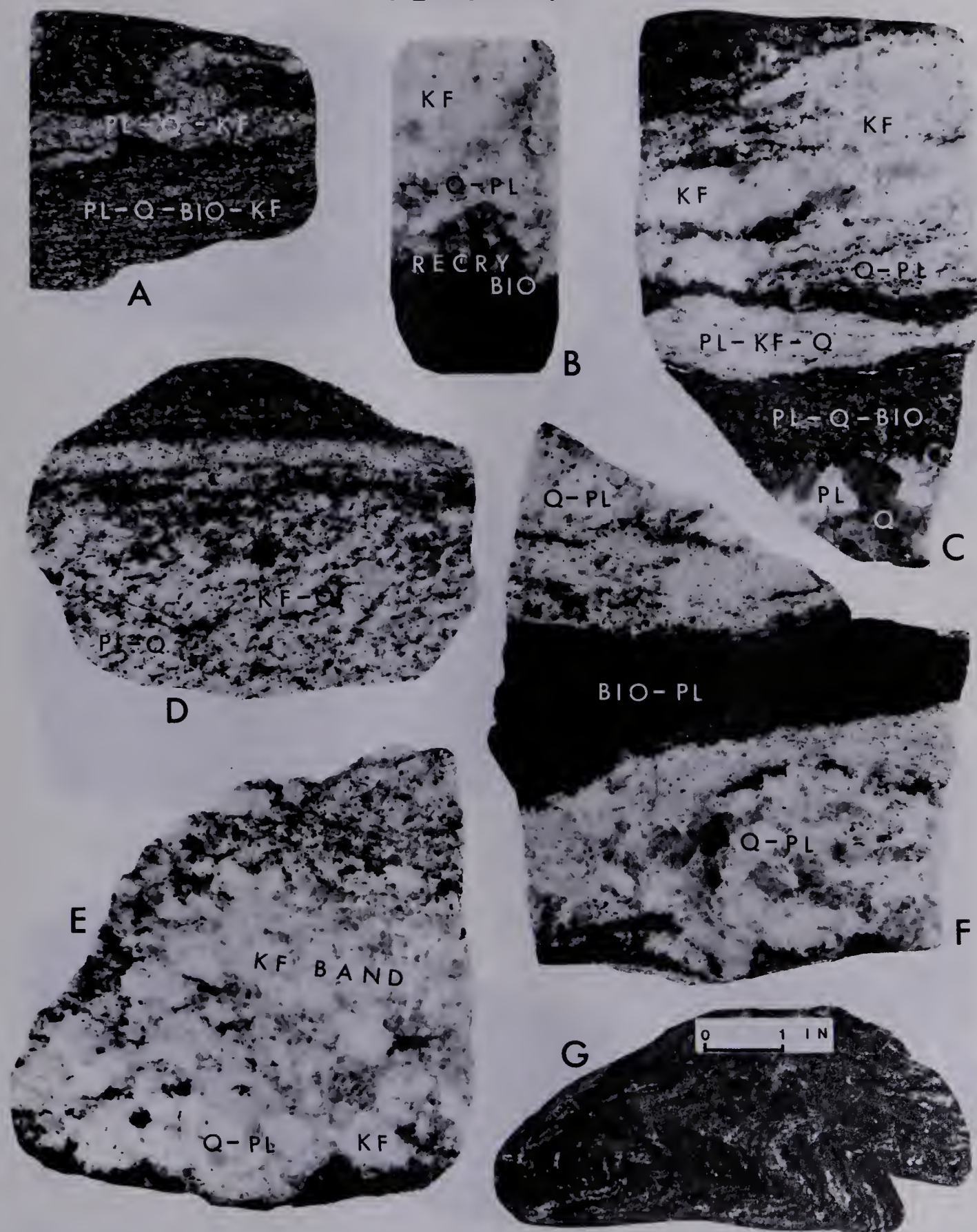


Photographs illustrating field relationships. A. Tazin Group metasediments tightly folded. B. Uniformly banded biotite gneiss away from the migmatized zone. C. Boudinaged and contorted xenoliths of migmatized biotite gneiss. D. Blocks of banded gneiss rotated 90 degrees by the intruding white pegmatite.





# PLATE 4



Photographs of migmatized biotite gneiss. Scale 1x except G. A. No 9. Folding and associated granitization of the gneiss. B. No 8. Note biotite recrystallized along the pegmatite/gneiss contact. C. No 10. Note the variations in grain size and degree of K-metasomatism. D. No 17. K-feldspar blastesis in the leucocratic band. E. No 22. Development of potash-feldspar bands in this migmatized gneiss. F. No 27. Trondhjemitic white pegmatite infiltrating gneissic layers. G. No 22. Folded biotite-rich gneiss.

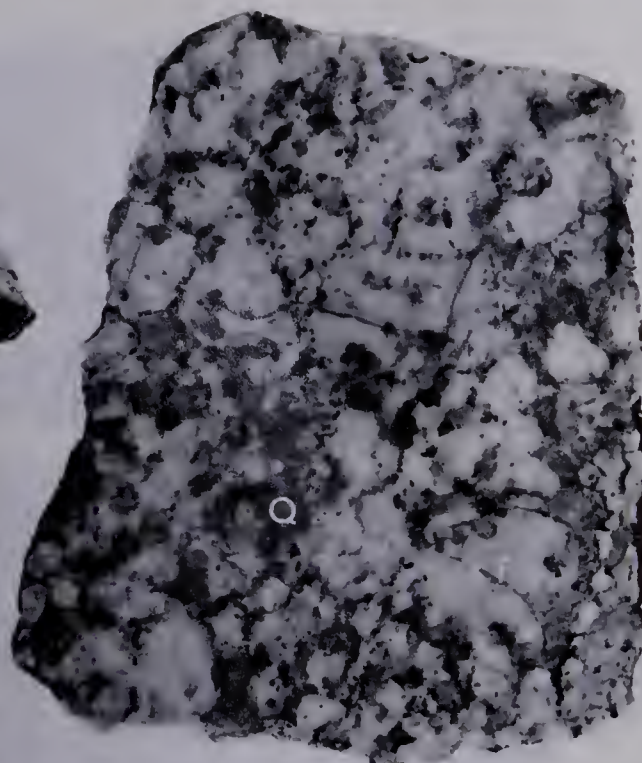




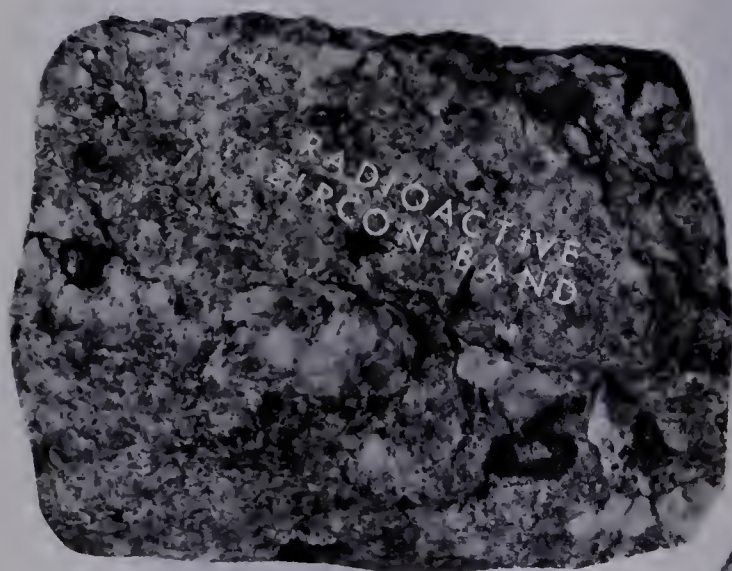
# PLATE 5



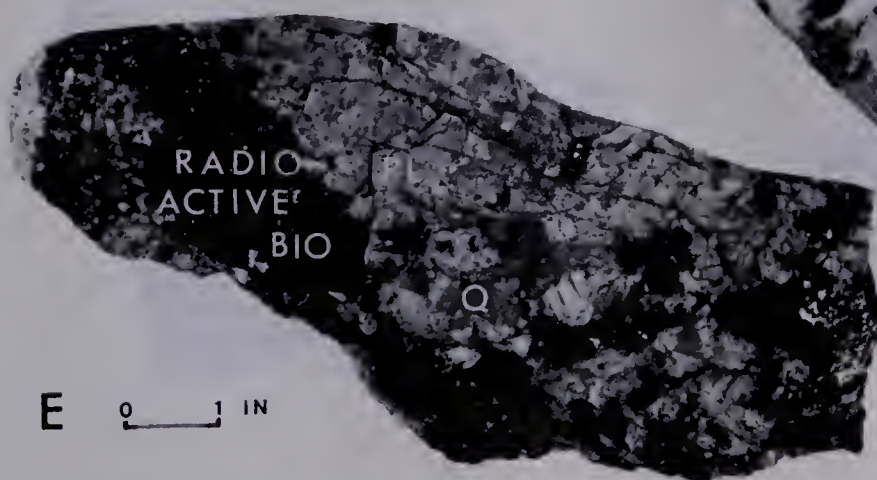
A 0 1 IN



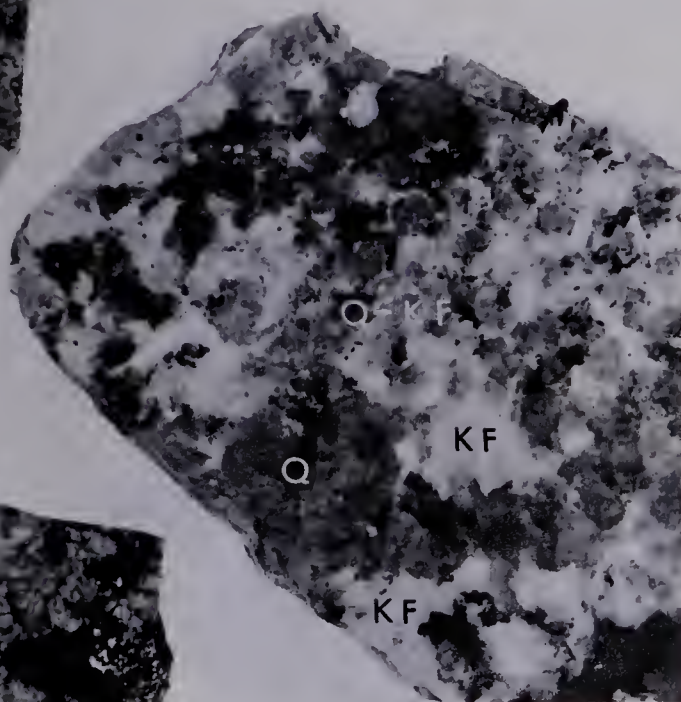
B 0 1 IN



C 0 1 IN



E 0 1 IN



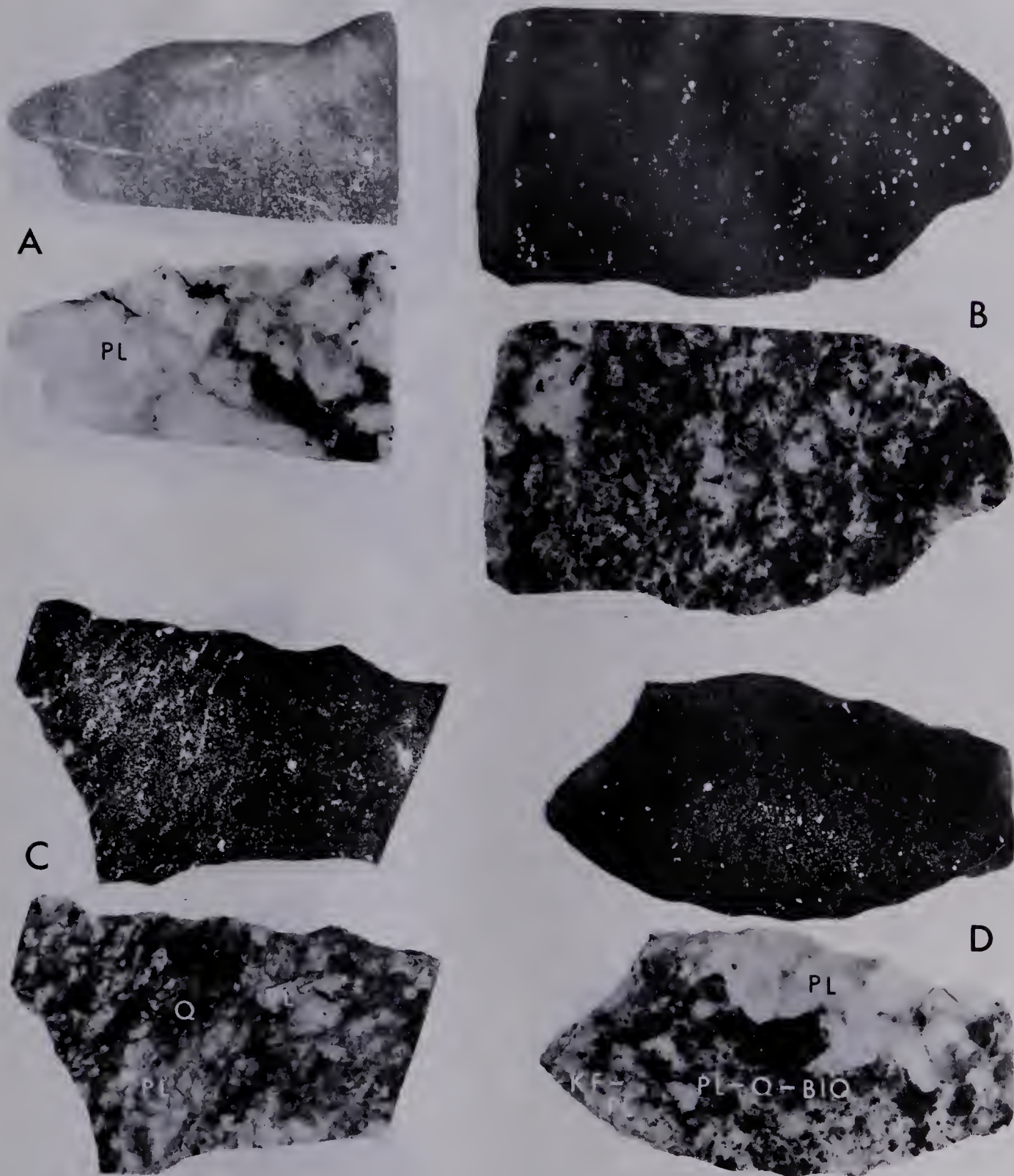
D 0 1 IN

Photographs of White Pegmatite. A. No 2. V. coarse-grained alkali-feldspar granite. Sl. radioactivity. B. No 5. Coarse-grained granofels of granite composition. C. No. 6. Sheared quartz-rich granitoid rock containing radioactive zircons and secondary mineralization. D. No 21. K-feldspar quartz-rich granitoid granofels. E. No D9. Radioactive trondhemitic pegmatite.





# PLATE 6

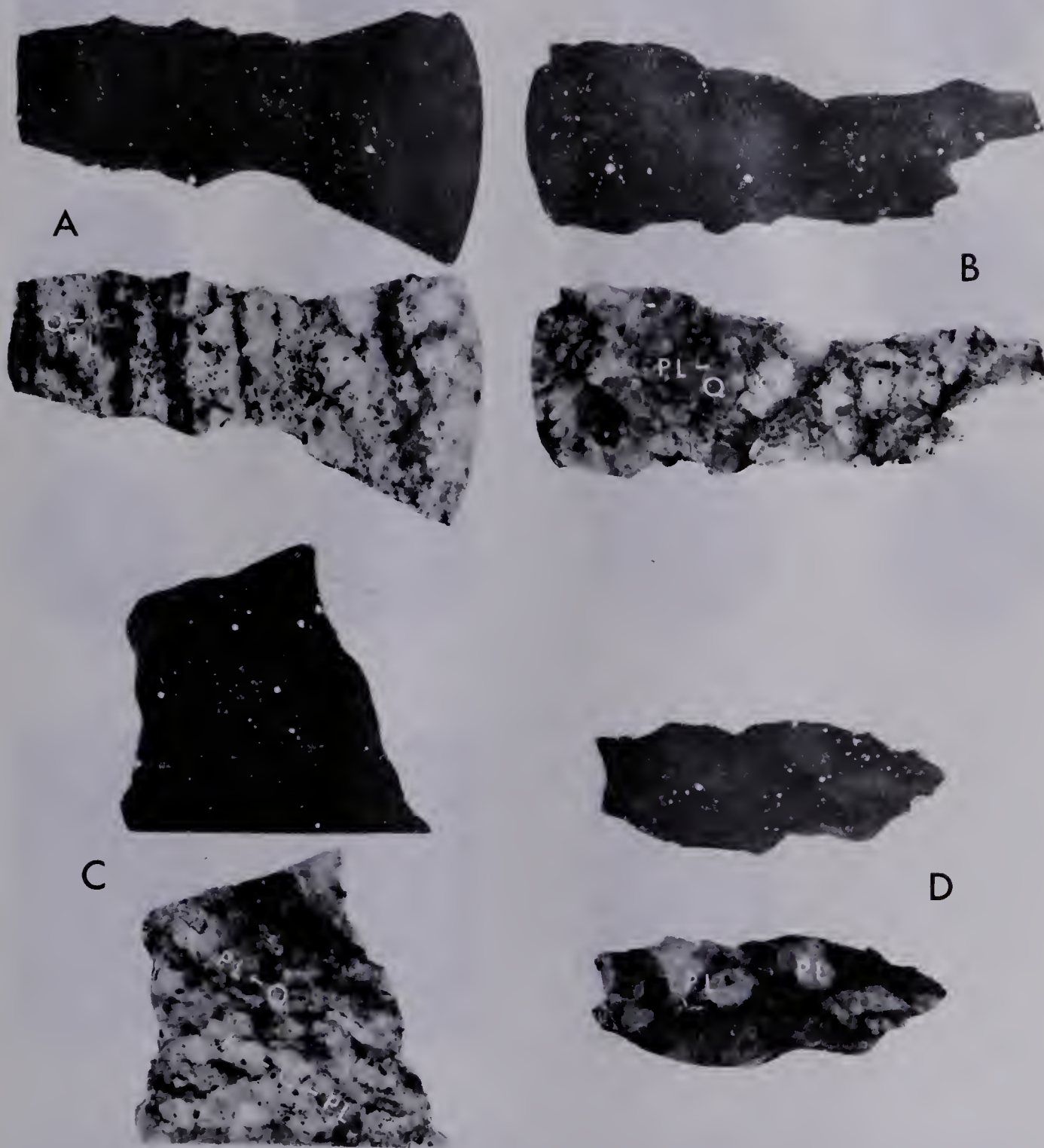


Photographs and radioluxographs of radioactive samples. Scale 1x.

A. No 1. E.T.-10 hrs. Primary and secondary (along cracks) radioactivity. B. No 14. E.T.-2 hrs. Scattered primary mineralization confined mostly to darker quartz-rich area. C. No 15. E.T.-21 hrs. Uraninite and zircon bearing quartz-rich granitoid migmatite. D. No 17. E.T.-29 hrs. Zircon and allanite bearing granite migmatite dated at 2230 Ma.



# PLATE 7

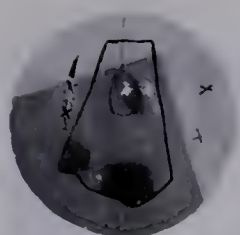


Photographs and radioluxographs of radioactive samples. Scale 1x.  
 A. No 20. E.T.-36 hrs. Granitized gneiss slightly mineralized.  
 B. No 24. E.T.-7 hrs. Isolated uraninite grains somewhat aligned  
 along a fracture. C. No 30. E.T.-3 hrs. Scattered radioactivity  
 in the bic-plag-qtz portions. D. No D9. E.T.-1.5 hrs. Uraninite  
 associated with biotite books in trondhjemitic pegmatite.





## PLATE 8



10



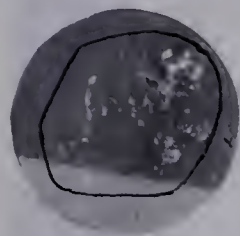
12



14



15



7615



18



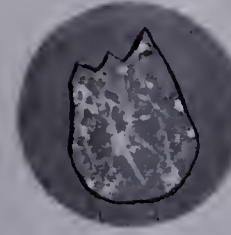
24



30



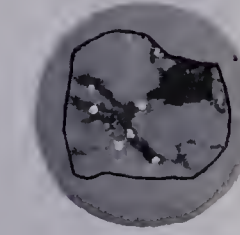
31



32



34



D9



14



15



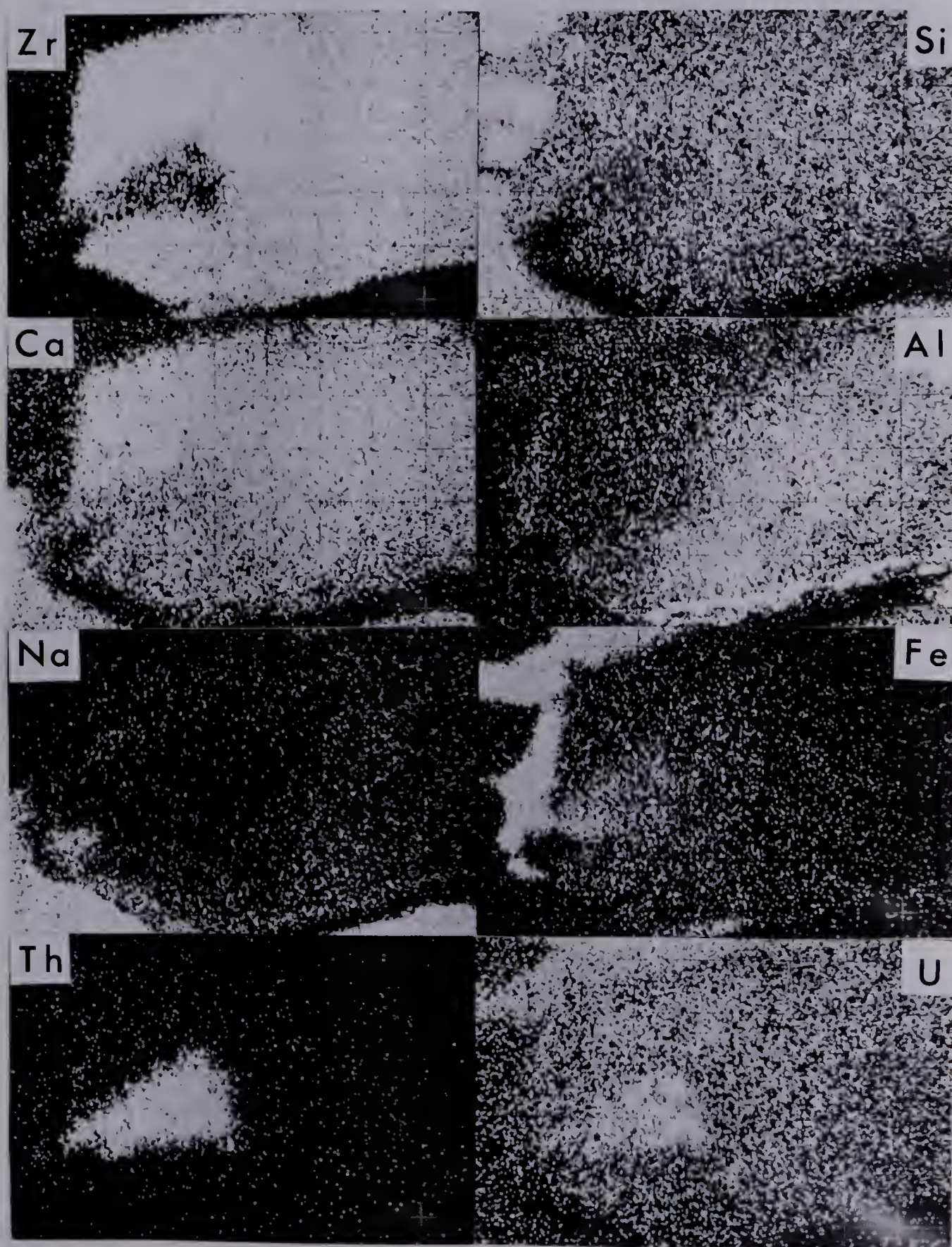
30

Radioluxographs of EMP thin-sections (10, 15, 7615, 18, 24, 30, 31, 32, 34 and D9), EMP thick sections (12, 14) and petrographic thin-sections (14, 15 and 30). Scale 1x. Processing times include 2 hrs. exposure to zinc film, 10 secs. exposure to light and 50 secs. for print development. The darker shades of grey observed in samples 10, 15, 7615, and 18 are due to weights used to ensure maximum contact between rock and film surfaces. Points of interest include; (1) close proximity of biotite and radioactive grains in EMP mounts 10, 15, 24, 30, D9 and petrographic sections 14 and 30; (2) the streaked nature of burn marks in sample 12, 7615, and 32 caused by the dispersion of U along cracks; (3) the weak radioactivity caused by allanite crystals in sample 18.





# PLATE 9

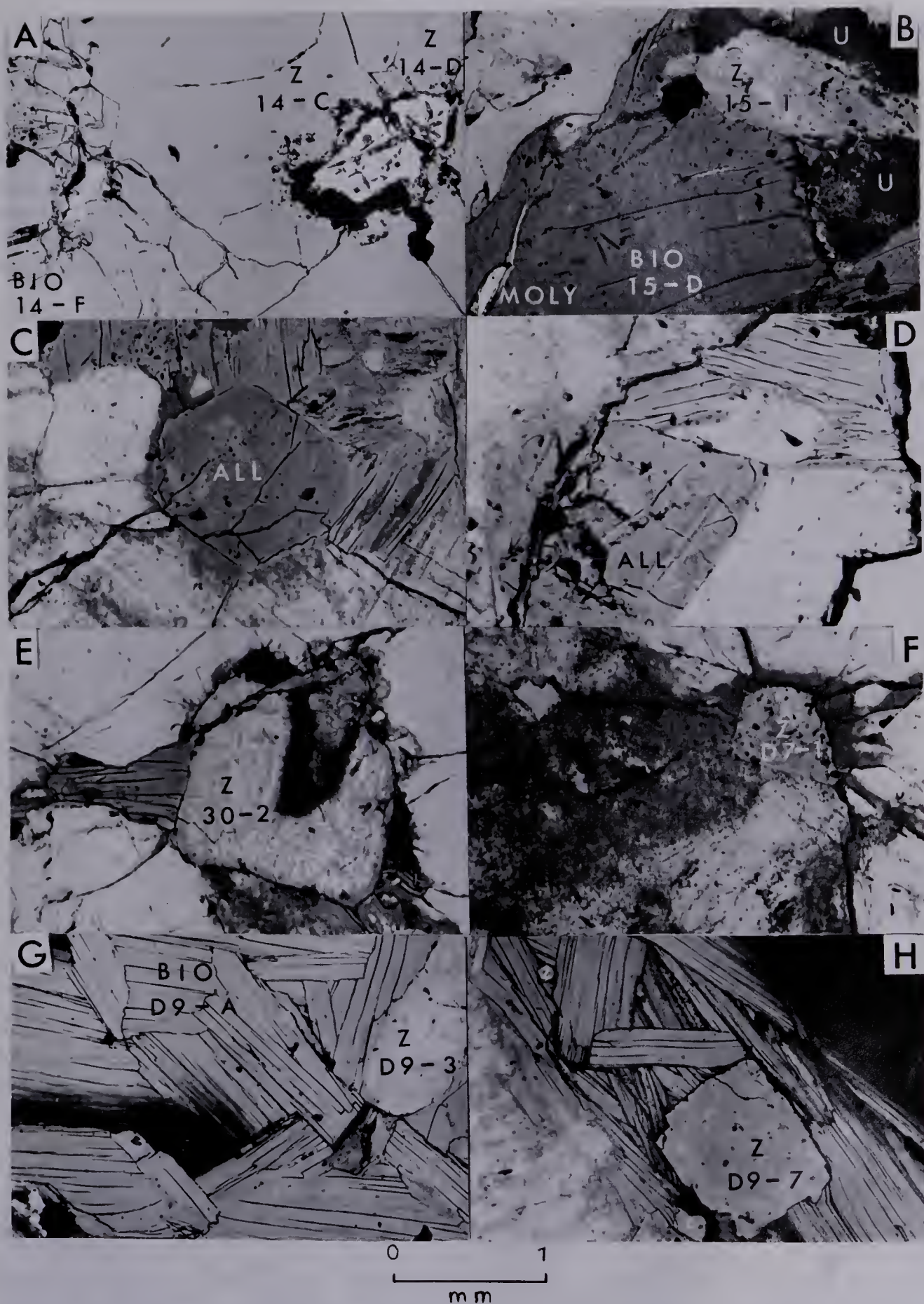


Elemental photographs of zircon D9-6.





# PLATE 10



Reflected light photomicrographs of zircon and allanite. A. No 14. Zircon. B. No 1. Uraninite and zircon intergrown. C. No 17. Allanite. D. No 18. Allanite with rutile ? inclusion. E. No 30. Zircon and a thorium-bearing mineral intergrown. F. No D7. Corroded zircon in altered granitic pegmatite. G, H. No D9. Large and small subhedral zircons intergrown with biotite.





THE  
JOURNAL OF THE

THE JOURNAL OF THE  
THE JOURNAL OF THE  
THE JOURNAL OF THE

## PLATE 11

Reflected light photomicrographic mosaic of trondhjemitic pegmatite sample 14 containing biotite, zircon, molybdenite, uraninite and Th-rich phases.

0 1  
mm

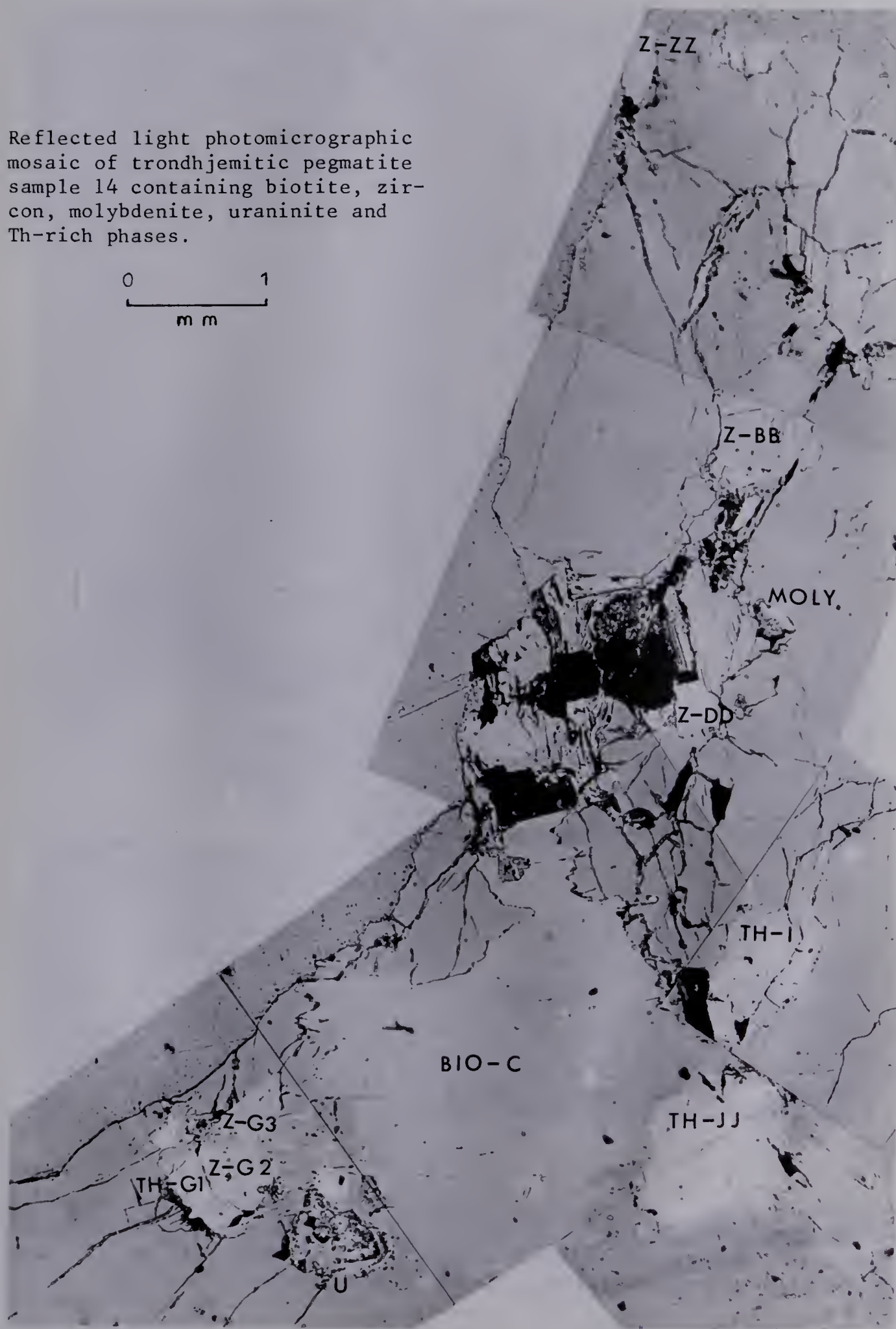
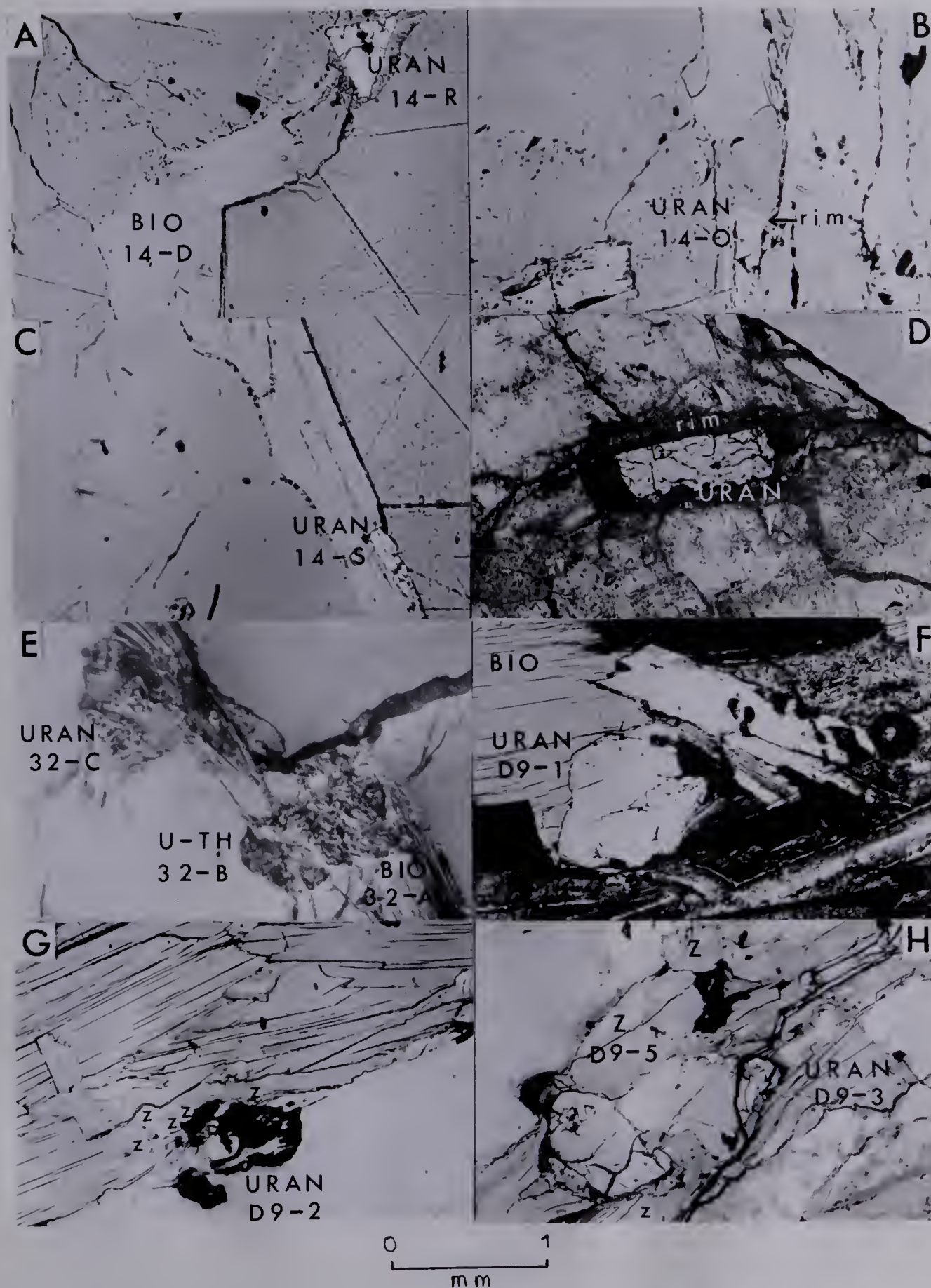






## PLATE 12

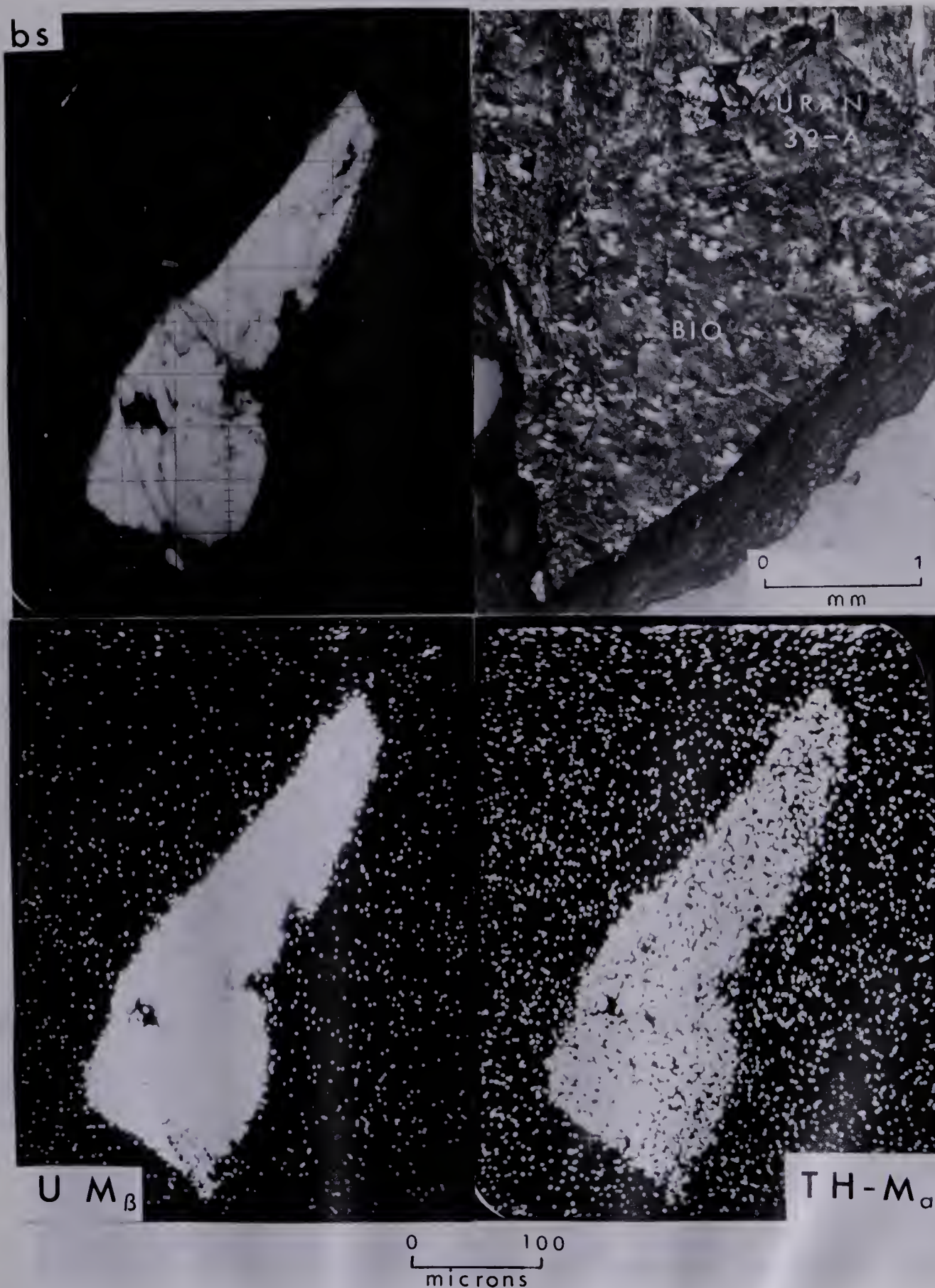


Reflected light photomicrographs of uraninite. A,B,C. No 14. Euhedral uraninite associated with biotite. D. No 31. Uraninite with alteration rim. E. No 32. Phase contrast photomicrograph of corroded uraninites. F,G,H. No D9. Uraninite associated with biotite, muscovite and zircons of variable sizes.





# PLATE 13



Backscatter electron and elemental photographs of uraninite 32-A. Included is a phase contrast photomicrograph of the grain in biotite.





# PLATE 14

SAMPLES

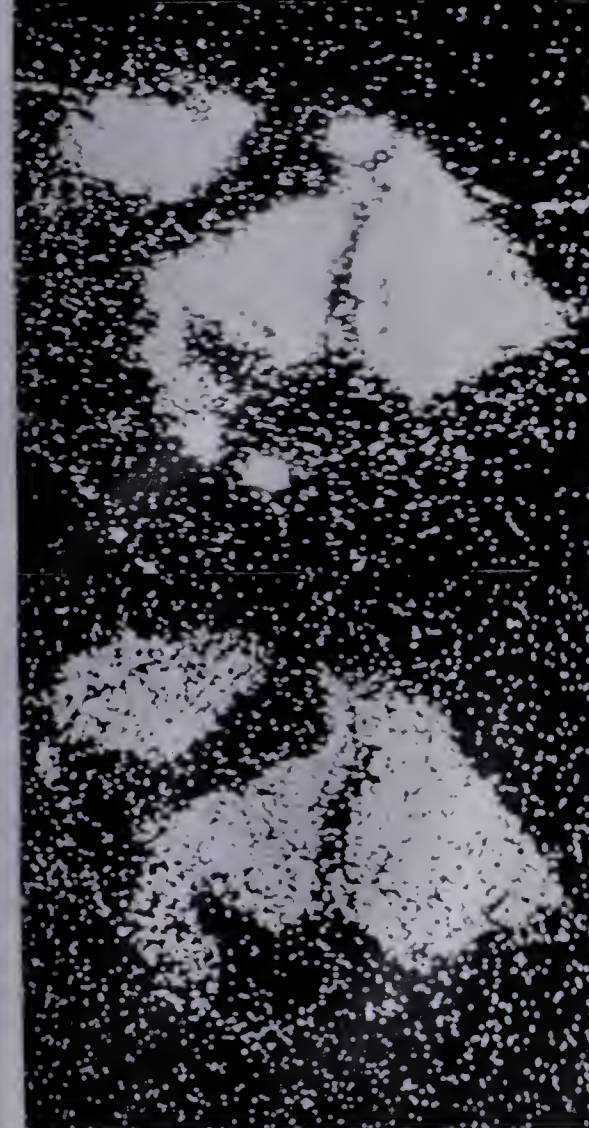
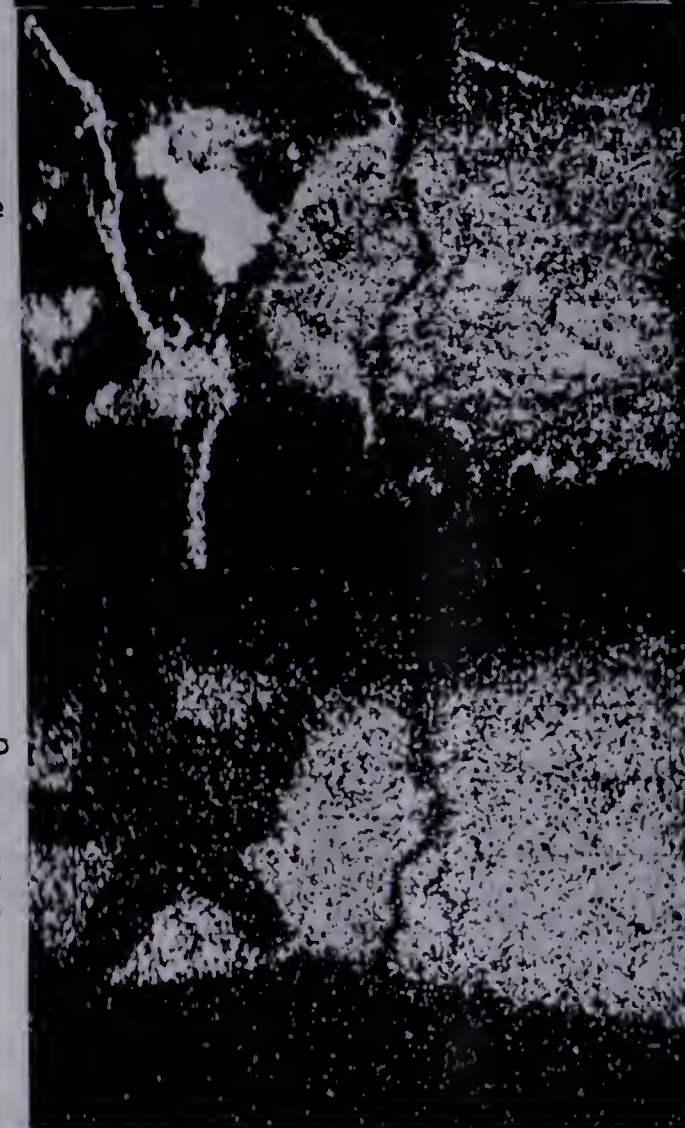
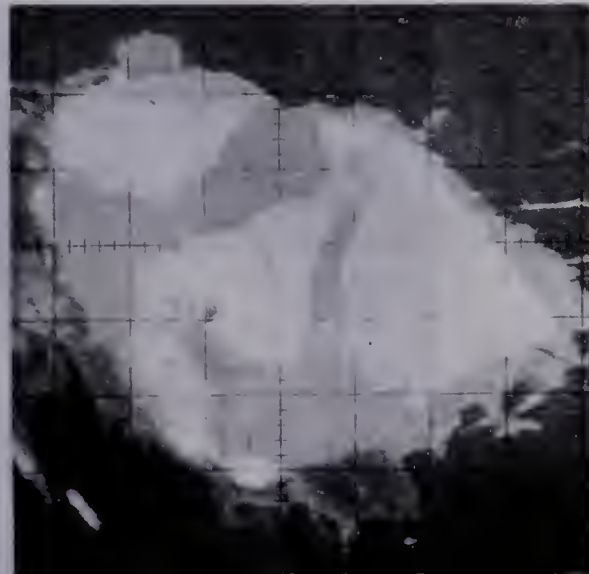
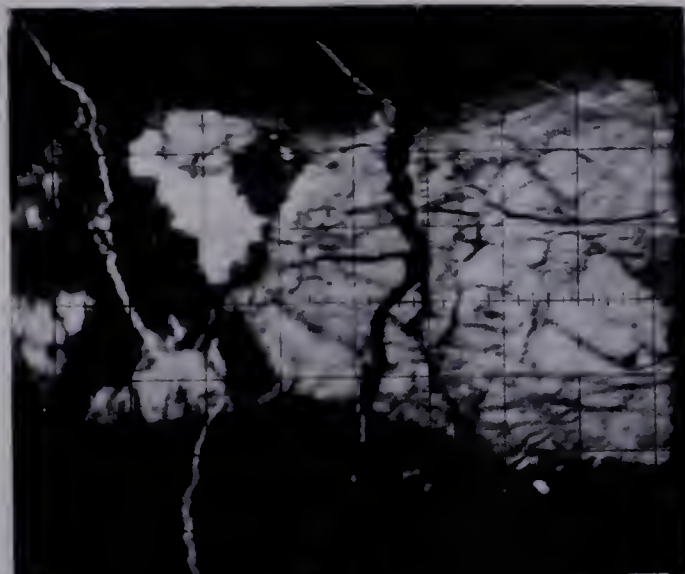
32-B

32-C

bs

U  $M_{\beta}$

TH  $M_{\alpha}$



0 100  
microns

Backscatter electron and elemental photographs of uraninites 32-B and 32-C.





## REFERENCES

- Alcock, F.J. 1936. Geology of the Athabaska region, Saskatchewan. Geol. Surv. Can., Mem. 196.
- Augustithis, S.S. 1973. Atlas of the textural patterns of granites, gneisses and associated rock types. Elsevier Scientific Publishing Co., Amsterdam, London, New York.
- Baadsgaard, H. 1964. Geochronology: a series of lecture notes. University of Alberta, Edmonton.
- Baadsgaard, H., and Godfrey, J.D. 1967. Geochronology of the Canadian Shield in Northeastern Alberta. 1, Andrew Lake Area. Can. J. Earth Sci. 4, pp. 541-563.
- Baer, A.J. 1968. The Precambrian geology of Fond-du-Lac. Map Area (74-0), Saskatchewan. Geol. Surv. Can., Paper 68-61.
- Bailey, R.V., and Childers, M.O. 1977. Applied mineral exploration with special references to uranium. Westview Press, Boulder, Colorado.
- Barnaby, F. 1978. Nuclear South Africa. New Scientist 80, 1125, 168-170.
- Bayly, B. 1968. Introduction to petrology. Prentice-Hall of Canada, Ltd., Toronto.
- Beck, L.S. 1966. Structural environment and genesis of the uranium deposits in the Athabasca region, Saskatchewan, Canada. University of Leeds, Dept. of Earth Science, PH.D. Thesis.
- 1969. Uranium deposits in the Athabasca region, Saskatchewan. Sask. Dept. Miner. Resour. Report No 126.
- Beesley, T.J. 1977. Report on an airborne radiometric survey and geological and radiometric surveying and sampling, Grease River, Saskatchewan. Urangesellschaft Canada Ltd. Project K-19. unpublished.
- Berman, R.M. 1957. The role of lead and excess oxygen in uraninite. Am. Min. 42, 11, pp. 704-731.
- Berning, J., Cooke, R., Hiemstra, S.A., and Hoffman, U. 1976. The Rossing uranium deposit, South West Africa. Econ. Geol. 71, pp.351-368.
- Berry, L.G., and Mason, B. 1959. Mineralogy. W.H. Freeman, San Francisco. 619p.
- Bibikova, Ye, V. 1977. Zircon as an isotopic geochromometer. Geochem. Int. 14, 2, pp. 46-56.



- Bowie, S.H.U. 1970. World uranium deposits. In Uranium exploration geology. IAEA, Panel Proc. Ser. Vienna. pp. 23-33.
- Bursill, L.A. and McLaren A.C. 1966. Transmission electron microscope of natural radiation damage in zircon ( $ZrSiO_4$ ). *Phys. Status Solidi*. 13, pp. 331-343.
- Burwash, R.A. 1978. Metamorphism of the Athabasca mobile belt, a subsurface extension of the Churchill province. *Geol. Sur. Can.*, Paper 78-10, pp. 123-127.
- \_\_\_\_\_. 1979. Uranium and thorium in the Precambrian basement of western Canada. II. Petrologic and tectonic controls. *Can. J. Earth Sci.* 16, 3, pp. 472-483.
- Burwash, R.A., Baadsgaard, H. and Peterman, Z.E. 1962. Precambrian K-Ar dates from the Western Canada Sedimentary Basin. *J. Geophys. Res.* 67, 4, pp. 1617-1675.
- Burwash, R.A. and Krupicka, J. 1969. Cratonic Reactivation in the PE. basement of Western Canada. Part I. Deformation and chemistry. *Can. J. Earth Sci.* 6, pp. 1381-1396.
- \_\_\_\_\_. 1970. Cratonic reactivation in the Precambrian basement of western Canada. Part II. Metasomatism and isostasy. *Can. J. Earth Sci.* 7, pp. 1275-1294.
- Cameron-Schimann, M. 1978. Election microprobe study of Uranium minerals and its application to some Canadian deposits. Ph.D. thesis. University of Alberta, Edmonton, Alta. unpublished.
- Can. Dept. Mines Tech. Serv. 1952. Gravity anomaly map of Saskatchewan.
- Carmichael, I.S.E., Turner, F.J. and Verhoogen, J. 1974. *Igneous Petrology*. McGraw-Hill, New York. 739p.
- Clayton, R.N. and Mayeda, T. 1963. The use of bromine pentafluoride in the extraction of oxygen from oxides and silicates for isotopic analysis. *Geochim. Cosmochim. Acta*. 27, pp. 43-52. *Geol.* 8, pp. 173-174.
- Colborne, G.L. 1962. The geology of the Wiley Lake area (East half), Sask. *Sask. Geol. Surv. Report No.* 69.
- Colborne, G.L. and Rosenberger, E., 1963. The geology of the Wiley Lake area (West half) Sask. *Sask. Geol. Surv. Report No.* 79.
- Craig, H. 1961. Isotopic variations in meteoric waters.





Science. 133, pp. 1702-1703.

Dahlkamp, F.J. 1978. Classification of uranium deposits. Mineral Deposits. 13, pp. 83-104.

Darnley, A.G., Cameron, E.M. and Richardson, K.A. 1975. The federal-provincial uranium reconnaissance program. Geol. Surv. Can., Paper 75-26, pp. 49-68.

Deer, W.A., Howie, R.A. and Zussman, J. 1962. Rock forming minerals. Longmans, London. 560p.

Donaghy, T.J. 1975. Reconnaissance and radioactivity survey of CBS 3424 and CBS 5398, Grease River, N. Sask. Fosago Exp. Ltd. Edm. Alta. unpublished.

\_\_\_\_\_ 1976. An autoradiograph study of uraniferous pegmatites, Grease River area, N. Sask. Geol. research project 607. Uni. of Alberta, Edm. Alta. unpublished.

Dooley, Jr. J.R. 1977. Fast autoradiographs for localizing uranium with the radioluxograph. Econ. Geol. 72, p. 727.

Engel, A.E.J. and Engel, C.G. 1960. Progressive metamorphism and granitization of the major paragneiss, Northwest Adirondack Mountains, New York. Geol. Soc. Am., Bull. 71, pp. 1-58.

Folinsbee, R.E. and Leech, A.P. 1974. Report on uraniferous pegmatites, Grease River area, Sask. Fosago Exp. Ltd. Edm. Alta. unpublished.

Geol. Surv. Can. 1967. Magnetic anomaly map of Canada. Map 1255A.

Grandstaff, D.E. 1976. A kinetic study of the dissolution of uraninite. Econ. Geol. 71, pp. 1493-1506.

Harper, C.T. 1978. Geology of the Cluff Lake uranium deposits. 80th Ann. Gen. Meeting, Can., Vancouver, B.C. April 1978.

Hauseux, M.A. 1976. Mode of uranium occurrence in a migmatitic granite terrain, Baie Johan Beetz, Quebec. paper present to 78th Ann. Gen. Meeting, Can. Inst. Min. Met., Quebec City, April 1976.

Heinrich, E. Wm. 1958. Mineralogy and geology of radioactive raw materials. McGraw-Hill Book Company, Inc. Toronto. 654 pg.

Henoc, J., Heinrich, K.F.L., and Myklekust, R.L. 1973. A rigorous correction procedure for quantitative electron probe microanalysis (COR-2). NBS TN-769.



- Heywood, W.W., and Schau, M. 1978. A subdivision of the northern Churchill structural province. Geol. Surv. Can., Paper 78-1A, pp. 139-143.
- Hoeve, J. 1978. Classification of uranium deposits in northern Saskatchewan. In: Kimberley, M.M. ed.; Short course in uranium deposits. Min. Ass. Can. 3, 397-402.
- I.U.G.S. 1973. Plutonic rocks: classification and nomenclature recommended. Geotimes pp. 26-30.
- Jaffey, A.H., Flynn, K.F., Glendenin, L.E., Bentley, W.C. and Essling, A.M. 1961. Precision measurement of half-lives and specific activities of  $U^{235}$  and  $U^{238}$ . Phys. Rev. C4, pp. 1889-1906.
- Kesler, S.E., Issigonis, M.J., Brownlow, A.H., 1975. Geochemistry of biotites from mineralized and barren intrusive systems. Econ. Geol. 70, pp. 559-567.
- Kimberley, M.M. 1978. High-temperature uranium geochemistry. In: Kimberley, M.M. ed., Short course in uranium deposits. Min. Ass. Can. 3, pp. 101-104.
- Klepper, M.R. and Wyant, D.G. 1956. Uranium provinces. In: Nininger, R.D. ed. Exploration for nuclear raw materials. D. Van Nostrand Company, Inc. Toronto. pp. 71-82.
- Koeppel, V. 1968. Age and history of the uranium mineralization of the Beaverlodge area, Saskatchewan. Geol. Surv. Can., Paper 67-31, 111 p.
- Koeppel, V., and Sommerauer, J. 1974. Trace elements and the behavior of the U-Pb system in inhibited and newly formed zircons. Contrib. Mineral. Petrol. 43, pp. 71-82.
- Krasnobayer, A.A., Polezhayer, Yu. M., Yunikov, B.A., and Novoselov, B.K. 1974. Laboratory evidence on radiation and genetic nature of metamict zircons. Geochem. Int. 195, pp. 195-209.
- Koster, F. and Baadsgaard, H. 1970. On the geology and geochronology of northwestern Saskatchewan. I. Tazin Lake region. Can. J. Earth Sci. 7, pp. 919-930.
- Krogh, T.E. 1973. A low-contamination method for hydrothermal decomposition of zircon and extraction of U and Pb for isotopic age determination. Geochim. Cosmochim. Acta. 37, pp. 485-494.
- Lang, A.H., Griffith, J.W., and Steacy, H.R. 1962. Canadian deposits of uranium and thorium. Geol. Surv. Can., Econ. Geol. Ser. 16. 324 p.





- Langmuir, D. 1978. Uranium solution - mineral equilibria at low temperatures with applications to sedimentary ore deposits. *Geochim. Cosmochim. Acta.* 42, pp. 547-569.
- LeRoux, L.J. and Glendenin, L.L. 1963. Half-life of thorium<sup>232</sup>. Proc on Nat'l Conf. Nuclear Energy, Pretoria, S. Africa. April 1963.
- Levinson, A.A. 1977. Hydrogen - a reducing agent in some uranium deposits. *Can. J. Earth Sci.* 14, pp. 2679-2681.
- Lewry, J.F., Sibbald, T.I.I., and Rees, C.J. 1978. Metamorphic patterns and their relationship to tectonism and plutonism in the Churchill province in northern Saskatchewan. *Geol. Surv. Can.*, Paper 78-10, pp. 139-154.
- Little, H.W. 1970. Distribution of types of uranium deposits and favourable environments for uranium exploration. *In: Uranium exploration geology. IAEA Panel Proc. Ser.*, Vienna. pp. 35-48.
- Longstaffe, F.J. 1979. Oxygen isotope geochemistry of Archean granitoids. *In: Barker, F. ed., Trondhjemites and related rocks. Elsevier Scientific Publishing Co.*, pp. 363-399.
- Lowdon, J.A. 1961. Age determinations by the Geological Survey of Canada, Rept. 2, Isotopic ages. *Geol. Surv. Can.*, Paper 61-17.
- 1963. Age determinations and geological studies. *Geol. Surv. Can.*, Paper 62-17, p. 49.
- Mawdsley, J.B. 1957. The geology of the Charlebois Lake area. *Sask. Geol. Surv. Report No. 24.*
- McMillan, R.H. 1978. Genetic aspects and classification of important Canadian uranium deposits. *In: Kimberley, M.M. ed.; Short course in uranium deposits. Min. Ass. Can. 3*, pp. 187-204.
- Medenbach, O., and El Goresy, A. 1978. Chemical variation in hydrated zircons. *Int. Min. Ass. Abst. General Meeting.*
- Mehnert, K.R. 1968. Migmatites and the origin of granitic rocks. *Elsevier Scientific Publishing Co., Amsterdam* 393p.
- 1973. The origin of granitic rocks. *Geol. Soc. S. Af. Spec. Pub. 3*, pp. 7-11.
- Meyer, C. and Hemley, J.J. 1967. Wall rock alteration. *In: Barnes, H.L. ed. Geochemistry of hydrothermal*





- oredeposits. Holt, Rinehart and Winston, Inc. New York. pp. 166-235.
- Mitchell, R.S. 1973. Metamict minerals: a review. Parts I and II. Mineral. Rec. 4, pp. 177-182, 214-223.
- Moorbath, S. 1970. Dating by radioisotopes. Sigma Series of Science Surveys. Francis Hodgson Ltd. Great Britain.
- Morra, F.P. 1977. Geology and uranium deposits of the Charlebois - Higginson Lake area, N. Saskatchewan. M.Sc. thesis. University of Alberta, Edmonton, Alta. unpublished.
- Morton, R.D., and Sassano, G.P. 1972. Reflectance and micro-indentation hardness versus chemical composition in some Canadian uraninites. N. Jb. Miner. Mh. 8, pp. 350-360.
- Munday, R J.C. 1977. The geology of the Mudjatik (east) area, Sask. Sask. Dept. Miner. Resour. Report No 168. 25 p.
- Nockolds, S.R. 1947. The relation between chemical composition and paragenesis in the biotite micas of igneous rocks. Am. J. Sci. 245, 7, pp. 401-420.
- Northern Miner, 1978. Uraniumania Sweeps Saskatchewan. July 27, 1978.
- Page, L.R. 1950. Uranium in pegmatites. Econ. Geol. 45, pp. 12-34.
- Park, C.F. and MacDiarmid, R.A. 1970. Ore deposits. W.H. Freeman and Co., San Francisco. 522p.
- Pavshukov, V.V., Komlev, L.V. Anderson, Ye.B. and Smyslova, I.G. 1975. X-ray microprobe data on the state of the U-Pb system in uranium ores. Geochem. Int. 12, 2, pp. 251-261.
- Poldervaart, A. 1956. Zircons in rocks. 2. Igneous rocks. Am. J. Sci. 254, pp. 521-554.
- Pyatenko, Y.A. 1970. Behavior of metamict minerals on heating and the general problem of metamictization. Geochem. 9, pp. 758-763.
- Rich, R.A., Holland, H.D. and Petersen, U. 1977. Hydrothermal uranium deposits. Elsevier Scientific Publishing Co., Amsterdam.
- Richardson, K.A. and Carson, J.M. 1976. Regional uranium distribution in northern Saskatchewan. In: Dunn, V.E.



ed.; Uranium in Saskatchewan. Sask. Geol. Soc. Spec. Pub. 3. pp. 27-50.

Richardson, K.A., Holman, P.B. and Elliot, B. 1974. Radioactivity maps and profiles, N. Saskatchewan. Geol. Surv. Can., Open File 169.

Roubault, M. 1958. Geologie de L'Uranium. Masson et C, Editeurs, Paris.

Rucklidge, J.C. 1976. Instrumentation. In: Smith, D.G.W. ed.; Short course in microbeam techniques. Min. Ass. Can. 1. pp. 45-62.

Ruzicka, V. 1971. Geological comparison between East European and Canadian uranium deposits. Geol. Surv. Can., Paper 70-48, 196p.

\_\_\_\_\_ 1975. New sources of uranium, types of uranium deposits presently unknown in Canada. Geol. Surv. Can., Paper 75-26, pp. 13-20.

Sask. Dept. Miner. Resour. and Geol. Surv. Can., Dept. Mines Tech. Surv. 1962a. Aeromagnetic Series. Wiley Lake. 74 O/8. Map 1222G.

\_\_\_\_\_ 1962b. Aeromagnetic Series. Fontaine Lake. 74 O/8. Map 1223G.

\_\_\_\_\_ 1964. Aeromagnetic Series. Fond-du-Lac area. 74/0. Map 7021G.

Sassano, G.P. 1974. Preliminary report #3 on the geology and economic potential of Claim Block CBS. 3424 of Fosago Explorations Ltd. Grease River area, N. Sask. unpublished.

Sibbald, T.I.I., Munday, R.J.C., and Lewry, J.F. 1976. The Geological Setting of uranium mineralization in Northern Saskatchewan. In: Dunn, C.E., ed; Uranium in Saskatchewan. Sask. Geol. Soc. Spec. Publ. No. 3. pp. 51.

Smith, D.G.W. 1976. Quantitative energy dispersive microanalysis. In: Smith, D.G.W. ed.; Short course in microbeam techniques. Min. Ass. Can. 1, pp. 45-62.

Spry, A. 1969. Metamorphic textures. Pergamen Press. London England.

Steady, H.R., and Kaiman, S. 1978. Uranium minerals in Canada: their description, identification and field guides. In: Kimberley, M.M. ed.; Short course in uranium deposits. Min. Ass. Can. 3, pp. 107-140.





- Stephenson, N.C.N. 1977. Coexisting hornblendes and biotites from Precambrian gneisses of the south coast of Western Australia. *Lithos* 10, pp. 9-27.
- Tatsch, J.H. 1976. Uranium deposits. Totsch Associates. Sudbury, Massachusetts. 01776.
- Tauson, L.V. 1965. Factors in the distribution of trace elements during the crystallization of magmas. *Phy. Chem. Earth*. 6, pp. 215-249.
- Taylor, B.E., Foord, E.E. and Friedrichsen, H. 1979. Stable isotope and fluid inclusion studies of gem-bearing granitic pegmatite-aplite dikes, San Diego Co., California. *Contrib. Mineral. Petrol.* 68, pp. 187-205.
- Taylor, H.P. Jr. 1967. Oxygen isotope studies of hydrothermal mineral deposits. In: Barnes, H.L. ed. *Geochemistry of hydrothermal ore deposits*. Holt, Rinehart and Winston, Inc. Toronto. pp. 109-142. *Contrib. Mineral Petrol.* 19, pp. 1-71.
- \_\_\_\_\_ 1968. The oxygen isotope geochemistry of igneous rocks. *Contrib. Mineral. Petrol.* 19, pp. 1-71.
- Taylor, H.P. Jr. and Epstein, S. 1962. Relationship between  $O^{18}/O^{16}$  ratios in coexisting minerals of igneous and metamorphic rocks. Part 2. Application to petrologic problems. *Geol. Soc. Am. Bull.* 73, pp. 675-694.
- Tilton, G.R. 1960. Volume diffusion as a mechanism for discordant Pb ages. *J. Geophys. Res.* 65, 9, pp. 2933.
- Tremblay, L.P. 1972. Geology of the Beaverlodge mining area, Saskatchewan. *Geol. Surv. Can., Memoir* 367.
- \_\_\_\_\_ 1978. Uranium subprovinces and types of uranium deposits in the Precambrian rocks of Saskatchewan. *Geol. Surv. Can., Paper* 78-1A, pp. 427-435.
- Vernon, R.H. 1976. Metamorphic processes: reactions and microstructure development. George Allen and Univen Ltd. Great Britain. 247 p.
- \_\_\_\_\_ 1977. Microfabrics of mica aggregates in partly recrystallized biotite. *Contrib. Mineral Petrol.* 61, pp. 175-185.
- Viswanathan, S. 1974. Oxygen isotope studies of early Precambrian granitic rocks from the giants Range batholith, northern Minnesota, U.S.A. *Lithos*. 7, pp. 29-34.
- Wetherill, G.W. 1956. Discordant uranium lead ages. *Trans.*





Am. Geophys. Union 37, pp. 320-326.

Whitten, E.H.T. 1966. Structural geology of folded rocks.  
Rand McNally and Company. U.S.A.

Winkler, H.G.F. 1974. Petrogenesis of metamorphic rock. 4th  
Edition. Springer - Verlag. New York.

Yelisseyeva, O.P., Ryabchikov, I.D. and Bogatyreva, N.A.  
1974. On the types of distribution in accessory zircon.  
Geochem. Int. 11, 5, pp. 960-968.

Yermolayev, N.P., Verlichkin, V.I., Averina, A.S., and  
Laktionova, N.V. 1976. Geochemical characteristics of  
granitization in the Erygekirge. Geochem. Int. 13, 3,  
pp. 49-58.

Zhukova, A.M., Bergman, I.A., and Zhukov, G.V. 1975.  
Distribution of uranium in the geological formations of  
the Ukrainian Shield. Geochem. Int. 12, 4, pp. 103-116.



## Appendix A

### Sample Descriptions

<u>Sample No.</u>	<u>Rock Name</u>
1	coarse-grained plagioclase-quartz-biotite white pegmatite
1a	coarse-grained microcline-quartz-plagioclase-biotite white pegmatite.
2	fine-grained quartz-microcline-biotite gneiss
2a	coarse-grained microcline-quartz-biotite plagioclase granophyric white pegmatite
3	coarse- to medium-grained plagioclase-quartz-biotite trondhjemitic migmatite
4	medium-grained plagioclase-quartz-biotite migmatite
4a	medium-grained thinly banded plagioclase-quartz biotite-garnet porphyroblastic gneiss
5	coarse-grained microcline-plagioclase-quartz-biotite granofels
6	coarse-grained quartz-plagioclase-biotite trondhjemitic pegmatite with minor zircon and molybdenite
6a	coarse-grained quartz-rich plagioclase-microcline biotite granitoid
7	medium-grained plagioclase-microcline-quartz biotite migmatite
8	fine-grained thinly-banded plagioclase-quartz-biotite gneiss in contact with zoned white pegmatite (8a)
8a	coarse-grained plagioclase-quartz white pegmatite grading into very coarse-grained microcline-quartz granophyric white pegmatite.
9	medium-grained plagioclase-quartz-biotite microcline folded gneiss



- 10 medium- to coarse-grained  
plagioclase-microcline-quartz-biotite migmatite  
with distinct mineralogical and textural  
banding.
- 10a medium-grained plagioclase-quartz-microcline  
leucocratic granite
- 11 coarse- to very coarse-grained  
quartz-plagioclase-microcline biotite migmatite  
with coarse layering.
- 12 coarse- to very coarse-grained  
quartz-plagioclase-biotite zircon-bearing  
pegmatitic quartzolite
- 13 medium-grained  
K-feldspar-quartz-biotite-plagioclase migmatite  
with folds developed in some layers
- 14 coarse-grained quartz-plagioclase-biotite  
trondhjemitic granofels
- 15 coarse-grained quartz-plagioclase-biotite  
radioactive granitoid migmatite
- 16 medium- to coarse-grained  
plagioclase-microcline-quartz biotite granofels
- 17 medium-grained  
plagioclase-microcline-quartz-biotite layers in  
contact with a porphyritic  
plagioclase-quartz-microcline pegmatitic portion  
of a migmatite
- 18 medium- to coarse-grained  
plagioclase-microcline-quartz-biotite  
zircon-bearing gneissic granite
- 19 medium-grained plagioclase-quartz-biotite  
migmatite
- 20 medium-grained  
plagioclase-microcline-quartz-biotite granitized  
gneiss
- 20a coarse-grained  
microcline-quartz-plagioclase-biotite  
granophyric granofel
- 21 medium- to very coarse-grained quartz-rich  
microcline-biotite granitoid granofel
- 22 medium- to coarse-grained





plagioclase-microcline-quartz-biotite granitized  
gneiss

- 23 medium- to coarse-grained  
microcline-plagioclase-quartz-biotite granofel
- 24 medium- to coarse-grained quartz-rich  
microcline-plagioclase-biotite uraninite bearing  
granitoid granofel with fine-grained  
biotite-rich gneissic xenoliths.
- 25 very coarse-grained microcline-quartz-biotite  
porphyritic pegmatite of alkali-feldspar granite  
composition
- 26 very coarse-grained microcline-quartz-biotite  
porphyritic pegmatite of alkali-feldspar granite  
composition
- 27 fine-grained biotite-plagioclase zones layered  
with medium-grained plagioclase-quartz zones in  
a trondhjemitic migmatite
- 28 coarse-grained  
microcline-plagioclase-quartz-biotite granite
- 29 coarse-grained microcline-quartz-biotite  
alkali-feldspar granitic migmatite
- 30 medium- to coarse-grained  
quartz-microcline-plagioclase-biotite granitic  
migmatite
- 31 medium- to coarse-grained  
plagioclase-quartz-biotite zircon-bearing  
trondhjemitic granofel
- 32 medium-grained quartz-microcline-plagioclase  
granitic granofel
- 33 very coarse-grained  
plagioclase-microcline-biotite granite pegmatite
- 34 coarse-grained  
plagioclase-quartz-microcline-biotite granitized  
gneiss
- D7 coarse-grained  
plagioclase-microcline-quartz-biotite pegmatite
- D9 very coarse-grained plagioclase-quartz biotite  
trondhjemitic pegmatite



Table 16: Heavy minerals found in gneissic and pegmatitic rocks from the Grease River area, N. Saskatchewan

Table 20. Heavy Minerals, Rock Analyses and Pyroxene Rock from the Great River Area, N. Saskatchewan																																		
Rock Type Sample No.		Hand <sup>1</sup> Specimen	Thin Section								Heavy Mineral Separate										Electron Microprobe Mount													
			Zr	Ap	Ep	Sp	Al	Gn	Ra	Fe	Zr	Ap	Ep	Sp	Al	Gn	Ra	U <sup>6</sup>	Fe	Py	Mo	Zr	Ap	Ep	Sp	Al	Gn	U <sup>4</sup>	U <sup>6</sup>	Th <sup>4</sup>	Fs	Mo		
Biotite Gneiss		4 9 13	Gn	X	X	X			X		X																							
				X	X					X	X																							
				X	X					X																								
Granitized Gneiss		3 5 6 7 11 16 17 18 19 20 22 23 27 28 30 32 33 34	Zr, Mo	X	X				X	X	X			?						X	X													
				X	X		?																											
				X	X		X			X	X																							
				X			X			X	X		X				X				X													
				X	?			X			X	X		X						X	X	X	X			X						X		
				X	X					X			X	X																			X	
				X	X		X																										X	
				X	X	X	X			X																								
				X	X	?	X			X				?			X	X			X	X						X		X				
				X			X					X	X	X			X				X													
Alkali Feldspar Granite		2 25 26 29							X																									
					X	X	?																											
				X																														
Quartz-Rich Granitoid		15 21 24		X	X				X		X			?				X			X	X							X	X			X	
				X	X					X	X		X	X			X				X								X		X			X
Quartzolite		12	Zr, U <sup>4</sup>	X	?	?	?			X	X	X		?	X		X	X			X													X
Quartz Diorite		1			X					X	X																		X					
Tonalitic Rocks		8 10 14 31 D7 D9		X X X X		?			X		X																					X		X
				X	X				X	X		X		X		X		X		X		X						X		X				
			Ilm	X						X	X									X									X					X
				X						X	X		X							X								X						

note: 1. Minerals listed here are large enough to be seen without a hand lens.



## Appendix C

### Geochronology Analytical Procedures

#### Heavy Mineral Analysis

This section will include a brief description of the rock samples selected, the heavy mineral procedures followed and the heavy mineral separates obtained for geochronological study.

#### Isolation of Mineral Separates

Rock samples were crushed in a jaw crusher then in a rotary mill. The fine fractions passing through a 120 mesh sieve were selected for heavy mineral analysis. Preparatory treatment of the fine fractions involved (1) H<sub>2</sub>O wash in an ultrasonic bath in order to remove adhering rock powder and (2) exposure to a hand magnet to remove tramp iron and any strongly magnetic minerals.

Heavy liquids and a Franz magnetic separator were used to further fractionate the crushed rock samples. Bromoform, tetrabromethane, methyl iodide and clerici with respective specific gravities of 2.90, 3.05, 3.30 and 4.25, were used to sink the heavy mineral fractions containing zircon and uraninite. Magnetic separations ensured the isolation of non-magnetic zircon and uraninite fractions.

Non-magnetic fractions containing zircon and uraninite were obtained from the clerici 'sink' material. Samples rich





in zircon were acid washed; initially in hot dilute HCl in order to dissolve any apatite and pyrite present, then in hot 6N HNO<sub>3</sub> in order to clean the zircons. However, those samples containing radioactive opaques were not acid washed since these minerals decomposed in acids.

Although not used for age dating, the heavy liquid 'float' material and magnetic fractions isolated were also examined under a binocular microscope. The heavy minerals (S.G. > 2.90) found in the samples crushed and processed appear in Appendix B.

#### Notes on Zircon and Uraninite Separates

Although these samples contained seemingly good quality zircon and uraninite populations, it was soon realized that many of the accessories could not be isolated within clean, monomineralic populations required for geochronological studies. Therefore, only five zircon and two uraninite heavy mineral separates were acceptable for further chemical and isotopic processing.

The majority of the zircon separates were rejected for these reasons: (1) unattainability of zircon populations isolated within narrow magnetic and density limits; (2) too low concentrations of high quality zircon populations with similar properties such as colour, size, shape, clarity and lack of metamict character. Iron stained zircons were acid washed but essentially all were discarded because the surfaces had been too severely corroded.

Several uraninite samples were excluded because of



these factors: (1) lack of recognizable crystal faces or cleavage planes; (2) uneven colour or luster; (3) abundance of secondary uranium mineralization present as fine-grained yellow coating.

### Chemical Procedure

The method used for the decomposition of zircon and the extraction of U and Pb isotopes has been described by Krogh (1973). Although a brief outline of the procedure followed in this study is given below, the reader is referred to the original paper.

Hand-picked zircon separates weighing from 3 to 30 mg were decomposed at 160°C in an HF:HNO<sub>3</sub> solution. The resulting sample solutions were divided into isotope dilution (ID) and isotope ratio (IR) fractions.

Isotope tracers containing 99.9 percent U<sup>235</sup> and 99.7 percent Pb<sup>208</sup> were utilized in the isotope dilution analyses. U and Pb were recovered from the ID-fraction, while, the IR-fraction was processed for Pb only. The apparatus, reagents and chemical steps used to process Pb in each aliquot were essentially the same. A brief account of the more involved treatment of the ID-fraction follows.

A Ba(NO<sub>3</sub>)<sub>2</sub> solution was added to the ID-sample solution in order to separate the major elements. Pb was co-precipitated with Ba(NO<sub>3</sub>)<sub>2</sub>, while U and Th were held in the supernatant liquid and decanted off. Pb-ID and U-ID were isolated on the respective Cl and NO<sub>3</sub> anion exchange



columns.

The initial processing of uraninite separates was simpler than the method followed for zircons. Approximately .3 mg samples of uraninite were dissolved in warm nitric acid. The resulting sample solutions were aliquotted and subsequently processed according to Krogh's method (1973) . In addition to the  $U^{235}$  and  $U^{208}$  spikes mentioned in the zircon procedure, a 92 percent  $Th^{230}$  tracer was included in the ID-fraction.

### Isotope Analysis

The zircon Pb and U, and uraninite Pb, U, and Th solutions isolated from the anion columns were isotopically analyzed by mass spectroscopy. The Pb fractions were dissolved in  $H_3PO_4$  and mounted onto a Re filament coated with silica gel. The U and Th samples were similarly dissolved but mounted on a Re filament coated with  $Ta_2O_5$ . The Pb, U and Th phosphates were ionized on a 12-inch mass spectrometer and isotopically analyzed.





## Appendix D

### Electron Microprobe Methodology

Cleaned polished mounts were carbon coated under vacuum. Their edges were marked with silver in order to ensure electrical conductivity during electron bombardment. Mineral analyses were obtained with either EDA or WDA techniques.

### Energy Dispersive Analysis

#### Instrumentation and Operating Conditions:

EDA results were obtained using the following parameters:

operating voltage	15 KV
emission current	200 UA
beam current	1.0 UA
probe current	.1 UA

An electron source was generated from a heated tungsten filament. Random x-ray photons emitted from the excited region of the bombarded specimen positioned under the electron beam were detected by a silicon-lithium drifted, [Si(Li)] semi-conductor maintained at liquid nitrogen temperatures. Detected photons resulted in the creation of signals transmitted as electrical pulses to a series of amplifiers, pulse pile-up rejector and multichannel analyzer for amplification, discrimination and storing, respectively. For greater detail, the reader is referred to Smith (1976).



### Standardization of Operating Conditions:

The use of willemite ( $\text{Zn}_2\text{SiO}_4$ ), a calibration standard, at the start of each set of analyses, ensured that no drift and main amplifier gain (commonly known as shift and stretch, respectively) of the spectrum appeared on the cathode ray tube (CRT) visual output mode. The utilization of calibration standards as such ensures reproducibility of analyses over periods of months.

The beam current was monitored (using an aperture in the electron beam column) during electron emission and acceleration towards the point of impact in the sample chamber. A continual check on the beam current coupled with the periodic measurement of the probe current (using a Faraday cage) was used to estimate the probe current for any given time during data accumulation.

### Standards used to obtain Chemical Results:

Mineral standards known to closely approximate the sample specimens in elemental concentrations, composition and average atomic number were used to calculate the elemental composition in the samples according to

$$\frac{C_{st}}{I_{st}} \propto \frac{C_{sp}}{I_{sp}}$$

where

$C_{st}$  = element concentration in the standard  
 $C_{sp}$  = element concentration in the sample  
 $I_{st}$  = peak intensity measured for the standard  
 $I_{sp}$  = peak intensity measured for the sample



The standards used for quantitative analysis of biotite and zircon samples are listed in Table 17. Other criteria used to ensure proper standard selection included: (1) chemical homogeneity to ensure reproducibility and (2) stability under the beam so as to maintain the chemical composition.

#### Data Accumulation:

Probe data on mineral standards and samples were accumulated over live counting times of 400 seconds. Dead time corrections were dealt with by the pulse pile-up rejector. In order to avoid damaging the more volatile biotite and zircon samples, a defocussed beam was moved whenever possible.

#### Data Processing:

Probe data accumulated on biotites and zircons was transferred directly to magnetic tapes. An APL program was used to verify beam:probe current stability. Following the subtraction of background spectrums, the sample data were compared to standards of known composition. An EDTA-II program used for such calculations, also performed absorption, atomic number and fluorescence effect corrections.

Oxygen in the silicates was calculated by cation concentrations, with any excesses of oxygen over 100% believed to be combined with hydrogen to give H<sub>2</sub>O. Where the





Table 17 : Standards used for the elements detected in biotites and zircons analyzed using EDA and WDA methods.

El.	<u>biotite analyses</u>		<u>zircon analysis</u>	
	standard	el conc.	standard	el. conc.
H <sup>1</sup>				
O <sup>1</sup>				
F <sup>2</sup>				
Na	sanidine	2.2	obsidian	3.0
Mg	diopside	11.2	kaersutite	7.7
Al	sanidine	9.9	kaersutite	7.3
Si	sanidine	30.2	zircon	15.2
P <sup>3</sup>				
S <sup>3</sup>				
Cl <sup>2</sup>	biotite	0.5		
K	sanidine	10.1	kaersutite	1.8
Ca	diopside	18.4	kaersutite	7.4
Ti	ilmenite	28.6	kaersutite	3.0
Mn	ilmenite	0.2		
Fe	ilmenite	38.7	kaersutite	8.5
Y <sup>2</sup>	n.d.		zircon	1.2
Zr	n.d.		zircon	48.9
Hf <sup>2</sup>	n.d.		zircon	1.2

Notes: 1. H and O calculated by difference. 2. Qualitative analysis using WDA methods. 3. Standard concentrations obtained from internal standards in the computer program.



totals of all the analyzed and calculated elements exceeded 100%, a recalculation of oxides was performed to bring the total to 100%.

#### Semi-Qualitative Analysis:

Facilities other than the EDA system were used to acquire additional compositional information. When simultaneous WDA data was accumulated, crystal spectrometer data was transferred to a typewriter and later accessed by the author. Also, an oscilloscope and polaroid camera facility was useful in delineating compositional varieties existing in the zircons.

#### Wavelength Dispersive Analysis

##### Instrumentation and Operating Conditions:

The observed instability of uraninite grains under the electron beam required that less destructive operating conditions be employed during WDA analysis. Using a 15KV operating potential, data was collected with the following parameters:

```

probe current..... 0.1 u Amp.
beam current..... 0.01 u Amp.
beam diameter..... 0.5 to 20 microns
counting periods.... 50.0 seconds
number of counting periods on peaks : 10
number of counting periods on backgrounds : 5

```

Characteristic x-ray emissions were detected simultaneously by three crystal spectrometers set to measure two heavy elements (with atomic numbers greater than 40) and one lighter element.



### Data Accumulation:

The strategy used in gathering quantitative WDA data is different from that outlined in the EDA section. Counts are accumulated on lower and higher energy level background portions of the electromagnetic spectrum bordering the characteristic lines measured on the standards and samples. The wavelengths used to measure element concentrations are listed in Table 18 along with the standards employed. Suitable standards were chosen on the same principals discussed earlier.

### Data Processing:

Corrections for fluctuations in the beam:probe current ratios were applied to raw probe data acquired on typewriter paper. Following the subtraction of average background values for each element, ratios of sample:standard peak intensities were calculated. Absorption, atomic number and fluorescence effect corrections were applied using the computer programme COR-2 (Henoc et al. 1973).

All of the elements measured (except S) were calculated as oxides. When present, sulfur was combined with lead to form PbS. The total weight percentages of constituents measured in the uraninites never reached 100 percent. The difference was attributed to water and helium.





Table 18: Basic data regarding the elements (El) analyzed and the standards used to obtain EMP-WDA compositional analyses of uraninite.

El.	Line	W length	Crystal	Standards
H <sup>1</sup>				
O <sup>1</sup>				
Na	Ka	11.9090	RAP <sup>2</sup>	sanidine
Mg	Ka	9.8889	RAP	diopside
Al	Ka	8.3390	RAP	sanidine
Si	Ka	7.7261	EDDT <sup>3</sup>	sanidine
S	Ka	5.3728	EDDT	galena
K	Ka	3.7424	ADP <sup>4</sup>	sanidine
Ca	Ka	3.3596	ADP	diopside
Fe	Ka	1.9373	LiF <sup>5</sup>	hematite
Pb	Ma	5.2916	EDDT	galena
Th	Ma	4.1448	ADP	ThO <sub>2</sub> (cintered)
U	M <sub>B</sub>	3.7160	EDDT	UO <sub>2.1</sub> (cintered)

- notes:
1. H and O calculated by difference
  2. RAP - Rb acid phthalate
  3. EDDT - ethylene diamine dextrotartrate
  4. ADP - ammonium dihydrogen phosphate
  5. LiF - lithium fluoride









# MAP 1

## GREASE RIVER : MAIN SHOWING GEOLOGICAL MAP

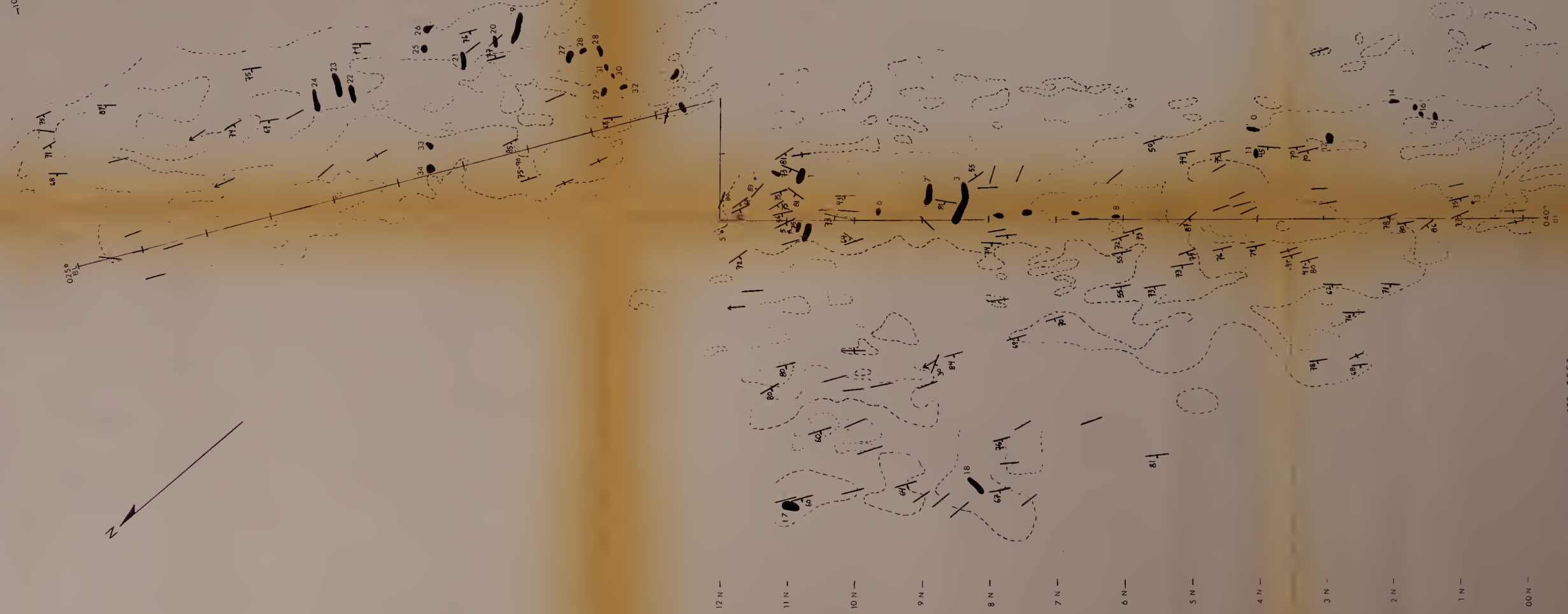
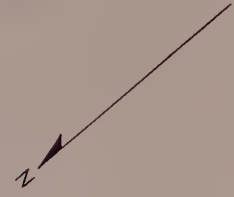
BY URANGESELLSCHAFT CANADA LIMITED  
WITH SLIGHT MODIFICATIONS BY S. COSTASCHUK

### LEGEND

- Diagonal lines (top-left to bottom-right) : Mineralized waste zone
- Diagonal lines (bottom-left to top-right) : Waste zone
- Stippled pattern : Pink to white pegmatite
- Dashed line : Outcrop boundary
- Wavy line : Geological contact
- Circle with number : Trench, and number
- Circle with cross : Strike and dip of inclusion (inlined, vertical)



-10N  
 -9N  
 -8N  
 -7N  
 -6N  
 -5N  
 -4N  
 -3N  
 -2N  
 -1N  
 -00N



LEGEND

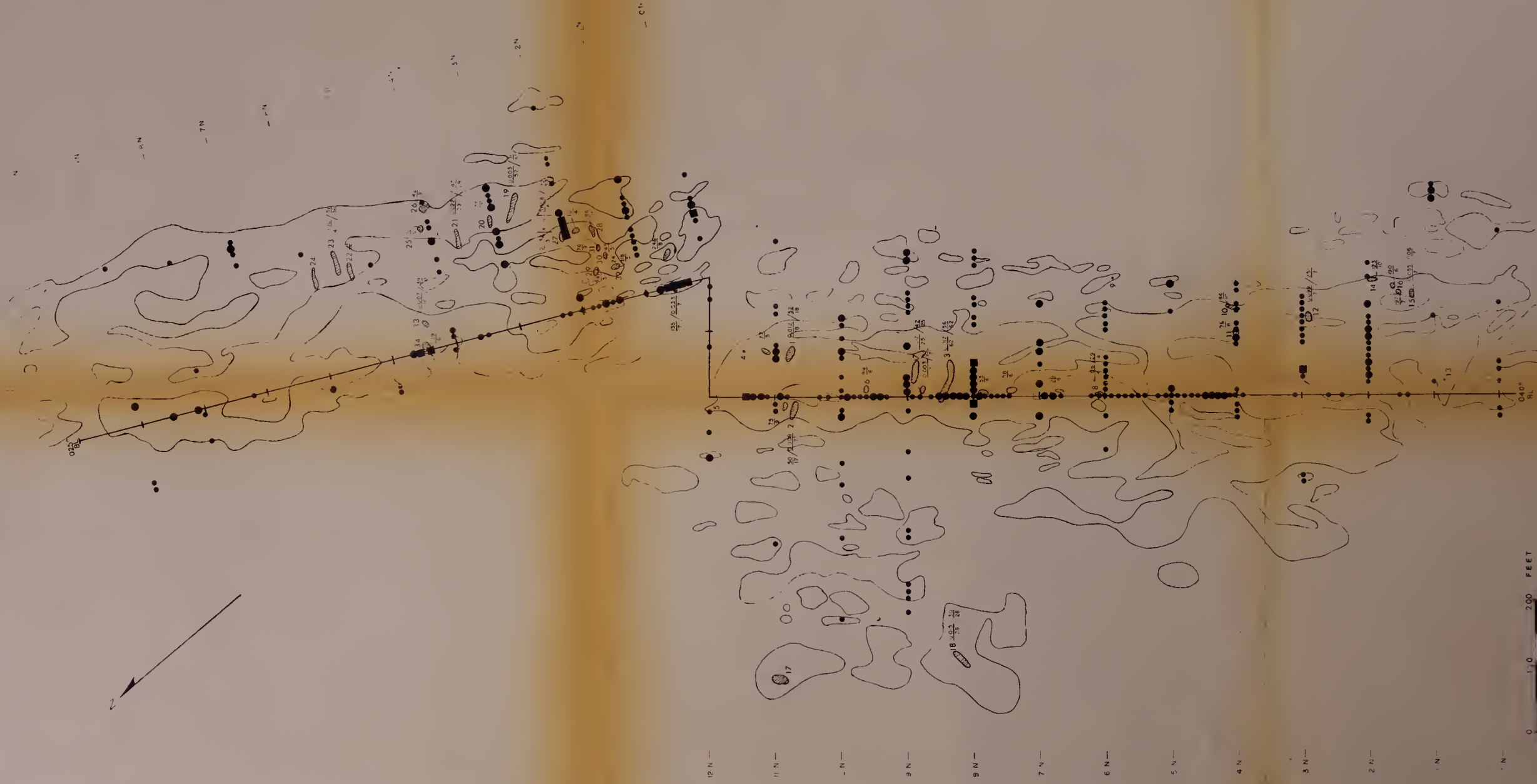
- Outcrop boundary
- Trench and number
- Strike and dip of gneissosity, inclined vertical
- Trend and plunge of folds

MAP 2

GREASE RIVER : MAIN SHOWING

STRUCTURAL GEOLOGY

BY S. COSTASCHUK



#### LEGEND

- Outcrop
- Scintillometric anomalies
  - 500-1000 cps
  - 1000-2000 "
  - 2000-4000 "
- Trench and number
- Trench chip sample assay result
  - 42 cps
  - 43 cps
  - 44 cps
  - 45 cps
  - 46 cps
  - 47 cps
  - 48 cps
  - 49 cps
  - 50 cps
  - 51 cps
  - 52 cps
  - 53 cps
  - 54 cps
  - 55 cps
  - 56 cps
  - 57 cps
  - 58 cps
  - 59 cps
  - 60 cps
  - 61 cps
  - 62 cps
  - 63 cps
  - 64 cps
  - 65 cps
  - 66 cps
  - 67 cps
  - 68 cps
  - 69 cps
  - 70 cps
  - 71 cps
  - 72 cps
  - 73 cps
  - 74 cps
  - 75 cps
  - 76 cps
  - 77 cps
  - 78 cps
  - 79 cps
  - 80 cps
  - 81 cps
  - 82 cps
  - 83 cps
  - 84 cps
  - 85 cps
  - 86 cps
  - 87 cps
  - 88 cps
  - 89 cps
  - 90 cps
  - 91 cps
  - 92 cps
  - 93 cps
  - 94 cps
  - 95 cps
  - 96 cps
  - 97 cps
  - 98 cps
  - 99 cps
  - 100 cps
- Spectrometer reading
  - 42 cps
  - 43 cps
  - 44 cps
  - 45 cps
  - 46 cps
  - 47 cps
  - 48 cps
  - 49 cps
  - 50 cps
  - 51 cps
  - 52 cps
  - 53 cps
  - 54 cps
  - 55 cps
  - 56 cps
  - 57 cps
  - 58 cps
  - 59 cps
  - 60 cps
  - 61 cps
  - 62 cps
  - 63 cps
  - 64 cps
  - 65 cps
  - 66 cps
  - 67 cps
  - 68 cps
  - 69 cps
  - 70 cps
  - 71 cps
  - 72 cps
  - 73 cps
  - 74 cps
  - 75 cps
  - 76 cps
  - 77 cps
  - 78 cps
  - 79 cps
  - 80 cps
  - 81 cps
  - 82 cps
  - 83 cps
  - 84 cps
  - 85 cps
  - 86 cps
  - 87 cps
  - 88 cps
  - 89 cps
  - 90 cps
  - 91 cps
  - 92 cps
  - 93 cps
  - 94 cps
  - 95 cps
  - 96 cps
  - 97 cps
  - 98 cps
  - 99 cps
  - 100 cps

### MAP 3

GREASE RIVER : MAIN SHOWING

RADIOMETRIC SURVEY AND  
TRENCH SAMPLING RESULTS

BY URANGESELLSCHAFT CANADA LIMITED  
WITH SLIGHT MODIFICATIONS BY S. COSTASCHUK



B30247